Sex Dependent Vulnerability of Fetal Nonhuman Primate Cardiac Mitochondria to Moderate Maternal Nutrient Reduction

Brief title: Maternal Nutrient Reduction Remodels Fetal Heart Mitochondria

Susana P. Pereira PhD [a,b,c,*], Ludgero C. Tavares PhD [a,b], Ana I. Duarte PhD [a], Inês Baldeiras PhD [a,d], Teresa Cunha-Oliveira PhD [a], João D. Martins MSc [a], Maria S. Santos PhD [a,b], Alina Maloyan PhD [c,#], António J. Moreno PhD [b], Laura A. Cox PhD [e], Cun Li MD [f], Peter W. Nathanielsz MD [f], Mark J. Nijland PhD [c], and Paulo J. Oliveira PhD [a]

Departments and institutions

[a] CNC-Center for Neuroscience and Cell Biology, University of Coimbra, 3004-517 Coimbra, Portugal.
[b] Department of Life Sciences, University of Coimbra, 3004-517 Coimbra, Portugal.
[c] Center for Pregnancy and Newborn Research, University of Texas Health Science Center at San Antonio, 78229-3900 San Antonio, Texas, United States
[d] Neurological Clinic, Faculty of Medicine, University of Coimbra, 3004-517 Coimbra, Portugal.
[e] Department of Genetics, Texas Biomedical Research Institute, 78245-0549 San Antonio, Texas, United States.
[f] Wyoming Pregnancy and Life Course Health Center, University of Wyoming, Laramie, Wyoming, 82071-3684
[*] New address: Research Centre in Physical Activity Health and Leisure (CIAFEL), Faculty of Sports, University of Porto, 4200-450 Porto, Portugal.
[#] New address: Knight Cardiovascular Institute, Oregon Health and Science University, Portland, Oregon, USA, 97239

Manuscript category: original article

Address for correspondence

Paulo J. Oliveira, PhD,
CNC-Center for Neuroscience and Cell Biology, UC Biotech, Biocant Park, University of Coimbra, 3060-197 Cantanhede, PORTUGAL
phone: +351-231-249-235
fax: +351-239-853409
email: pauloliv@cnc.uc.pt
ORCID: 0000-0002-5201-9948

Susana P. Pereira, PhD,
CNC-Center for Neuroscience and Cell Biology, UC Biotech, Biocant Park, University of Coimbra, 3060-197 Cantanhede, PORTUGAL
phone: +351-231-249-170
fax: +351-239-853409
email: pereirasusan@gmail.com
ORCID: 0000-0002-1168-2444

Tweet: Maternal nutrition reduction causes fetal sex-dependent cardiac mitochondrial remodelling, bioenergetic imbalance and later-life cardiac disease.

Acknowledgments

The authors dedicate this paper to the late Dr. Thomas J. McDonald from University of Texas Health Science Center at San Antonio. The authors acknowledge the contributions by Paulina Quezada and Greg Langone, Michelle Zavala, Ana Maria Silva, Leslie Myatt, Nagarjun Kasaraneni, Chunming Guo, Balasubashini Muralimanoharan, James Mele, Karen Moore and Susan Jenkins.

Abstract

Poor maternal nutrition in pregnancy affects fetal development, predisposing offspring to cardiometabolic diseases. The role of mitochondria during fetal development on later-life cardiac dysfunction caused by maternal nutrient reduction (MNR) remains unexplored.

We hypothesized that MNR during gestation causes fetal cardiac bioenergetic deficits, compromising cardiac mitochondrial metabolism and reserve capacity.

To enable human translation, we developed a primate baboon model (Papio spp) of moderate MNR in which mothers receive 70% of control nutrition during pregnancy, resulting in intrauterine growth restriction (IUGR) offspring and later exhibiting myocardial remodeling and heart failure at human equivalent ~25years. Term control and MNR baboon offspring were necropsied following cesarean-section, and left ventricle (LV) samples were collected. MNR adversely impacted fetal cardiac LV mitochondria in a sex-dependent fashion. Increased maternal plasma aspartate aminotransferase, creatine phosphokinase, and elevated cortisol levels in MNR concomitant with decreased blood insulin in male fetal MNR were measured. MNR resulted in a two-fold increase in fetal LV mtDNA. NMR resulted in increased transcripts for several respiratory chain (NDUFB8, UQCRC1, and cytochrome c) and ATP synthase proteins However, MNR fetal LV mitochondrial complex I and complex II/III activities were significantly decreased, possibly contributing to the 73% decreased ATP content and increased lipid peroxidation. MNR fetal LV showed mitochondria with sparse and disarranged cristae dysmorphology.

Conclusions: MNR disruption of fetal cardiac mitochondrial fitness likely contributes to the documented developmental programming of adult cardiac dysfunction, indicating a programmed mitochondrial inability to deliver sufficient energy to cardiac tissues as a chronic mechanism for later-life heart failure.

Keywords: cardiometabolic disease, cardiac metabolic flexibility, sexual dimorphism, heart, maternal nutrition, fetal development

Declarations

Funding

This work was supported by FEDER funds through the Operational Programme Competitiveness Factors-COMPETE and national funds by FCT-Foundation for Science and Technology, Portugal under fellowships [SFRH/BD/64694/2009 and SFRH/BPD/116061/2016 to S.P.P.; Post-Doctoral Researcher contract DL57/2016 #*SFRH/BPD/84473/2012* to A.I.D]; [PTDC/DTP-DES/1082/2014 and POCI-01-0145-FEDER-016657 to P.J.O.]; [UID/NEU/04539/2020 to CNC]; Program Project Grant (P01) from the National Institutes of Health, USA [PO1-HD21350 to P.W.N., C.L. and M.J.N.] and R24 RR021367. Resources and facilities were also supported by the Southwest National Primate Research Center, San Antonio,Texas, USA grant [P51-RR013986] from the National Center for Research Resources, NIH, currently supported by the Office of Research Infrastructure Programs through [P51-OD011133] and [C06-RR013556]. The funding agencies had no role in study design, data collection and analysis, decision to publish, or preparation of this document.

Conflicts of interest/Competing interests

The authors declare that they have no conflict of interest. relationship with industry.

Ethics approval

All animal procedures were approved by the Animal Care and Use Committees of the Texas Biomedical Research Institute and the University of Texas Health Science Center at San Antonio, TX (no. 1134PC), and were conducted in Association for Assessment and

Accreditation of Laboratory Animal Care-approved facilities and NIH Guide for the Care and Use of Laboratory Animals as detailed in the supplemental material.

Consent to participate

'Not applicable'

Consent for publication

All authors agreed with the content and gave explicit consent to submit and that they obtained consent from the responsible authorities at the institute/organization where the work has been carried out, before the work was submitted.

Code availability

'Not applicable'

1 Introduction

Cardiovascular disease (CVD) is the leading cause of mortality worldwide (1). Human epidemiologic studies have demonstrated that developmental programming by a suboptimal intrauterine environment increases later life CVD risk (2). Maternal nutrient reduction is a common cause of intrauterine growth restriction (IUGR) (3). IUGR is associated with increased later life risk for heart disease (4) coronary artery disease (2,5,6), hypertension, hypercholesterolemia, and stroke (5,7). There is a strong association between birthweight and mortality rate from ischemic heart disease, with smaller babies having a three-to-five-fold higher risk (8). Moreover, programming of CVD risk by adverse intrauterine conditions is transmitted across generations (9), increasing this condition's impact.

Epidemiological studies have provided compelling evidence on etiological factors that predispose to CVD. However, epidemiological studies can only indicate an association. Demonstration of causation requires precise control of environmental confounders, randomisation, and the introduction of specific interventions. While rodent models provide useful mechanistic information, those are polytocous, and thus pregnant dams carry a much more significant nutrient burden than monotocous species. Data from monotocous species are required to identify differences between humans and the polytocous, commonly-used laboratory animal species to provide firm information for translation to humans. Studies in nonhuman primates have particular strengths concerning the production of translational data. We have developed a well-established nonhuman IUGR primate model to evaluate the effects of moderate maternal nutrient reduction (MNR) in which baboon mothers were fed 70% of the global diet eaten by controls fed *ad libitum* during pregnancy and lactation (10–15). At birth, MNR offspring were IUGR weighing ~89% of control offspring (16). This degree of MNR was associated with offspring dysregulation in cardiac structure with extracellular

fibrosis, altered miRNA expression, and changed lipid metabolism at the cardiac structural and molecular level (13). Even when fed a regular diet after weaning, IUGR offspring of MNR mothers showed myocardial remodeling and impaired cardiac left (LV) and right ventricle (RV) physiological function in early adulthood (5.7 years, human equivalent approximately 25 years old). MNR offspring show established early adult cardiac dysfunction, impaired diastolic and systolic cardiac function (11,14), resembling changes reported in human IUGR (17,18). The dysfunction is similar to human cardiac failure with preserved ejection fraction. Notwithstanding the strong association between poor maternal nutrition and adverse fetal and life-course cardiac programming, direct and causal effects on fetal heart mitochondrial biology remain uninvestigated (19,20). Disturbance of the energy transformation process is a prime feature of heart failure in subjects with cardiomyopathy (20,21).

In this study, the innovation is to potentially explain postnatal cardiovascular health with fetal cardiac metabolism by characterizing the impact of MNR on fetal left ventricular myocardial mitochondrial function in near term fetuses, thereby providing a mechanistic framework for our findings of cardiac dysfunction and premature cardiac aging in young adult, 5.7years old MNR baboons (11,14). We hypothesized that moderate 30% global MNR during fetal development impairs fetal cardiac mitochondrial metabolism, decreasing cardiac mitochondrial reserve capacity, thereby affecting the cardiac metabolic ability to overcome postnatal life's high demands and contribute to the compromised cardiovascular function found in older MNR offspring. To test this hypothesis, we investigated mitochondrial and metabolic markers in control and MNR fetuses at 0.9 gestation (0.9G) and determine sex-specific fetal mitochondrial remodelling resulting from MNR.

2 Materials and Methods

2.1 Detailed *in vivo* procedures

2.1.1 Animal care and maintenance

All animal procedures, including pain relief, were approved by the Animal Care and Use Committees of the Texas Biomedical Research Institute and the University of Texas Health Science Center at San Antonio, TX (no. 1134PC), and were conducted in Association for Assessment and Accreditation of Laboratory Animal Care-approved facilities and NIH Guide for the Care and Use of Laboratory Animals.

As previously described (22), maternal morphometric determinations were made before pregnancy to guarantee the consistency of weight and general morphometrics in animals used in the present study. Non-pregnant outbred female baboons (*Papio* spp.) of the similar morphometric phenotype were selected for the study. Animals were housed at the Southwest National Primate Research Center at the Texas Biomedical Research Institute (TBRI) in Association for Assessment and Accreditation of Laboratory Animal Care (AAALAC)-approved facilities. Groups up to 16 female baboons were initially housed with a vasectomized male to establish a stable social group in outdoor gang cages, thereby providing full social and physical activity.

Each outdoor concrete gang cage was covered with a roof and had open sides that allowed exposure to normal lighting. Each cage holds 10-16 females and had a floor area of 21 x 37 m, being about 3.5 m high. The enrichment inside the cages included nylon bones (Nylabone, Neptune, New Jersey, USA), rubber Kong toys (Kong Company, Golden, Colorado, USA), and plastic Jolly Balls (Horseman's Pride, Inc., Ravenna, Ohio, USA). A 0.6 m-wide platform built from expanded metal grating was placed at the height of 1.7 m and ran the entire length of the cage. A similar perch was built at the front of the cage, running the entire cage's length. Tube perches were present at the back in the corner of each cage. Each cage

had an exit into a chute 0.6 m wide by 1 m high positioned along the side of each set of cages. A fine mesh was placed on the side of the chute adjacent to the other group cages between groups of animals as they passed along the chute to the individual feeding cages. The two chutes merged and passed over a scale and into individual feeding cages, which were 0.6 by 0.9 m in floor area and 0.69 m high. All metal components were made of galvanized steel. Before pregnancy, animals were trained to be fed in individual cages. Briefly, at feeding time, all baboons passed along a chute into individual feeding cages. Once in the individual cages, they were fed with the designated amount of normal primate chow (Purina Monkey Diet 5038, Purina, St. Louis, Missouri, USA).

Each baboon's weight was obtained while crossing an electronic scale (GSE 665; GSE Scale Systems, Milwaukee, Wisconsin, USA). A commercial software application designed to capture weight data was modified to record 50 individual measurements over 3 seconds. If the weight measurement's standard deviation was greater than 0.01 kg of the mean weight, the weight was automatically discarded, and the weighing procedure was re-initiated.

2.1.2 Animal study groups

All female baboons were observed twice a day for well-being and three times a week for turgescence (sex skin swelling) and signs of vaginal bleeding to assess their reproductive cycle and enable timing of pregnancy (22). After a 30-day period of adaptation to the feeding system, a fertile male was introduced into each breeding cage. Pregnancy was dated initially by following the changes in the swelling of the sex skin and confirmed at 30 days of gestation by ultrasonography. On day 30 of pregnancy (term ~ 183 days gestation), twenty-four female baboons were randomly assigned to eat standard primate chow ad libitum (control diet) or to receive 70% of the average daily amount of feed eaten by the female control baboons (MNR group) on a body weight-adjusted basis at same gestational age (12 baboons/dietary group, 6

male control fetuses – C-M, 6 female control fetuses – C-F, 6 MNR male fetuses – MNR-M, and 6 MNR female fetuses – MNR-F). Animals remained in these groups until cesarean section at 165 days gestation (0.9 gestation, see Figure 1 for study timeline). Each fetus from a singleton pregnant female baboon is considered an experimental unit; in some cases, the pregnant female baboon was also assumed as the experimental unit when maternal data is presented.

Food was provided once a day as Purina Monkey Diet 5038, standard biscuits. The biscuit is described as a "complete life-cycle diet for all Old-World Primates" and contains stabilized vitamin C as well as all other required vitamins. The basic composition includes crude protein (≥ 15%), crude fat (≥ 5%), crude fiber (≤ 6%), ash (≤ 5%) and added minerals (≤ 3%) (22).

At the beginning of the feeding period, between 7-9 h or 11-13 h, each baboon received 60 biscuits in the feeding tray at the individual feeding cage. After the baboon had returned to the group cage at the end of the 2 h feeding period, the remaining biscuits in the tray and on the floor of the cage were counted and weighted. Following confirmation of pregnancy, food intake was recorded in 8 female baboons fed *ad libitum* and was calculated as 50.61 ± 3.61 kcal/kg of body weight per day. Before the start of the controlled diet, baboons were fed the same diet without a biscuit limit. Water was continuously available in the feeding cages via individual waterers (Lixit, Napa, California, USA) and at several locations in the group housing. Food consumption of animals, their weights, and health status were recorded daily. This feeding system allowed us to manipulate and monitor food intake in a controlled fashion while still maintaining female baboons in group housing instead of individual cages, thereby permitting regular social and physical activity. More details of housing and environmental enrichment have been previously published (22).

2.1.3 Cesarean section, fetal and maternal morphometry, and blood sampling

Animal feeding and cesarean sections were performed at specific times to avoid circadian variations between animals. Mothers were fasted from their last feeding time in the day before, until the cesarean section at 8 a.m. the next day, around 18 h (22).

Cesarean section and fetal necropsy were performed under isoflurane anesthesia (2%, 2 L/min oxygen, tracheal intubation) following tranquilization with ketamine hydrochloride (10 mg/kg intramuscularly injection) at 165 days of gestation (0.9 of gestation) using standard sterile techniques as previously described. Following hysterotomy, the umbilical cord was identified and used for fetal exsanguination with maternal and fetal baboon under general anesthesia as approved by the American Veterinary Medical Association Panel on Euthanasia (22). Fetal hearts were collected and dissected into their four chambers. Cardiac samples were taken from the free wall of the left cardiac ventricle that was cut transversely in at least four pieces. Some pieces were flash-frozen and stored at – 80ºC until analyses, and one piece was fixed for histological analyses. Heparinized blood samples from the fetal umbilical vein and maternal uterine vein were obtained at cesarean section. Postoperatively mothers were placed in individual cages and watched until they were upright under their power and returned to their group cage at two weeks postoperatively (22). Maternal analgesia was administered for 3 days (buprenorphine hydrochloride intramuscularly injection; Hospira, Inc., Lake Forest, IL, USA; 0.015 mg/kg/day (23). Cesarean sections were evenly spread throughout the year and took place in the morning period, usually between 8 - 12 h. A fully certified M.D. or D.V.M. performed surgical procedures, and postsurgical care was prescribed and monitored by an accredited veterinarian.

2.1.4 Biochemical analyses

Within 1 h of collection, clotted blood was centrifuged at 10,000 g for 10 min and the serum

was removed within 1 h of collection. Biochemical determinations of glucose, blood urea nitrogen (BUN), creatinine, total protein, albumin, and globulin were made in serum using a Beckman Synchron CX5CE Analyzer (Beckman Coulter, Irving, Texas, USA) by a certificated laboratory.

Heparinised plasma samples (0.1 ml) were deproteinized with 0.1 ml of 1.5 M $HClO_4$ and neutralized with 0.05 ml of 2 M K_2CO_3. The solution was centrifuged at 12,000 g at 4°C for 1 min, and the supernatant was used for analyses. Amino acids were determined by HPLC involving pre-column derivatisation with o-phthaldialdehyde, as previously described in detail (24). All amino acids were quantified using appropriate standards (Sigma-Aldrich, St. Louis, Missouri, USA) using Millenium-32 Software (Waters, Milford, Massachusetts, USA).

2.2. Analysis of mtDNA copy number by quantitative real-time PCR

Total DNA was extracted from ~20 mg of cardiac left ventricle tissue using the QIAamp DNA mini-kit (#50951304 Qiagen, Düsseldorf, Germany), following the manufacturer's instructions and the protocol previously described (25). Briefly, the tissue was cut into small pieces and lysed with proteinase K in buffer ATL (tissue lysis buffer for use in purification of nucleic acids) provided by the kit. When the tissue was lysed entirely, buffer AL (tissue lysis buffer containing guanidine salts and detergent) and ethanol 96% were added. The mixture was applied to the QIAamp column and centrifuged at 6,000 *xg* for 1 min in Eppendorf 5415R benchtop centrifuge equipped with a FA-45-24-11 rotor (Eppendorf, Hamburg, Germany). After centrifugation, the column was placed in a new collection tube, and the DNA was washed sequentially with buffers AW1 (washing buffer 1) and AW2 (washing buffer 2). Ethanol was completely removed by centrifugation at full speed for 1 min. DNA was eluted with 200 µl Buffer AE and quantified using a Nanodrop 2000 device

(ThermoFisher Scientific, Waltham, Massachusetts, USA).

RT-PCR was performed using the SsoFast Eva Green Supermix (Bio-Rad, Hercules, California, USA), in a CFX96 real time-PCR system (Bio-Rad), with the primers for ND1 (accession code NC_001992.1; sense sequence CCTATGAATCCGAGCAGCGT; antisense sequence GCTGGAGATTGCGATGGGTA) and for B2M (accession code NC_018158.1, sense sequence CAGGGCCCAGGACAGTTAAG; antisense sequence GGGATGGGACTCATTCAGGG) at 500 nM each. Amplification of 25 ng DNA was performed with an initial cycle of 2 min at 98ºC, followed by 40 cycles of 5 sec at 98ºC plus 5 sec at 60ºC. At the end of each cycle, Eva Green fluorescence was recorded to enable for Ct determination. For quality control, melting temperature of the PCR products was determined after amplification by performing melting curves, and no template controls were run.

For absolute quantification and amplification efficiency, standards at known copy numbers were produced by purifying PCR products. After optimizing the annealing temperature, products were amplified for each primer pair using the HotstarTaq Master Mix Kit (#203445 Qiagen). Briefly, 1 µl of a DNA sample was added to a PCR tube containing the HotStar Taq Master Mix and the specific primers and placed in a CFX96 real time-PCR system. The amplification protocol started with an initial activation step of 15 min at 95ºC degrees, followed by 35 cycles of 1 min at 94ºC (denaturation) plus 1 min at 60ºC (annealing), plus 1 min at 72ºC (extension), and a final extension step of 10 min at 72ºC. After amplification, the products were purified using the MiniElute PCR purification kit (#280006 Qiagen) following the manufacturer's instructions. Eluted DNA was quantified in a Nanodrop 2000 device, the copy numbers were adjusted to 5 x 10^9 copies/µl, and tenfold serial dilutions were prepared. mtDNA copy number was determined by the ratio between the absolute amounts of mitochondrial gene *ND1* versus the absolute amount of the *B2M* nuclear gene in each sample, using the CFX96 Manager software (v. 3.0; Bio-Rad).

2.3 Gene expression analysis by PCR array

RNA extraction was performed following the protocol previously described by Cox et al.(26). Briefly, approximately 20 mg transversal section of frozen tissue was cut. The tissue was homogenized in 1 ml Trizol Reagent using a Power General Homogenizer (Omni International, Wilmington, Delaware, USA). Genomic DNA in the sample was sheared by passing the homogenate three times through a 22-gauge needle attached to a 1 ml syringe. The homogenized samples were incubated for 5 min at 25°C. Two hundred µl of chloroform was added to each sample, and the samples were shaken vigorously by hand for 15 s and incubated at 25ºC for 3 min. Samples were then centrifuged at 12,000 *xg* for 15 min at 4ºC. The aqueous phase containing RNA was transferred to a fresh tube, and RNA precipitated by the addition of 0.5 ml of isopropyl alcohol. Samples were incubated for 10 min at 25ºC and then centrifuged at 12,000 *xg* for 10 min at 4ºC. The RNA precipitate was washed with 1 ml of 75% ethanol and centrifuged at 7,500 *xg* for 5 min at 4ºC. After air-drying, the RNA pellet was dissolved in diethylpyrocarbonate (DEPC)-treated ddH_2O. The RNA was quantified spectrophotometrically using Thermo Scientific NanoDrop 2000 spectrophotometer (ThermoFisher Scientific) and stored at −80ºC. The RNA purity and quality were checked by Ultraviolet spectrophotometry by the ratios of A_{260}/A_{280} and A_{260}/A_{230} and electrophoretically by visualization of the ribosomal band integrity for both the 18S and 28S ribosomal RNA. Only RNA samples that demonstrated consistent quality were used.

After RNA preparation, the samples were treated with DNase to eliminate genomic DNA, while extracted RNA was converted to cDNA using the RT^2 First Strand Kit from SuperArray Bioscience Corporation (SA Biosciences, Qiagen, Valencia, California, USA) according to the manufacturer's instructions. Briefly, 1 µg RNA was combined with 2 µL gDNA elimination buffer and brought up to a final volume of 10 µL using RNAse-free H_20.

This mixture was incubated at 42ºC for 5 min, then chilled in ice. Ten µL of RT Cocktail was then added to this mixture and incubated at 42ºC for precisely 15 min followed by 5 min at 95ºC to stop the reaction. Ninety-one µL ddH20 was added to each 20 µL cDNA synthesis reaction and well mixed. The cDNA mixture was stored at -20ºC until used for gene expression profiling.

The RT^2 Profiler polymerase chain reaction (PCR) Array System (SuperArray Bioscience, SA Biosciences, Qiagen), was used to evaluate the different cardiac mitochondrial transcripts between control and MNR fetuses. We used the Human Mitochondrial Energy Metabolism and the Human Mitochondria PCR Pathway Arrays. Real-time PCR detection was carried out per the manufacturer's instructions. The experimental cocktail was prepared by adding 1,350 µL of the SuperArray RT^2 qPCR master mix and 1,248 µL ddH_20 to 102 µL of the diluted cDNA mixture. For real-time PCR detection, 25 µL of this cocktail was added to each well in the 96-well PCR array. The array was then processed on a real-time thermal cycler (Applied Biosystems StepOnePlus, ThermoFisher Scientific, Applied Biosystems) by using the following program: 1 cycle of 10 min at 95ºC followed by 40 cycles of 15 seconds at 95ºC and 1 min at 60ºC. A melting curve program for quality control was immediately performed after the cycling program. SYBR Green fluorescence was detected from each well during the annealing step of each cycle, and values were exported to an Excel template file for analysis. Each PCR array contained 84 transcripts of the corresponding signaling pathway, a set of five housekeeping genes as internal controls, and additional controls for efficiency of reverse transcription, PCR, and the absence of contaminating genomic DNA. Data were normalized with three endogenous controls that did not differ between groups [hypoxanthine phosphoribosyltransferase 1 (*HPRT1*), ribosomal protein L13a (*RPL13A*), and Beta-actin (*ACTB*) and analyzed with the ΔΔCt method (where Ct is threshold cycle) using the PCR Array Data Analysis Web Portal (SA Biosciences).

2.4. Protein analyses by Western Blotting

Protein analyses by Western Blotting was performed following standard protocols (27). A small piece of frozen tissue (≈30 mg) was used for whole tissue protein extraction. All the extraction procedures were performed on ice. Tissue was homogenized in a 20% (w/v) RIPA buffer (150 mM NaCl, 50 mM Tris pH 8.0 (HCl), 0.5% sodium deoxycholate (DOC), 1% IGEPAL (CA-630) and 0.1% sodium dodecyl sulfate (SDS)), supplemented with 5 µl/100 mg (tissue) of protease inhibitors cocktail (P8340, Sigma-Aldrich) and sodium orthovanadate, a phosphatase inhibitor, using an electric homogenizer PowerGen Model 125 (ThermoFisher Scientific, Fisher Scientific). The suspension was kept on ice for 5 min and then centrifuged at 14,000 *xg* for 5 min at 4ºC to remove cellular debris. The pellet was discarded and protein concentration in the supernatant was determined by the Bicinchoninic acid assay (BCA) using the commercial Pierce BCA assay kit protocol (#9981, ThermoFisher Scientific, Fisher Scientific), using bovine serum albumin (BSA type V, Sigma-Aldrich) ranging from 0.25 to 2 mg/ml as standard. The amount of protein was calculated after determining the absorbance of the dye at 545 nm in a Victor X3 plate reader (PerkinElmer, Waltham, Massachusetts, USA). Standards and unknown samples were performed in triplicates. After protein determination, all the proteins were diluted for the same final concentration with RIPA and stored at -80ºC until further use.

Extracted proteins were solubilized to achieve a working concentration of 1mg/ml or 2 mg/ml of protein with Laemmli buffer (62**.**5mM Tris pH 6.8 (HCl), 50% glycerol, 2% SDS, 0.005% bromophenol blue, supplemented with 5%β-mercaptoethanol) and boiled for 5 min in a water bath and then centrifuged at 14,000 *xg* for 5 min to remove cellular debris. Equivalent amounts of total protein (10 µg per lane) were loaded in a 10-20% gradient Tris-HCl polyacrylamide gel as well two different standards for molecular weight estimation and for

monitoring electrophoresis progress, the Precision Plus Protein Dual Color Standards (Bio-Rad) and the SeeBlue Plus2 Pre-Stained Standard (ThermoFisher Scientific, Invitrogen). Electrophoresis was carried at room temperature in a Criterion system (Bio-Rad) using 150 V until the sample buffer (blue) reaches the bottom of the gel (≈ 90 min).

After separation by SDS-PAGE, proteins were electrophoretically transferred in a TransBlot Cell system (Bio-Rad) to a polyvinylidene difluoride (PVDF) membrane previously activated, a constant amperage (0.5 A) during 2 h at 4ºC using a CAPS transfer buffer (10 mM 3-(Cyclohexylamino)-1-propanesulfonic acid pH 11 (NaOH), 10% methanol). Good electrophoretic transfer was indicated by the complete transfer of pre-stained molecular weight markers below 100 kDa and by Ponceau staining. Ponceau results were also used to confirm an equal amount of protein loading and to normalize band density. After Ponceau removal, the membranes were blocked in 5% non-fat milk/PBS overnight at 4ºC with agitation. Before incubation with primary antibodies, the membrane was washed for 10 min in PBS 0.05% Tween-20 (PBS-T). Primary antibodies described in the supplemental table were prepared in 1% non-fat milk/PBS to a final volume of 5 ml and incubated overnight at 4ºC. After incubation with primary antibodies, membranes were washed with PBS-T solution three times, 5 min each, and incubated with the correspondent alkaline phosphatase-conjugated secondary antibodies for 2 h at room temperature with stirring (see Suppl. Table S1 and S2).

For immunodetection, membranes were washed three times for 5 min each with PBS-T, rinsed in PBS to remove any Tween-20, which can be inhibitory to the detection method, dried and incubated with an enhanced chemifluorescence (ECF) system (#RPN5785, GE Healthcare, Little Chalfont, Buckinghamshire, UK) during a maximum of 5 min. Density analysis of bands was carried out with VisionWorks.LS Image Acquisition and Analysis Software (UVP).

Resulting images were analyzed and densities were normalized to Ponceau (28–30). The average value of the control males (C-M) group was assumed as one unit, and the values of each sample were determined proportionally.

2.5. Tissue Immunohistochemistry

Tissue immunohistochemistry was performed by a standard avidin-biotin histochemical technique, as previously described (31), and using the antibodies listed in Table S3. After optimizing the final dilution of the primary antibody that yielded the cleanest immunostaining achievable, all sections were immunostained in the same assay to assure identical conditions. Briefly, fixed tissues sections (5 µm) were deparaffinized with xylene and rehydrated to decrease ethanol grades to water (100, 95, 70, and 50%). Antigen retrieval was performed for 15 min using boiling citrate buffer (0.01 M citrate buffer, pH 6.0). After cooling for 15 min, the section was rinsed for 5 min in potassium PBS (KPBS; 0.04 M K_2HPO_4, 0.01 M KH_2PO_4, 0.154 M NaCl, pH 7.4) and washed for 10 min in a solution of 1.5% H_2O_2/methanol and then for 5 min in KPBS. Sections were placed in diluted (10%) normal serum for 10 min and covered with primary antibody (Table S3) overnight at 4ºC and incubated for 1 h at room temperature with the appropriate biotinylated secondary antibody (1:1,000; Vector Laboratories (Burlingame, California, USA)): goat anti-rabbit (BA-1000) and horse anti-mouse (BA-2000). Negative controls were also run in the absence of the primary antibody but in normal serum. Three slides per animal were analyzed, and six pictures/slide per section were randomly taken and analyzed with ImageJ software (National Institutes of Health, New York, USA) for the fraction (area immunostained/area of the field of interest x 100%) and the density (arbitrary density units).

2.6 Enzymatic activity of mitochondrial proteins

Mitochondrial respiratory chain activities were determined in LV tissue homogenates according to previously published methods.

The activity of complex I was measured by the method described by Long (32) with some modifications. Briefly, 30 μg of tissue homogenate was resuspended in reaction buffer containing 25 mM KH_2PO_4 pH 7.5, 5 mM $MgCl_2$, 300 μM KCN, 4 μM antimycin A, 3 mg/mL BSA, 60 μM coenzyme Q1, 160 μM 2,6-dichlorophenolindophenol (DCPIP). Complex I activity was determined by the measurement of DCPIP absorbance at 600 nm, 37ºC, in a Victor X3 plate reader, upon the addition of 100 μM freshly-prepared NADH. Enzymatic activity was determined through the mean of slopes obtained during the linear phase of duplicates. Specific mitochondrial complex I activity was computed as the difference among basal activity in the absence or presence of 10 μM rotenone, a specific inhibitor of complex I. Normalization was performed to the protein concentration and an $\varepsilon 600 = 19.1\ mM^{-1}.cm^{-1}$. Complex I activity is expressed as nmol DCPIP/min/mg protein.

The activity of complex II/III was analyzed as defined by Tisdale (33), with minor modifications. Concisely, 100 μg of tissue homogenate was pre-incubated in 200 μL of phosphate buffer (166 mM KH_2PO_4/K_2HPO_4, pH 7.4) supplemented with 100 mM KCN and 500 mM sodium succinate for 5 min at 37°C. The reaction was initiated by adding 120 μL of phosphate buffer supplemented with 2 mM oxidized cytochrome c (cyt c ox) plus 15 mM EDTA-dipotassium. Complex II/III activity was determined by following the reduction of cyt c ox (increased absorbance at 550 nm), using a Victor X3 plate reader. Enzyme activity was measured through the mean of slopes obtained during the linear phase for duplicates. Mitochondrial complex II/III specific activity was calculated as the difference between basal activity in the absence or presence of 4 mM antimycin A (a specific inhibitor of complex III). Normalization was performed to the protein concentration and an $\varepsilon 550 = 18.5\ mM^{-1}.cm^{-1}$.

Results are expressed as nmol cyt c ox/min/mg protein.

The activity of complex III was analyzed according to Luo (34), with minor adaptations. Briefly, 100 μg of tissue homogenate was suspended in reaction buffer containing 25 mM KH_2PO_4 pH 7.5, 4 μM rotenone, 0.025% Tween-20, 100 μM fresh decylubiquinone solution at 37°C. Enzymatic activity was measured as an increase in absorbance of cyt c ox at 550 nm, upon addition of 75 μM cyt c ox in a VICTOR X3 plate reader. Enzyme activity was determined through the mean of slopes obtained during the linear phase for duplicates. For determination of the specific complex III activity, 2.5 mM antimycin A (complex III specific inhibitor) was used, and the difference between basal activity in the absence or presence of antimycin A was determined. Normalization was performed to the protein concentration and an $\varepsilon 550 = 18.5\ mM^{-1}.cm^{-1}$. Results were expressed as nmol cyt cox min/mg protein.

The activity of complex IV was measured by adapting the method described by Brautigan (35). Briefly, 25 μg of tissue homogenate was suspended in reaction buffer containing 50 mM KH_2PO_4 pH 7.0, 4 μM antimycin A, 0.05% n-dodecyl-β-D-maltoside at 37°C. Enzymatic activity was followed in a VICTOR X3 plate reader as a decrease in absorbance of reduced cytochrome c (cyt c red) at 550 nm, upon addition of 57 μM freshly-prepared cyt c red. Enzyme activity was calculated through the mean of slopes obtained during the linear phase for duplicates. Cyanide, a complex IV-specific inhibitor, was used to determine mitochondrial complex IV specific activity, that was calculated as the difference between basal activity in the absence or presence of 10 mM of KCN. Normalization was performed to the protein concentration and an $\varepsilon 550 = 18.5\ mM^{-1}.cm^{-1}$. Activity is expressed as nmol cyt c red min/mg protein.

The activity of citrate synthase was analyzed by adapting the method described by Core (36). Concisely, 25 μg of tissue homogenate was suspended in a reaction buffer containing 100 mM Tris pH 8.0 plus 200 μM Acetyl-CoA, 200 μM 5,5-dithiobis-2-nitrobenzoic acid at 37°

C. Enzymatic activity was measured by following the increase in absorbance (412 nm) upon adding 100 μM freshly-prepared oxaloacetate in a VICTOR X3 plate reader 37°C. Enzyme activity was calculated through the mean of slopes obtained during the linear phase for duplicates. Specific citrate synthase activity was determined by subtracting the basal activity in the presence of 0.1% Triton-X100. Normalization was performed to the protein concentration and an ε412 = 13.6 mM−1·cm−1. Enzyme activity is expressed as nmol of oxaloacetate min/mg protein.

2.7. Analysis of adenine nucleotides by HPLC

Adenine nucleotide levels were measured according to the method described by Santos et al. (37). Briefly, tissue was homogenized in 0.3 M perchloric acid (equal parts of PBS and 0.6 M perchloric acid) and kept for 5 min on ice. The acid homogenates were centrifuged at 14,000 *xg* for 10 min and at 4°C. Supernatants were brought to neutral pH with 3 M KOH in 1.5 mM Tris, centrifuged at 14,000 *xg*, for 10 min at 4ºC, and stored at -80ºC. Then, the supernatants were assayed for ATP, ADP, and AMP by separation in a reverse-phase high-performance liquid chromatography (HPLC), as described by Stocchi and collaborators (38). The chromatographic apparatus used was a Beckman-System Gold (Beckman Instruments, Fullerton, California, USA), consisting of a binary pump (model 126) and a variable UV detector (model 166), controlled by a computer. The detection wavelength was 254 nm, and the column used was a LiChrospher 100 RP-18 (5 μm) from Merck. An isocratic elution with 100 mmol/l phosphate buffer (KH_2PO_4; pH 6.5) and 1.0% methanol was performed with a flow rate of 1 ml/min. The required time for each analysis was 6 min. Peak identity was determined by the retention time compared with standards. A concentration standard curve was used to determine the concentrations of nucleotides and metabolites. Concentration of adenylates was expressed as nmol/mg of protein and adenylate energy charge (AEC) was

determined according to the formula (ATP + 1/2 ADP) /(ATP + ADP + AMP).

2.8. Oxidative stress evaluation

Oxidative stress was evaluated by measuring malondialdehyde (MDA) levels and oxidized glutathione (GSSG), while the antioxidant capacity was evaluated by determination of the contents on reduced glutathione (GSH) and vitamin E. The enzymatic activity of glutathione peroxidase (Gl-Px) and glutathione reductase (Gl-Red) was also determined.

Lipid peroxidation was given by the fluorimetric measurement of MDA adducts separated by high-performance liquid chromatography (HPLC; Gilson, Lewis Center, Ohio, USA) with the ClinRep complete kit (RECIPE, Munich, Germany), at an excitation wavelength of 515 nm and an emission wavelength of 553 nm (FP-2020/2025, Jasco, Tokyo, Japan), according to the method described by Draper et al. (39). Results are expressed as mM of MDA.

Reduced and oxidized glutathione (GSH and GSSG) were evaluated according to Tsao et al. (40), with minor adaptations, by using a commercial kit (Immunodiagnostik AG, Bensheim, Germany) and an HPLC system (Gilson) with fluorimetric detection (excitation at 385 nm and emission at 515 nm; FP-2020/2025, Jasco). Results are expressed as mM of GSH and mM of GSSG.

Vitamin E present in tissue was extracted in *n*-hexane (Merck) and quantified by reverse-phase HPLC (Gilson), using an analytic column Spherisorb S10w (250 x 4.6 mm), eluted at 1.5 ml/min with n-hexane modified with 0.9% of methanol (Merck) and spectrophotometric detection at 287 nm. Results are expressed as mM vitamin E.

The activity of glutathione peroxidase (Gl-Px) was evaluated spectrophotometrically as described by Palia et al. (41) with minor adaptations by using *tert*-butylperoxide (Sigma-Aldrich) as substrate. The formation of oxidized glutathione was given by quantifying the oxidation of NADPH (Sigma-Aldrich) to $NADP^+$ at 340 nm in a thermostatized

spectrophotometer (UVIKON 933 double bean UV/Visible spectrophotometer, Kontron instruments, Milan, Italy). Results are expressed in international units of enzyme per liter (U/l).

Glutathione reductase (Gl-Red) activity was evaluated according to Goldberg et al. (42), with some modifications, by following the reduction of GSSG (Sigma) to GSH through the quantification of NADPH (Sigma) oxidation at 37ºC at 340 nm, in a thermostatized spectrophotometer (UVIKON 933 double bean UV/Visible spectrophotometer). Results are expressed in international units of enzyme per liter (U/l).

2.9. Transmission Electron Microscopy

Samples were processed by the certificated Electron Microscopy Laboratory at the Department of Pathology at UTHSCSA using the Transmission Electron Microscope (TEM) JEOL 1230 (JEOL, Peabody, Massachusetts, USA). After the primary fixation at the cesarean section samples were rinsed with PBS and post-fixed for 30 min with 1% buffered osmium tetroxide, according to Malhotra (43). Samples were dehydrated in increasing grades of ethanol (70, 95 and 100%) and placed in propylene oxide for 20 min. Then, samples were infiltrated with a mixture 1:1 of propylene oxide/resin followed by 30 min in 100% resin under 25 psi vacuum. Longitudinal pieces were flat-embedding in molds and filled to the top with resin. The resin was polymerized at 80ºC overnight. Tissues were sectioned in 0.5-1 μm sections and stained with T-blue for 10 seconds on a hot plate. Sections quality was checked using a light microscope. Cardiac sections were either left unstained or stained with uranyl acetate followed by Reynold's Lead Citrate stain for 20 s. A series of 5-6 images at 3,300x magnification demonstrating areas of interest were obtained.

2.10. Data analyses and statistics

The hypothesis to be tested in this study is that MNR by 30% during gestation affects cardiac mitochondria heritage and function in the progeny. A secondary question is whether these effects are dependent on fetal sex.

In this study, each pregnant female baboon and the correspondent fetus was considered as an experimental unit. Outbred pregnant female baboons were randomly assigned to control or MNR groups. Whenever possible, we performed a blind assessment of the diet effects and blind determination of the parameters to be statistically analyzed. Data are expressed as mean ± standard error of the mean. Normality and homoscedasticity were assessed by the Kolmogorov-Smirnov normality test and Levene variance homogeneity test. Since the variables do not comply with the assumptions required for parametric tests, namely lack of normality and homoscedasticity, the equivalent non-parametric Mann-Whitney U test was employed. Statistical tests were performed considering a significance level of $\alpha=0.05$. Statistical analyses were performed using SPSS version 17.0 (IBM corporation, Armonk, New York, USA) with significance set at $P<0.05$ by two independent investigators to minimize the influence of natural human biases and corroboration. Graphical representations were obtained using GraphPad Prism version 8.0 (GraphPad Software, San Diego, California, USA).

3 Results

3.1 Pregnancy-related morphometric and blood biochemistry changes

Non-pregnant outbred female baboons (Papio spp.) of the similar morphometric phenotype were studied in this nutritional intervention and randomly assigned to the Control (C) or MNR group, resulting in groups with similar pre-pregnancy body weight (16.3±0.7vs16.6±1.2 kg, mean+SEM, $p<0.05$, Table S4). At 0.9G, control mothers weighed more than MNR mothers, controls gained 12.8±2.1% of their body weight during pregnancy while MNR mothers lost weight (-3.1±3.0%). Maternal weight loss was greater in MNR mothers carrying male than female fetuses (MNR-M vs., MNR-F, -7.1±3.7vs1.8±4.2%). Placental weight was also decreased with MNR-M fetuses.

Aspartate aminotransferase (AST) increased approximately 72% in MNR mothers (Table S5), while creatine phosphokinase (CPK) increased by 27.2%. Remarkably, circulating enzyme levels were significantly higher in control mothers carrying male fetuses (Table S5).

Cortisol levels agreed with previously published data (31,44) (Figure S1A) being increased in MNR mothers and with a more pronounced effect in MNR mothers carrying male fetuses. No difference was observed in glucose levels between control and MNR fetuses when sexes were either combined or separated (Figure S1B). Only MNR-M mothers showed an increase in glucose levels compared with C-M mothers. MNR reduced fetal insulin in male fetuses, while sex differences were observed for MNR-M vs. MNR-F for maternal and fetal samples, with MNR-F presenting higher insulin levels than MNR-M (Figure S1C).

3.2 Cardiac left ventricular mitochondrial DNA copy number

To evaluate MNR effects on fetal LV cardiac mitochondrial capacity, we measured mtDNA copy number by qRT-PCR. mtDNA copy number was calculated by determining the

ratio between the absolute amounts of mitochondrial gene ND1versus the absolute amount of the B2M nuclear gene in each sample (Figure 2A). The average mtDNA in control fetuses was 714.5±84.9 copies per nucleus. Increased mtDNA was measured in MNR-F (1351±160) but not in MNR-M (836±117) (Figure 2A).

3.3 Mitochondrial transcript changes in the fetal cardiac left ventricular myocardium

Human Mitochondrial Energy Metabolism and the Human Mitochondria Pathway Arrays were used for fetal LV RNA expression profiling. Summarized data are shown in Figure2 (see also Table S6). The heat maps in Figure S2 and S3 provide a graphical summary representation of RNA expression fold regulation in response to the maternal diet in the fetal LV (Figure S2) and sex-dependent differences in control fetuses (Figure S3). Our results support the general conclusion that MNR increased fetal cardiac mitochondrial transcripts, more noticeable in MNR-F fetuses. When sexes were combined (Figure 2B) twenty-one transcripts were differentially expressed between C and MNR fetuses, with 85% of significant differences being upregulation in MNR. Most upregulated transcripts encoded subunits of the mitochondrial oxidative phosphorylation system (OXPHOS), three complex I subunits: *NDUFB6, NDUFB7,* and *NDUFV1*; two complex II subunits: *SDHC* and *SDHD*; one complex III subunits: *UQCR11*; and five ATP synthase subunits: *ATP5A1, ATP5B, ATP5F1, ATP5G3* and *ATP5L*. Besides, transcripts for regulators and mediators of mitochondrial molecular transport, namely small-molecule transporters (*SLC25A24* and *SLC25A27*); one member of the inner membrane translocation system (*TOMM34*); mitochondrial outer membrane import complex protein 2 (*MTX2*); a mediator of mitochondrial fusion (*MFN2*); heat shock protein 1 (*HSPD1*) and pro-apoptotic factor and autophagy mediator (*BNIP3*) were also upregulated in MNR fetuses. Finally, two members related to the apoptosis pathway (*PMAIP1* and *TP53*) and one related to cholesterol

transporter (*TSPO*) were downregulated.

Maternal diet-induced transcript differences were also observed within the same sex (Figures 2C, 2D). Multiple components of the mitochondrial respiratory chain were increased in MNR-M fetuses, including two complex I subunits (*NDUFA1*, *NDUFS6*), one complex II subunit (*SDHD*), one complex III subunit (*UQCR11*) and two ATP synthase subunits (*ATP5A1*, *ATP5G3*). Increased transcripts also included *SLC25A24*, *MTX2*, *HSPD1*, *BNIP3*, and one member of the outer membrane translocase complex (*TOMM70A*) (Figure 2D).

Comparing MNR-F and C-F fetuses, increased abundance of two mitochondrial respiratory chain transcripts, *NDUFB6* and *NDUFB7* and decreased transcripts related to cell death pathways, e.g. pro-apoptotic Bcl-2-binding component 3 (*BBC3*), *BID*, a mediator of mitochondrial damage induced by caspase-8, *PMAIP1*, which is related to the activation of caspases and apoptosis, *TP53*, *TIMM22*, an inner mitochondrial membrane protein translocase and *TSPO*, involved in cholesterol homeostasis, were observed (Figure 2C).

Significant sexual dimorphism was present in the cardiac mitochondrial-related gene expression profile in control fetuses (C-F vs C-M, Figure 2E). Female fetuses presented a higher content of transcripts for *NDUFB5* and *NDUFC1*, complex I subunits; *COX6C*, a cytochrome c oxidase subunit; *MSTO1*, a regulator of mitochondrial morphology and distribution; *SLC25A3*, *SLC25A4*, *SLC25A20*, regulators and mediators of mitochondrial molecular transport, and *SOD1*, encoding for cytosolic superoxide dismutase. However, sex differences were attenuated by MNR, with only one transcript being different between sexes for this group, complex I subunit *NDUFB7* (MNR-F vs MNR-M, Figure 2F).

3.4 Left ventricle cardiac mitochondrial protein content

To assess whether transcriptional changes were translated into altered protein production, we performed Western blot (WB) and immunohistochemical analyses. In

agreement with the observed increase in transcripts related to OXPHOS, WB analysis (Figure 3) revealed an increase in cardiac mitochondrial respiratory chain proteins in MNR fetuses, including complex I subunit NDUFB8, complex II subunit UQCRC1, and cytochrome c (CYT C), a major factor in cell death regulation. Protein for the outer membrane channel VDAC1 (a structural protein), and cyclophilin D (CYC D), a modulator of the mitochondrial permeability transition pore, increased in MNR fetuses. However, the most significant increase was observed for the mitochondrial fission 1 protein (Fis1, 0.89±0.08vs1.33±0.16 A.U.).

Maternal diet-induced cardiac protein expression differences were also observed within the same sex. In summary, from the 14 mitochondrial proteins tested, 11 increased in MNR-M vs C-M fetuses and only two in MNR-F vs C-F fetuses (COX6C and Fis1), denoting a more significant effect of MNR on male fetuses at the protein level. Pronounced sexual dimorphism was present in control fetuses, with female fetuses displaying a higher content in nine mitochondrial proteins (C-M vs C-F, UQCRC1, UQCRC2, MT-CO2, ATP5A1, ATP5A, CYT C, VDAC, CYC D, and CAT). Interestingly, MNR attenuated this sex-related difference decreasing to four the number of mitochondrial proteins whose expression differed between sexes in MNR fetuses (MNR-M vs MNR-F, NDUFB8, COX6C, CAT, and FIS1).

Tissue content of mitochondrial proteins (COX6C, CYC1, MFN2, and TIMM9A) was further measured by immunohistochemistry (Figure 4). In agreement with the overall mitochondrial proteins pattern, mitofusin 2 (MFN2), which participates in mitochondrial fusion, was increased in the LV of MNR female fetuses (C-F vs. MNR-F, Figure 4A, F). Although under control diet conditions, female fetuses had decreased content of MFN2 compared to male fetuses (C-M vs. C-F, % fraction stained and density (AU)), Figure 4A, E), there were no other differences between diets or sexes in the quantitative immunohistochemistry of CYC1, COX6C or TIMM9A in LV cardiac tissue (Figure 4B-D).

3.5 Activity of mitochondrial proteins and tissue adenine nucleotide content in the fetal cardiac left ventricle

Citrate synthase (CS), a mitochondrial matrix enzyme commonly used as a mitochondrial marker, was decreased in MNR (C 1798.7±145.9vsMNR 1011.4±189.9 nmol/min/mg protein, Table 1), with female fetuses demonstrating a more significant effect, reaching a difference of 51% between C-F and MNR-F (1527±187vs741±98 nmol/min/mg protein). CS activity was also sex-dependent in control fetuses, being 26% lower in C-F than C-M. Considering that the decrease in CS activity may reflect inherent mitochondrial dysfunction caused by MNR, we calculated the activities of mitochondrial respiratory chain complexes before and after normalization with CS (Table 1).

Mitochondrial complex I, complex II/III, and complex IV activities were decreased in MNR fetuses, with complex II/III being the most severely affected, decreasing 80% in activity (Table 1). In MNR-M fetuses, complex I and complex II/III activities were decreased, with complex II/III activity decreasing 77%. Conversely, complex IV activity increased 3.5 fold in male MNR fetuses. We found a similar pattern in female fetuses with MNR inducing an 84% decrease in complex II/III activity and a 10.4-fold increase in complex IV activity. Sexual dimorphism was present in control fetuses, with female fetuses presenting higher complex III and lower II/III activity. MNR abolished these sex-related differences (Table 1).

After normalization for CS activity, an effect of MNR on respiratory chain activities persisted with a significant decrease in complex II/III and an increase in complex IV activity in both sexes. However, only complex III activity remained different between sexes in control fetuses (C-M vs. C-F, 0.45±0.04vs1.18±0.32).

We assessed possible differences in adenine nucleotide levels between control and

MNR fetuses (Table 1). Although mitochondrial ADP and AMP levels were similar in C and MNR fetuses, ATP decreased by 73% in MNR fetuses. Notably, this difference mainly resulted from MNR-M fetuses. Diet-induced reduction of adenylate energy charge was also observed for male fetuses. Once again, sex dimorphism was noted in control fetuses, with males exhibiting 5.2-fold higher ATP content and an increase of 2.2-fold in adenylate energy charge than females.

3.6 Cardiac left ventricle redox state

We evaluated cardiac LV oxidative stress with the lipid peroxidation marker malondialdehyde (MDA) and measured antioxidant enzymes and molecules, including activity of glutathione peroxidase (Gl-Px), glutathione reductase (Gl-Red), and quantification of reduced and oxidized glutathione (GSH and GSSG), and vitamin E (Table 2). There was a 40% increase in MDA in MNR fetuses, which was significantly higher in males (60% increase). GSH quantification also showed sex-related differences in MNR. MNR-F fetuses showed a 2.4-fold greater GSH concentration than MNR-M.

3.7 Cardiac left ventricle mitochondrial morphology

We used transmission electron microscopy (TEM) to analyze changes in mitochondrial morphology and overall organization (Figure 5). MNR markedly altered mitochondrial ultrastructure, especially the number and shape of the cristae. Abundant cristae were found in mitochondria from control fetal cardiac LV of both sexes, whereas in MNR fetal LV samples, both sexes displayed mitochondria with sparse, disarranged, and distorted cristae, partial or total cristolysis, and electron-lucent matrix. Maternal diet-induced mitochondrial morphological alterations were more prominent in MNR-M fetuses, presenting defective mitochondria with few cristae, some resembling an onion-like structure, characterized by

multi-layered inner membranes suggesting concentric spherical rings (arrow in Figure 5). Multiple panels in the NMR group of images show several double-membrane structures, resembling autophagic vacuoles.

4 Discussion

Suitable healthy human fetal tissues, uncomplicated by confounding pathology, are very rarely, if ever, available to investigate prenatal mitochondrial bioenergetics. Human fetal cardiac samples are obtained at autopsy in pathological situations after a variable period without a functioning circulation. A further limitation of human studies is the lack of homogenous subjects and ensure that the challenges introduced are very carefully controlled. To overcome these limitations, we have developed and characterized a baboon, nonhuman primate model of IUGR that shows an overall offspring cardiac phenotype similar to that described in human IUGR (11,14,45) in order to investigate the nature of the specific in utero nutritional-induced alterations in fetal cardiac mitochondrial function that could explain the greater susceptibility of IUGR offspring to CVD later in life.

We show here for the first time that MNR adversely impacts fetal cardiac LV mitochondria in a sex-dependent fashion. MNR increased 50% of the fetal LV mtDNA content, which was more pronounced in female fetuses, in which a two-fold increase in mtDNA was observed. Transcription of key mitochondrial genes involved in mitochondrial dynamics and oxidative phosphorylation was up-regulated in NMR fetuses, resulting in increased content of several mitochondrial proteins, namely components of the mitochondrial respiratory chain (NDUFB8, UQCRC1, and cytochrome c) and ATP synthase. However, the activity of OXPHOS enzymes was significantly decreased in MNR fetuses (complex I and complex II/III activities), possibly contributing to the 73% decreased ATP content and increased oxidative stress in the cardiac left ventricle tissues, as seen by increased lipid peroxidation marker, MDA. Microscopy of the fetal cardiac left ventricles reflected the mitochondrial

dysmorphology induced by MNR, revealing mitochondria with sparse and disarranged cristae.

In our baboon model, we observed a fetal brain-to-liver weight ratio of 3.31 for control fetuses and 4.18 for MNR fetuses was determined, supporting the view that fetal IUGR was present in the MNR fetuses. Our previous study demonstrated that 5.7 years old offspring of MNR mothers exhibited myocardial remodeling with reduced systolic and diastolic function, as detected by magnetic resonance imaging. Of importance, when compared with aged baboons (mean age 15.9 years – normal baboon life span 23 years), levels of dysfunction similar to a premature ageing cardiac phenotype were observed (14). Both LV and RV dysfunction, with reduced wall thickness, reduced filling rates, prolonged diastolic filling times, reduced ejection fraction, reduced 3D sphericity indices, and decreased cardiac output with lower stroke volume, was determined (14). Similar changes have been shown in IUGR human fetuses and children (46–52). In humans, IUGR is significantly associated with preterm birth. Human cardiac magnetic resonance imaging studies reported altered cardiac postnatal growth after preterm birth. Preterm born babies had increased left ventricular mass at 3 months postnatal age, and exhibited at 20 to 39 years increase in LV free wall mass, abnormal LV wall geometry, and impaired LV systolic/diastolic function relative to term-born subjects (53). Bensley et al showed an inverse relationship between the percentage of proliferating cardiac cells and gestational age, with a reduction in the proliferation of cardiomyocytes in the hearts of the preterm infants. In contrast, cardiomyocyte proliferation was still ongoing in age-matched control fetuses. This reduced cardiomyocyte proliferation in preterm infants may adversely impact the final number of cardiomyocytes which may reduce cardiac functional reserve and impair the reparative capacity of the myocardium (54).

Analogous results were described in animal models such as rodents and sheep (52,55–60), suggesting cross-species similarity for IUGR cardiac effects.

Here, we sought to identify cardiac LV mitochondrial phenotype changes in MNR-induced IUGR fetuses of both sexes.

Disruption of mitochondrial function will have more significant effects on organs with higher metabolic demands and/or limited regenerative capacity, such as the heart. Impairment of mitochondrial oxidative phosphorylation and fatty acid oxidation have been measured in dilated cardiomyopathies in young infants (61,62). Effects on cardiac function of MNR programming are likely exacerbated during the transition from pre-natal to postnatal life, a critical period in which mitochondrial ATP synthesis is determinant (63).

We observed a significant increase in mtDNA copy number in MNR fetuses, possibly a compensatory response to decreased glucose influx into MNR fetal cardiac tissue due to the decreased insulin signaling. Increased circulating mtDNA levels was also found in diabetic patients and fetal blood of IUGR and premature pregnancies (64–66). We demonstrate that fetal undernutrition up-regulates several relevant mitochondrial transcripts and proteins in the fetal baboon cardiac LV, suggesting an increased mitochondrial capacity. However, the measured activity of mitochondrial proteins is significantly decreased in MNR fetuses, accompanied by 73% decreased ATP content and increased oxidative stress. Thus, reduced mitochondrial enzyme activity and ATP production is likely not due to a reduction in mitochondrial content or the expression of the respiratory chain complexes. Instead, observed differences may be due to functionally damaged mitochondria that produce less ATP and produce more reactive oxygen species (ROS), since MNR induced a 40% increase in MDA, reflecting the pro-oxidative environment in the MNR fetal cardiac LV tissue.

ROS play a physiological role at low concentrations (67) but are an important cause of cellular dysfunction and CVD at high concentrations (68,69). Mitochondria are also a key

target of oxidative stress, resulting from ROS generation by the respiratory chain under stress conditions (70). The fact that oxidized mtDNA is not repaired as efficiently as nuclear DNA, contributes to a loss of mtDNA fitness because of the higher persistence of damaged mitochondrial genomes (71). Damaged mitochondria and increased ROS production may also lead to cell death, features equally described in CVD and cardiac aging (72), and in line with the increased mRNA levels for the mitochondrial-specific protein BNIP3 found in the hearts of MNR fetuses. Recent studies demonstrated that cardiomyocytes BNIP3 overexpression is associated with aberrant mitochondrial function, loss of mitochondrial membrane potential, induction of mitochondrial permeability transition pore, development of cardiac hypertrophy, activation of aberrant mitophagy, and induction of cardiac cell death (73,74). Growing evidence also attests significant relationship between BNIP3 and mitochondrial morphology (75).

TEM demonstrated that LV MNR fetal cardiac tissues display mitochondrial cristae abnormalities. Mitochondrial cristolysis is related to mitochondrial inner membrane potential decrease and severe respiratory chain defects (76). The inner mitochondrial membrane hosts key oxidative phosphorylation enzymes, so there is a close relationship between the number of cristae and the surface area of that membrane and cellular metabolic activity capacity (77). Abnormalities in mitochondrial morphology, reflected as disorganized cristae, have been described in cardiac and skeletal muscle biopsies from children aged 0.5 to 12 years with non-compaction cardiomyopathy (78). The degree of cristolysis observed in MNR baboon fetuses suggests that the capacity of the fetal LV to generate energy by mitochondrial OXPHOS is critically compromised, priming cardiomyocytes to a low energy bioenergetic state, in agreement with the observed low adenine nucleotides and energy charge.

In agreement with the mitochondrial abnormalities observed, we found alterations of mitochondrial fission/fusion involved proteins in the cardiac LV of MNR offspring.

Imbalance in mitochondrial fission/fusion process leads to mitochondrial deformities associated with numerous human diseases (79,80). We found elevated *MFN2* transcripts in the MNR fetal LV, accompanied by increased immunoreactive protein in MNR-F fetuses. Outer mitochondrial membrane MFN2 induces the fusion of this membrane with the membranes of neighboring organelles, being also a mitochondrial assembly regulatory factor (79,80). Changes in mitochondrial fission/fusion may contribute to the mitochondrial degeneration in the cardiac LV of MNR near-term offspring observed by TEM.

The present work clearly indicates fetal sex-dependent outcomes. Male MNR fetuses seem more affected by in utero nutritional deprivation. These findings agree with the considerable body of data documenting sex dissimilarities in the frequency and severity of coronary artery disease, cardiac hypertrophy, heart failure and sudden cardiac death with mitochondrial dysfunction playing a role in these diseases (81–83).

Sex-based differences in human disease are caused by the levels of endogenous sex steroid hormones that now we know regulate mitochondrial metabolism (83,84).

We have demonstrated increased myocardial fibrosis and autophagy in male MNR fetuses by term, indicating impaired stiffness and predisposition to diastolic dysfunction (13). This increased stiffness in the fetal hearts is demonstrated in the postnatal dynamic cardiac MRI data (14,85). Sex-specific hypertensive effects have been reported in MNR-M offspring (86). Sex differences can be in part explained by intrinsic sex-specific mitochondrial differences (87,88). It has been described that estrogens and androgens protect mitochondria against aging-related degenerative effects in a tissue-specific manner by activating their respective receptors (89). While the mechanisms and targets by which estrogens act directly and indirectly to regulate mitochondrial function are not entirely clarified, it is clear that estradiol regulates mitochondrial metabolism and morphology via nuclear and mitochondrial-mediated events, including stimulation of nuclear respiratory factor-1 (NRF-1) transcription,

one of NRF-1 target is TFAM that binds mtDNA to regulate its transcription (reviewed in (84)). However, mechanisms for sex differences include not only estrogens and androgens but also sex chromosome-encoded genes.

Since overall effects were more severe in MNR-M fetuses, energy production, cardiac function, and the ability to withstand "second hits" later in life would likely be more compromised in males who were IUGR at birth, decreasing metabolic resilience.

MNR-M fetuses exhibited higher MDA levels than females indicating a more elevated prooxidative environment in male cardiac LV tissue, a critical factor in the pathogenesis development of CVD (69). In a rat model of MNR (86), plasma from 21-day-old male offspring showed increased carbonyls content, decreased GSH, and decreased superoxide anion scavenging activity while MNR female plasma did not show a prooxidative status. Women show slower progress of atherosclerosis, lesser incidence of heart failure (90,91), and usually acquire heart disease advanced in life than men (92). Also, abnormal cardiac morphology and function in healthy humans and animal models are plausible risk factors for sex-associated CVD development (93). Additionally, hearts from females show greater contractility (93) and better calcium handling (94), functions in which mitochondria play important roles. Our data strengthen the view that pregnancy responses to metabolic stressors can have differential LV mitochondrial effects in male and female fetal hearts that reflect sex differences in production and handling of oxidative stress.

To our knowledge, the present study is the first demonstrating the sensitivity of fetal LV cardiac mitochondrial function to moderate MNR. Our model consistently shows important human parallels regarding responses to prenatal stressors that lead to later life disease vulnerabilities. In this model, postnatal dysfunction has also been demonstrated in offspring carbohydrate metabolism by the early development of peripheral insulin resistance (95). We demonstrate here several fetal alterations that potentially predispose to the early

adult impaired cardiac ventricular dysfunction previously reported (11,14,85). Numerous studies establish that mitochondrial alterations produced by gestational exposure persist into adulthood or across generations (20).

This study offers a unique view of the sensitivity of cardiac mitochondria during fetal development in an animal model that has consistently shown important parallels with the human in terms of responses to stressors in the womb that lead to later life disease vulnerabilities. This model enables qualitative and quantitative assessment of biological processes, exposing new mechanisms that regulate cardiac tissue metabolism and function. Potential therapeutic interventions that address the decreased mitochondrial function have been investigated in rodents. There is a need for similar studies in nonhuman primates, addressing interventions to prevent the programmed mitochondrial dysfunction *in utero* as well as to reverse the postnatal effects due to lifestyle habits. Among the future studies, we propose dietary and/or exercise interventions to improve cardiac mitochondrial function and increase reserve cardiovascular response in MNR/IUGR offspring and measurement of cardiac function and mitochondrial capacity throughout in longitudinal studies in this baboon model.

Although this is a relatively short-term study, perform a longer-term follow-up will better understand the sex-specific outcomes, identify sex-specific biomarkers for cardiac dysfunction, and evaluate the effect of developing programming in premature cardiac aging and mortality. Afterward, the longstanding implications on well-being and illness risk is accumulative throughout time, so any alteration (relative insufficiencies) in cardiac biology that arise earlier in the life continuum tend to produce larger magnitudes than those (with equivalent magnitude) that happen later in life. Mitochondria are the heart of cellular bioenergetics, so we expect that gestational dysfunction of cardiac mitochondria will have pronounced consequences later in life. Significant knowledge is missing, such as the extent

and duration of the long-term consequences of developmental conditions on initial mitochondrial function, the clinical implication of these effects on pathophysiology susceptibility over the life span, the molecular mechanism(s) perpetuating long-term effects and their plasticity, the establishment of non-invasive biomarkers of mitochondrial function across tissues, and the influence of sex differences on long-term mitochondrial function and outputs. Both sexes were studied and revealed fetal sex-dependent outcomes. Male MNR fetuses were more severely affected by in utero nutritional deprivation. Understanding the sex-specific underlying pathogenesis of IUGR and the sex-specific cellular mechanisms responsible for in utero programmed predisposition to cardiac disease will allow the development of sex-specific biomarkers for early diagnosis in both sexes provide an opportunity for more timely and sex-target interventions to improve life course cardiovascular health.

5 Conclusion

Alterations in cardiac mitochondrial structure/function are implicated in cardiac developmental programming and likely influence long-term cardiac health (Figure 6). A better understanding of the underlying pathogenesis of IUGR and the cellular mechanisms responsible for in utero programmed predisposition to cardiac disease will allow the development of biomarkers for early diagnosis that provides an opportunity for more timely interventions to improve life course cardiovascular health.

6 Study Limitations

The sample size used in this study (n=6 by sex and treatment, total n=12 with sexes pooled) may appear small compared with rodent studies; however, the power of our analysis is very high compared with other primate studies. We published a paper surveying different

publications with primates as research models (96), which averaged 6 with sexes pooled, lower than our study.

Although we have shown early left and right ventricular heart failure with preserved ejection fraction in MNR offspring in the same model (11,14,85,97), we did not perform cardiac mitochondrial functional analysis in the fetal or adult cardiac muscle under basal or stress conditions. However, we reported a significant reduction in maximum respiration rate of adult skin-derived fibroblasts from MNR compared to control (98). MNR-induced mitochondrial dysfunction may be defined as priming pathological deviance from the physiologic program of a healthy cell. The effects of the MNR-induced state may range from mild to severe alteration of metabolic and signaling pathways leading to increased or accelerated cell death, depending on the cell type, its energy requirements, its underlying expression program, and its accumulation of second-hit stresses. We do not anticipate that MNR-programmed effects to be exclusively cardiac, but instead affect the whole organism leading to tissue-specific MNR-implications. This raises the pertinence to study other tissues.

Further studies are warranted to establish how early cardiac implications of IUGR can be detected. It is primordial to establish cardiac-impairment IUGR biomarkers to use in a clinical setting. More research in this area is clearly needed. Hence, it may be prudent for clinicians to consider periodic echocardiographic examinations of IUGR offspring to monitor cardiac performance and potentially intervene early, as this group may be at greater risk of cardiovascular disease at an earlier age.

7 Clinical Perspectives

- There is a lack of knowledge on the role of mitochondria during fetal development on later-life cardiac dysfunction caused by maternal nutrient reduction (MNR).

- Our nonhuman primate baboon model of moderate MNR revealed a sex-dependent relationship between MNR, fetal cardiac mitochondrial remodeling and bioenergetic imbalance that may ultimately predispose the offspring to cardiometabolic disorders later in life.
- Uncovering the precise mechanisms underlying the IUGR pathogenesis and the in utero programmed predisposition to cardiac disease will allow the development of biomarkers for an early diagnosis, and to establish timely and efficient interventions to improve a life course cardiovascular health.

8 Availability of data and material

All data and materials are available upon request.

9 References

1. WHO. Noncommunicable diseases [Internet]. 2018 [cited 2020 May 13]. Available from: https://www.who.int/en/news-room/fact-sheets/detail/noncommunicable-diseases
2. Thornburg KL. The programming of cardiovascular disease. J Dev Orig Health Dis [Internet]. 2015 Oct 15 [cited 2018 Jan 7];6(05):366–76. Available from: http://www.journals.cambridge.org/abstract_S2040174415001300
3. Masoumy EP, Sawyer AA, Sharma S, Patel JA, Gordon PMK, Regnault TRH, et al. The lifelong impact of fetal growth restriction on cardiac development. Pediatr Res [Internet]. 2018;84(4):537–44. Available from: http://www.ncbi.nlm.nih.gov/pubmed/29967522
4. Rich-Edwards JW, Stampfer MJ, Manson JE, Rosner B, Hankinson SE, Colditz G a, et al. Birth weight and risk of cardiovascular disease in a cohort of women followed up since 1976. BMJ. 1997;315(7105):396–400.
5. Barker DJ, Osmond C, Golding J, Kuh D, Wadsworth ME. Growth in utero, blood pressure in childhood and adult life, and mortality from cardiovascular disease. BMJ. 1989;298(6673):564–7.
6. Rich-Edwards J, Kleinman K, Michels K, Stampfer M, Manson J, Rexrode K, et al. Longitudinal study of birth weight and adult body mass index in predicting risk of coronary heart disease and stroke in women. BMJ. 2005;330(7500):1115.
7. Barker DJ, Martyn CN, Osmond C, Hales CN, Fall CH. Growth in utero and serum cholesterol concentrations in adult life. BMJ. 1993;307(6918):1524–7.
8. Syddall H, Aihie Sayer A, Dennison E, Martin H, Barker D, Cooper C. Cohort Profile: The Hertfordshire Cohort Study. Int J Epidemiol. 2005 Dec 1;34(6):1234–42. Available from: http://academic.oup.com/ije/article/34/6/1234/707357/Cohort-Profile-

The-Hertfordshire-Cohort-Study

9. Cheong JN, Wlodek ME, Moritz KM, Cuffe JSM. Programming of maternal and offspring disease: impact of growth restriction, fetal sex and transmission across generations. J Physiol. 2016 Sep 1;594(17):4727–40. Available from: http://www.ncbi.nlm.nih.gov/pubmed/26970222

10. Bishop AC, Libardoni M, Choudary A, Misra B, Lange K, Bernal J, et al. Nonhuman primate breath volatile organic compounds associate with developmental programming and cardio-metabolic status. J Breath Res. 2018 May 14;12(3):036016. Available from: http://www.ncbi.nlm.nih.gov/pubmed/29593130

11. Kuo AH, Li C, Huber HF, Schwab M, Nathanielsz PW, Clarke GD. Maternal nutrient restriction during pregnancy and lactation leads to impaired right ventricular function in young adult baboons. J Physiol. 2017;13(13):4245–60. Available from: http://doi.wiley.com/10.1113/JP273928%0Ahttp://www.ncbi.nlm.nih.gov/pubmed/28439937

12. Kuo AH, Li C, Huber HF, Clarke GD, Nathanielsz PW. Intrauterine growth restriction results in persistent vascular mismatch in adulthood. J Physiol. 2017 Nov 3; Available from: http://doi.wiley.com/10.1113/JP275139

13. Muralimanoharan S, Li C, Nakayasu ES, Casey CP, Metz TO, Nathanielsz PW, et al. Sexual dimorphism in the fetal cardiac response to maternal nutrient restriction. J Mol Cell Cardiol. 2017 Jul;108:181–93. Available from: http://dx.doi.org/10.1016/j.yjmcc.2017.06.006

14. Kuo AH, Li C, Li J, Huber HF, Nathanielsz PW, Clarke GD. Cardiac remodelling in a baboon model of intrauterine growth restriction mimics accelerated ageing. J Physiol [Internet]. 2017;595(4):1093–110. Available from: http://doi.wiley.com/10.1113/JP272908

15. Li C, Jenkins S, Mattern V, Comuzzie AG, Cox LA, Huber HF, et al. Effect of moderate, 30 percent global maternal nutrient reduction on fetal and postnatal baboon phenotype. J Med Primatol. 2017;46(6):293–303.
16. Li C, McDonald TTJ, Wu G, Nijland MMJ, Nathanielsz PWP. Intrauterine growth restriction alters term fetal baboon hypothalamic appetitive peptide balance. J Endocrinol. 2013 Jun;217(3):275–82. Available from: http://www.ncbi.nlm.nih.gov/pubmed/23482706
17. Mäkikallio K, Räsänen J, Mäkikallio T, Vuolteenaho O, Huhta JC. Human fetal cardiovascular profile score and neonatal outcome in intrauterine growth restriction. Ultrasound Obstet Gynecol. 2008 Jan 1;31(1):48–54. Available from: http://doi.wiley.com/10.1002/uog.5210
18. Severi FM, Rizzo G, Bocchi C, D'Antona D, Verzuri MS, Arduini D. Intrauterine growth retardation and fetal cardiac function. Fetal Diagn Ther. 2000;15(1):8–19. Available from: http://www.ncbi.nlm.nih.gov/pubmed/10705209
19. Lock MC, Tellam RL, Botting KJ, Wang KCW, Selvanayagam JB, Brooks DA, et al. The role of miRNA regulation in fetal cardiomyocytes, cardiac maturation and the risk of heart disease in adults. J Physiol. 2018;596(23):5625–40.
20. Gyllenhammer LE, Entringer S, Buss C, Wadhwa PD. Developmental programming of mitochondrial biology: a conceptual framework and review. Proc R Soc B Biol Sci [Internet]. 2020 May 13;287(1926):20192713. Available from: https://royalsocietypublishing.org/doi/10.1098/rspb.2019.2713
21. Scheuermann-Freestone M, Madsen PL, Manners D, Blamire AM, Buckingham RE, Styles P, et al. Abnormal cardiac and skeletal muscle energy metabolism in patients with type 2 diabetes. Circulation. 2003;107(24):3040–6.
22. Schlabritz-Loutsevitch NE, Howell K, Rice K, Glover EJ, Nevill CH, Jenkins SL, et

al. Development of a system for individual feeding of baboons maintained in an outdoor group social environment. J Med Primatol. 2004 Jun;33(3):117–26. Available from: http://www.ncbi.nlm.nih.gov/pubmed/15102068

23. Schlabritz-Loutsevitch NE, Hubbard GB, Dammann MJ, Jenkins SL, Frost P a, McDonald TJ, et al. Normal concentrations of essential and toxic elements in pregnant baboons and fetuses (Papio species). J Med Primatol. 2004 Jun;33(3):152–62. Available from: http://www.ncbi.nlm.nih.gov/pubmed/15102072

24. Wu A, Ying Z, Gomez-Pinilla F. Dietary omega-3 fatty acids normalize BDNF levels, reduce oxidative damage, and counteract learning disability after traumatic brain injury in rats. J Neurotrauma. 2004 Oct;21(10):1457–67. Available from: http://www.ncbi.nlm.nih.gov/pubmed/15672635

25. Pereira SP, Deus CM, Serafim TL, Cunha-Oliveira T, Oliveira PJ. Metabolic and Phenotypic Characterization of Human Skin Fibroblasts After Forcing Oxidative Capacity. Toxicol Sci. 2018 Jul 1;164(1):191–204. Available from: https://academic.oup.com/toxsci/article/164/1/191/4947784

26. Cox L, Nijland M, Gilbert J, Schlabritz-Loutsevitch N, Hubbard G, McDonald T, et al. Effect of 30 per cent maternal nutrient restriction from 0.16 to 0.5 gestation on fetal baboon kidney gene expression. J Physiol. 2006 Apr;572(Pt 1):67–85. Available from: http://www.pubmedcentral.nih.gov/articlerender.fcgi?artid=1779656&tool=pmcentrez&rendertype=abstract

27. Machado NG, Baldeiras I, Pereira GC, Pereira SP, Oliveira PJ. Sub-chronic administration of doxorubicin to Wistar rats results in oxidative stress and unaltered apoptotic signaling in the lung. Chem Biol Interact. 2010 Dec;188(3):478–86. Available from: http://www.ncbi.nlm.nih.gov/pubmed/20932959

28. Romero-Calvo I, Ocón B, Martínez-Moya P, Suárez MD, Zarzuelo A, Martínez-

Augustin O, et al. Reversible Ponceau staining as a loading control alternative to actin in Western blots. Anal Biochem. 2010 Jun 15;401(2):318–20. Available from: http://www.ncbi.nlm.nih.gov/pubmed/20206115

29. Dittmer A, Dittmer J. β-Actin is not a reliable loading control in Western blot analysis. Electrophoresis. 2006;27(14):2844–5. Available from: http://doi.wiley.com/10.1002/elps.200500785

30. Aldridge GM, Podrebarac DM, Greenough WT, Weiler IJ. The use of total protein stains as loading controls: An alternative to high-abundance single-protein controls in semi-quantitative immunoblotting. J Neurosci Methods. 2008;172(2):250–4. Available from: http://www.pubmedcentral.nih.gov/articlerender.fcgi?artid=2567873&tool=pmcentrez&rendertype=abstract

31. Pereira SP, Oliveira PJ, Tavares LC, Moreno AJ, Cox L a., Nathanielsz PW, et al. Effects of moderate global maternal nutrient reduction on fetal baboon renal mitochondrial gene expression at 0.9 gestation. Am J Physiol - Ren Physiol. 2015 Jun 1;308(11):F1217–28. Available from: http://ajprenal.physiology.org/lookup/doi/10.1152/ajprenal.00419.2014

32. Long J, Ma J, Luo C, Mo X, Sun L, Zang W, et al. Comparison of two methods for assaying complex I activity in mitochondria isolated from rat liver, brain and heart. Life Sci. 2009 Aug 12;85(7–8):276–80. Available from: http://dx.doi.org/10.1016/j.lfs.2009.05.019

33. Tisdale HD. Preparation and properties of succinic-cytochrome c reductase (complex II-III). Methods Enzymol. 1967;10(C):213–5.

34. Luo C, Long J, Liu J. An improved spectrophotometric method for a more specific and accurate assay of mitochondrial complex III activity. Clin Chim Acta. 2008

Sep;395(1–2):38–41. Available from: http://www.ncbi.nlm.nih.gov/pubmed/18502205

35. Brautigan DL, Ferguson-Miller S, Margoliash E. Mitochondrial cytochrome c: Preparation and activity of native and chemically modified cytochromes c. Methods Enzymol. 1978;53(C):128–64.

36. Coore HG, Denton RM, Martin BR, Randle PJ. Regulation of adipose tissue pyruvate dehydrogenase by insulin and other hormones. Biochem J. 1971;125(1):115–27.

37. Santos MS, Moreno AJ, Carvalho AP. Relationships between ATP depletion, membrane potential, and the release of neurotransmitters in rat nerve terminals. An in vitro study under conditions that mimic anoxia, hypoglycemia, and ischemia. Stroke. 1996;27(5):941–50.

38. Stocchi V, Cucchiarini L, Magnani M, Chiarantini L, Palma P, Crescentini G. Simultaneous extraction and reverse-phase high-performance liquid chromatographic determination of adenine and pyridine nucleotides in human red blood cells. Anal Biochem. 1985;146(1):118–24.

39. Draper HH, Hadley M. Malondialdehyde determination as index of lipid peroxidation. Methods Enzymol. 1990;186:421–31.

40. Tsao S-MM, Yin M-CC, Liu W-HH. Oxidant stress and B vitamins status in patients with non-small cell lung cancer. Nutr Cancer. 2007;59(1):8–13.

41. Paglia DE, Valentine WN. Studies on the quantitative and qualitative characterization of erythrocyte glutathione peroxidase. J Lab Clin Med. 1967;70(1):158–69.

42. Goldberg D, Spooner R. Glutathione reductase. In: Bergmerye, editor. Methods in Enzymatic Analysis. New York.: Verlag Chemie Weinheim Academic Pres; 1983. p. 258–65.

43. Malhotra BSK. Experiments on fixation for electron microscopy. Small. 1962;103(March):5–15.

44. Li C, Ramahi E, Nijland MJ, Choi J, Myers D a., Nathanielsz PW, et al. Up-regulation of the fetal baboon hypothalamo-pituitary-adrenal axis in intrauterine growth restriction: Coincidence with hypothalamic glucocorticoid receptor insensitivity and leptin receptor down-regulation. Endocrinology. 2013;154(7):2365–73.
45. Kuo AH, Li J, Li C, Huber HF, Nathanielsz PW, Clarke GD. Poor perinatal growth impairs baboon aortic windkessel function. J Dev Orig Health Dis. 2017 Oct 11;5038:1–6. Available from: https://www.cambridge.org/core/product/identifier/S2040174417000770/type/journal_article
46. Crispi F, Hernandez-Andrade E, Pelsers MMAL, Plasencia W, Benavides-Serralde JA, Eixarch E, et al. Cardiac dysfunction and cell damage across clinical stages of severity in growth-restricted fetuses. Am J Obstet Gynecol. 2008;199(3). Available from: https://ac.els-cdn.com/S000293780800687X/1-s2.0-S000293780800687X-main.pdf?_tid=ef09df74-f411-11e7-98b1-00000aab0f6b&acdnat=1515374532_c2b22053d76d7dcb2792d04a3b4fbd87
47. Crispi F, Bijnens B, Figueras F, Bartrons J, Eixarch E, Le Noble F, et al. Fetal growth restriction results in remodeled and less efficient hearts in children. Circulation. 2010 Jun 8;121(22):2427–36. Available from: http://www.ncbi.nlm.nih.gov/pubmed/20497977
48. Leipälä JA, Boldt T, Turpeinen U, Vuolteenaho O, Fellman V. Cardiac hypertrophy and altered hemodynamic adaptation in growth-restricted preterm infants. Pediatr Res. 2003;53(6):989–93. Available from: https://www.nature.com/articles/pr2003440.pdf
49. Fouzas S, Karatza AA, Davlouros PA, Chrysis D, Alexopoulos D, Mantagos S, et al. Neonatal cardiac dysfunction in intrauterine growth restriction. Pediatr Res. 2014 May 12;75(5):651–7. Available from: http://www.nature.com/articles/pr201422

50. Comas M, Crispi F, Cruz-Martinez R, Figueras F, Gratacos E. Tissue Doppler echocardiographic markers of cardiac dysfunction in small-for-gestational age fetuses. YMOB. 2011;205:57.e1-57.e6. Available from: https://ac.els-cdn.com/S000293781100319X/1-s2.0-S000293781100319X-main.pdf?_tid=460bcaa6-f40f-11e7-bc81-00000aab0f01&acdnat=1515373390_0b26ed4eb9e7ae04d32fedda05434e98
51. Verburg BO, Jaddoe VWV, Wladimiroff JW, Hofman A, Witteman JCM, Steegers EAP. Fetal Hemodynamic Adaptive Changes Related to Intrauterine Growth: The Generation R Study. Circulation. 2008 Feb 5;117(5):649–59. Available from: http://www.ncbi.nlm.nih.gov/pubmed/7805194
52. Darby JRT, Varcoe TJ, Orgeig S, Morrison JL. Cardiorespiratory consequences of intrauterine growth restriction: Influence of timing, severity and duration of hypoxaemia. Theriogenology. 2020;150:84–95. Available from: https://doi.org/10.1016/j.theriogenology.2020.01.080
53. Lewandowski AJ, Augustine D, Lamata P, Davis EF, Lazdam M, Francis J, et al. Preterm heart in adult life: Cardiovascular magnetic resonance reveals distinct differences in left ventricular mass, geometry, and function. Circulation. 2013;127(2):197–206.
54. Bensley JG, Moore L, De Matteo R, Harding R, Black MJ. Impact of preterm birth on the developing myocardium of the neonate. Pediatr Res. 2018;83(4):880–8. Available from: http://dx.doi.org/10.1038/pr.2017.324
55. Wang KCW, Zhang L, Mcmillen IC, Botting KJ, Duffield JA, Zhang S, et al. Fetal growth restriction and the programming of heart growth and cardiac insulin-like growth factor 2 expression in the lamb. J Physiol. 2011;589(19):4709–22.
56. Morrison JL, Botting KJ, Dyer JL, Williams SJ, Thornburg KL, McMillen IC.

Restriction of placental function alters heart development in the sheep fetus. Am J Physiol - Regul Integr Comp Physiol. 2007;293(1).

57. Bubb KJ, Cock ML, Black MJ, Dodic M, Boon WM, Parkington HC, et al. Intrauterine growth restriction delays cardiomyocyte maturation and alters coronary artery function in the fetal sheep. J Physiol. 2007;578(3):871–81.

58. Master JS, Zimanyi MA, Yin K V., Moritz KM, Gallo LA, Tran M, et al. Transgenerational left ventricular hypertrophy and hypertension in offspring after uteroplacental insufficiency in male rats. Clin Exp Pharmacol Physiol. 2014;41(11):884–90.

59. Dong F, Ford SP, Fang CX, Nijland MJ, Nathanielsz PW, Ren J. Maternal nutrient restriction during early to mid gestation up-regulates cardiac insulin-like growth factor (IGF) receptors associated with enlarged ventricular size in fetal sheep. Growth Horm IGF Res. 2005;15(4):291–9.

60. Ge W, Hu N, George LA, Ford SP, Nathanielsz PW, Wang XM, et al. Maternal nutrient restriction predisposes ventricular remodeling in adult sheep offspring. J Nutr Biochem. 2013;24(7):1258–65.

61. Lipshultz SE, Sleeper LA, Towbin JA, Lowe AM, Orav EJ, Cox GF, et al. The Incidence of Pediatric Cardiomyopathy in Two Regions of the United States. N Engl J Med. 2003 Apr 24;348(17):1647–55. Available from: http://www.nejm.org/doi/abs/10.1056/NEJMoa021715

62. Kelly DP, Strauss AW, Strauss AW. Inherited cardiomyopathies. N Engl J Med. 1994 Mar 31;330(13):913–9. Available from: http://www.nejm.org/doi/abs/10.1056/NEJM199403313301308

63. Porter GA, Hom JR, Hoffman DL, Quintanilla RA, de Mesy Bentley K, Sheu S-SS, et al. Bioenergetics, mitochondria, and cardiac myocyte differentiation. Prog Pediatr

Cardiol. 2011 May;31(2):75–81. Available from: http://www.pubmedcentral.nih.gov/articlerender.fcgi?artid=3096664&tool=pmcentrez&rendertype=abstract

64. Novielli C, Mandò C, Tabano S, Anelli GM, Fontana L, Antonazzo P, et al. Mitochondrial DNA content and methylation in fetal cord blood of pregnancies with placental insufficiency. Placenta. 2017;55:63–70.

65. Czajka A, Ajaz S, Gnudi L, Parsade CK, Jones P, Reid F, et al. Altered Mitochondrial Function, Mitochondrial DNA and Reduced Metabolic Flexibility in Patients With Diabetic Nephropathy. EBioMedicine. 2015;2(6):499–512. Available from: http://dx.doi.org/10.1016/j.ebiom.2015.04.002

66. Zhou M, Zhu L, Cui X, Feng L, Zhao X, He S, et al. Reduced peripheral blood mtDNA content is associated with impaired glucose-stimulated islet β cell function in a Chinese population with different degrees of glucose tolerance. Diabetes Metab Res Rev. 2016 Oct 30;32(7):768–74. Available from: http://libweb.anglia.ac.uk/

67. Brand MD. Mitochondrial generation of superoxide and hydrogen peroxide as the source of mitochondrial redox signaling. Free Radic Biol Med. 2016;100:14–31. Available from: http://dx.doi.org/10.1016/j.freeradbiomed.2016.04.001

68. Cadenas S. ROS and redox signaling in myocardial ischemia-reperfusion injury and cardioprotection. Free Radic Biol Med. 2018 Mar;117:76–89. Available from: http://linkinghub.elsevier.com/retrieve/pii/S0891584918300340

69. Ballinger SW. Mitochondrial dysfunction in cardiovascular disease. Free Radic Biol Med. 2005;38(10):1278–95.

70. Zorov DB, Juhaszova M, Sollott SJ. Mitochondrial Reactive Oxygen Species (ROS) and ROS-Induced ROS Release. Physiol Rev. 2014;94(3):909–50.

71. Yakes FM, Van Houten B. Mitochondrial DNA damage is more extensive and persists

longer than nuclear DNA damage in human cells following oxidative stress. Proc Natl Acad Sci U S A. 1997;94(2):514–9. Available from: http://www.ncbi.nlm.nih.gov/pubmed/9012815%0Ahttp://www.pubmedcentral.nih.gov/articlerender.fcgi?artid=PMC19544

72. Wang Y, Li Y, He C, Gou B, Song M. Mitochondrial regulation of cardiac aging. Biochim Biophys Acta - Mol Basis Dis. 2019;(December):0–1. Available from: https://doi.org/10.1016/j.bbadis.2018.12.008

73. Regula KM, Ens K, Kirshenbaum LA. Inducible expression of BNIP3 provokes mitochondrial defects and hypoxia-mediated cell death of ventricular myocytes. Circ Res. 2002;91(3):226–31.

74. Dhingra A, Jayas R, Afshar P, Guberman M, Maddaford G, Gerstein J, et al. Ellagic acid antagonizes Bnip3-mediated mitochondrial injury and necrotic cell death of cardiac myocytes. Free Radic Biol Med. 2017;112(August):411–22. Available from: https://doi.org/10.1016/j.freeradbiomed.2017.08.010

75. Gao A, Jiang J, Xie F, Chen L. Bnip3 in mitophagy: Novel insights and potential therapeutic target for diseases of secondary mitochondrial dysfunction. Clin Chim Acta [Internet]. 2020;506(December 2019):72–83. Available from: https://doi.org/10.1016/j.cca.2020.02.024

76. Arismendi-Morillo G. Electron microscopy morphology of the mitochondrial network in gliomas and their vascular microenvironment. Biochim Biophys Acta [Internet]. 2010 Nov 9 [cited 2011 Oct 11];1807(6):602–8. Available from: http://www.ncbi.nlm.nih.gov/pubmed/21070743

77. Modica-Napolitano JS, Singh KK. Mitochondria as targets for detection and treatment of cancer. Expert Rev Mol Med. 2002;4(9):1–19.

78. Pignatelli RH, McMahon CJ, Dreyer WJ, Denfield SW, Price J, Belmont JW, et al.

Clinical Characterization of Left Ventricular Noncompaction in Children: A Relatively Common Form of Cardiomyopathy. Circulation. 2003;108(21):2672–8.

79. Filadi R, Pendin D, Pizzo P. Mitofusin 2: from functions to disease. Cell Death Dis [Internet]. 2018 Mar 28 [cited 2018 Aug 14];9(3):330. Available from: https://www.nature.com/articles/s41419-017-0023-6.pdf

80. Bach D, Pich S, Soriano FX, Vega N, Baumgartner B, Oriola J, et al. Mitofusin-2 determines mitochondrial network architecture and mitochondrial metabolism: A novel regulatory mechanism altered in obesity. J Biol Chem. 2003 May 9;278(19):17190–7. Available from: http://www.ncbi.nlm.nih.gov/pubmed/12598526

81. Gilbert JS, Nijland MJ. Sex differences in the developmental origins of hypertension and cardiorenal disease. Am J Physiol Regul Integr Comp Physiol. 2008 Dec;295(6):R1941-52. Available from: http://www.pubmedcentral.nih.gov/articlerender.fcgi?artid=2685301&tool=pmcentrez&rendertype=abstract

82. Khalifa ARM, Abdel-Rahman EA, Mahmoud AM, Ali MH, Noureldin M, Saber SH, et al. Sex-specific differences in mitochondria biogenesis, morphology, respiratory function, and ROS homeostasis in young mouse heart and brain. Physiol Rep. 2017;5(6):1–19.

83. Silaidos C, Pilatus U, Grewal R, Matura S, Lienerth B, Pantel J, et al. Sex-associated differences in mitochondrial function in human peripheral blood mononuclear cells (PBMCs) and brain. Biol Sex Differ. 2018;9(1):1–10.

84. Klinge CM. Estrogenic control of mitochondrial function. Redox Biol [Internet]. 2020;31(August 2019):101435. Available from: https://doi.org/10.1016/j.redox.2020.101435

85. Kuo AH, Li C, Huber HF, Nathanielsz PW, Clarke GD. Ageing changes in

biventricular cardiac function in male and female baboons (Papio spp.). J Physiol. 2018;596(21):5083–98. Available from: http://doi.wiley.com/10.1113/JP276338

86. Rodríguez-Rodríguez P, de Pablo ALL, Condezo-Hoyos L, Martín-Cabrejas MA, Aguilera Y, Ruiz-Hurtado G, et al. Fetal undernutrition is associated with perinatal sex-dependent alterations in oxidative status. J Nutr Biochem. 2015;26(12):1650–9. Available from: http://dx.doi.org/10.1016/j.jnutbio.2015.08.004

87. John C, Grune J, Ott C, Nowotny K, Deubel S, Kühne A, et al. Sex Differences in Cardiac Mitochondria in the New Zealand Obese Mouse. Front Endocrinol (Lausanne) [Internet]. 2018 Dec 4;9(December):1–9. Available from: https://www.frontiersin.org/article/10.3389/fendo.2018.00732/full

88. Cardinale DA, Larsen FJ, Schiffer TA, Morales-Alamo D, Ekblom B, Calbet JAL, et al. Superior intrinsic mitochondrial respiration in women than in men. Front Physiol. 2018;9(AUG):1–12.

89. López-Lluch G. Mitochondrial activity and dynamics changes regarding metabolism in ageing and obesity. Mech Ageing Dev. 2017;162:108–21.

90. Vassalle C, Simoncini T, Chedraui P, Pérez-López FR. Why sex matters: the biological mechanisms of cardiovascular disease. Vol. 28, Gynecological Endocrinology. 2012. p. 746–51.

91. Czubryt MP, Espira L, Lamoureux L, Abrenica B. The role of sex in cardiac function and disease. Can J Physiol Pharmacol. 2006;84(1):93–109.

92. Mosca L, Manson JE, Sutherland SE, Langer RD, Manolio T, Barrett-Connor E. Cardiovascular Disease in Women : A Statement for Healthcare Professionals From the American Heart Association. Circulation. 1997;96(7):2468–82.

93. Merz CN, Moriel M, Rozanski A, Klein J, Berman DS. Gender-related differences in exercise ventricular function among healthy subjects and patients. Am Heart J.

1996;131(4):704–9.

94. Regitz-Zagrosek V, Oertelt-Prigione S, Seeland U, Hetzer R. Sex and gender differences in myocardial hypertrophy and heart failure. Circ J. 2010;74(7):1265–73.

95. Choi J, Li C, McDonald TJ, Comuzzie A, Mattern V, Nathanielsz PW. Emergence of insulin resistance in juvenile baboon offspring of mothers exposed to moderate maternal nutrient reduction. Am J Physiol Regul Integr Comp Physiol. 2011 Sep ;301(3):R757-62. Available from: http://www.pubmedcentral.nih.gov/articlerender.fcgi?artid=3174762&tool=pmcentrez &rendertype=abstract

96. Pantham P, Rosario FJ, Nijland M, Cheung A, Nathanielsz PW, Powell TL, et al. Reduced placental amino acid transport in response to maternal nutrient restriction in the baboon. Am J Physiol Integr Comp Physiol. 2015;309(7):R740–6. Available from: http://ajpregu.physiology.org/lookup/doi/10.1152/ajpregu.00161.2015

97. Kuo AH, Li C, Nathanielsz PW. Accelerated aging of cardiac function in offspring of undernourished pregnant baboons. Reprod Sci. 2015;22(March):97A-98A. Available from: http://ovidsp.ovid.com/ovidweb.cgi?T=JS&PAGE=reference&D=emed13&NEWS=N &AN=71847347

98. Salmon AB, Dorigatti J, Huber HF, Li C, Nathanielsz PW. Maternal nutrient restriction in baboon programs later-life cellular growth and respiration of cultured skin fibroblasts: a potential model for the study of aging-programming interactions. GeroScience. 2018;40(3):269–78.

10 Figures Titles and Captions

Fig. 1 Timeline of maternal nutrition during baboon fetal development. Term baboon gestation occurs around 185 days.

Fig. 2 Variation of mitochondrial DNA (mtDNA) copy number and gene expression analysis of fetal cardiac left ventricle (LV) tissue from fetuses of control (C) and maternal nutrient reduction (MNR) mothers.

A: mtDNA was measured in fetal baboon cardiac LV tissue at 0.9G from control and NMR pregnancies in which mothers ate 70% of the food consumed by control mothers on a weight-adjusted basis. mtDNA copy number was calculated as the ratio between the mitochondrially encoded NADH dehydrogenase 1 (ND1) gene and the nuclear-encoded gene for beta-2-microglobulin (B2M). B-F: Gene expression analysis of control and MNR baboon fetuses at 0.9G. mRNA abundance for mitochondrial transcripts was assessed by PCR arrays in cardiac LV samples from offspring of C and MNR mothers. B: global diet-dependent effects in the mitochondrial gene expression profile; C and D comparison of transcripts expression between different maternal diets for the same sex [female fetuses (C) and male fetuses (D)]; and E and F: Sexual dimorphism in the mitochondrial profile of control (E) and MNR (F) fetuses. Transcripts related to oxidative phosphorylation system (OXPHOS), complex I (CI; NADH dehydrogenase), complex II (CII; succinate dehydrogenase), complex III (CIII; ubiquinol cytochrome c oxidoreductase), complex IV [CIV; cytochrome c oxidase (COX)], and complex V (CV; ATP synthase). Values were normalized to endogenous controls [hypoxanthine phosphoribosyltransferase 1 (HPRT1), ribosomal protein L13a (RPL13A), and Beta-actin (ACTB)] and are expressed relative to their normalized values. All transcripts presented have $P<0.1$ vs. respective paired group. C-M, male fetuses from control group (n=6); C-F, female fetuses from control group (n=6); MNR-M, male fetuses from MNR

group (n=6); MNR-F, female fetuses from MNR group (n=6) or n=12 (sexes combined) animals/group. Means±SEM Comparison between groups was performed using a non-parametric Mann-Whitney test. P-value<0.05 was considered significant. *P<0.05 vs. respective controls or as indicated. Consult Table S6 for gene abbreviations and also Figures S2 and S3.

Fig. 3 Protein content by immunoblot detection were determined in fetal cardiac LV tissue of control and MNR pregnancies, the latter characterized as 70% of the food consumed by control mothers on a weight-adjusted basis of baboons at 0.9G. C-M, male fetuses from the control group; C-F, female fetuses from the control group; MNR-M, male fetuses from MNR group; MNR-F, female fetuses from MNR group; T1, LV cardiac sample from an adult male baboon; T2, LV cardiac sample from an adult female baboon; T3, human cardiac sample, not used in all membranes. Ponceau staining for the respective membrane was used for normalization and as a loading control. Data are presented as arbitrary units and represent densitometry analysis of membranes by immunoblot detection after image acquisition. Data are means ± SEM; n=6 (when separated by sex) or n=12 (sexes combined) animals/group. Comparison between groups was performed using a non-parametric Mann-Whitney test. P-value less than 0.05 was considered significant. See also Table S1-S2.

[a] for these proteins, the sample size is different from the one previously indicated, being n=3 (when separated by sex) or n=6 (sexes combined) animals/group

[b] for the CS protein, the sample size is different from the one previously indicated, being n=4 (when separated by sex) or n=8 (sexes combined) animals/group.

Fig. 4 Quantitative immunohistochemistry of mitochondrial proteins in fetal cardiac LV tissue of control and MNR pregnancies, the latter characterized as 70% of the food consumed

by control mothers on a weight-adjusted basis of baboons at 0.9G. A-D: The mitochondrial subunits MFN2 (A), CYC1 (B), COX6C (C) and TIMM9A (D) were analyzed in cardiac left ventricle tissue of fetal baboons from mothers that were fed ad libitum (control group) or fed with 70% of the control (MNR group). A-D: representative micrographs (magnification: x20) from cardiac LV sections of C-M, male fetuses from control group; C-F, female fetuses from control group; MNR-M, male fetuses from MNR group; MNR-F, female fetuses from MNR group. Immunoreactivity of MNF2 was expressed as fraction stained (in %; E) and density [F; in arbitrary units (AU)]. Data are expressed as mean + SEM; n=5 (when separated by sex) or n=10 (sexes combined) animals/group. Comparison between groups was performed using a non-parametric Mann-Whitney test. P-value less than 0.05 was considered significant. *P<0.05 vs. respective controls.

Fig.5 Representative transmission electron microscopy of cardiac LV tissue of fetal baboon from mothers that were fed *ad libitum* (control group) or 70% of the control (MNR group). C-M, male fetuses from the control group; C-F, female fetuses from the control group; MNR-M, male fetuses from the MNR group; MNR-F, female fetuses from the MNR group. Arrow indicates one mitochondrion with multiple concentric sheets of the inner membrane. Method of staining: uranyl acetate/lead citrate. The rightmost panel is the image magnification of a sample from a female fetus of a control mother. Mitochondria are delimited by double membranes , the inner mitochondrial membrane (IMM) and the outer mitochondrial membrane (OMM), enclosing the matrix (Ma), the section that contains the mitochondrial DNA. The topology of the IMM is dynamically controlled, allowing a greater variation in the morphology of the cristae (Cri). The OMM is more uniform and establishes the organelle border. Method of staining: uranyl acetate/lead citrate. Micrographs were taken with a magnification of 3,300x. Scale bar = 500 nm.

Fig. 6 In utero cardiac mitochondrial alterations due to IUGR in a non-human primate model may explain the previously described sex-dependent later life cardiac pathologies.

11 Text Tables

Table 1. Effects of maternal diet on enzymatic activity of mitochondrial respiratory chain complex and changes in the fetal cardiac LV tissue adenine nucleotides and energy charge at 0.9G in control and MNR pregnancies, the latter characterized as a 70% reduction of the food eaten by the control mothers on a weight-adjusted basis.

	Sexes combined		Male		Female		P-value				
	Control	MNR	Control	MNR	Control	MNR	C vs MNR	Male C vs MNR	Female C vs MNR	Control M vs F	MNR M vs F
Number of animals/group	10	10	5	5	5	5					
Citrate Synthase (nmol/min/mg)	1799±146	1011±190	2070±154	1281±341	1527±187	741±98	0.008	-	0.016	0.047	-
Complex I (nmol/min/mg)	1814±84	1339±131	1955±124	1441±142	1673±79	1237±227	0.013	0.028	-	-	-
Complex II / III (nmol/min/mg)	839±143	170±66	1157±78	260±123	521±187	81±21	0.001	0.009	0.009	0.047	-
Complex III (nmol/min/mg)	1265±153	1111±278	929±108	834±291	1601±193	1388±475	-	-	-	0.028	-
Complex IV (nmol/min/mg)	154±55	845±51	219±89	761±69	90±60	928±59	<0.001	0.016	0.009	-	-
CompIex I / Citrate Synthase	1.1±0.1	1.6±0.2	1.0±0.1	1.4±0.4	1.2±0.3	1.7±0.3	-	-	-	-	-
(Complex II / III) / Citrate Synthase	0.47±0.07	0.19±0.06	0.58±0.08	0.3±0.1	0.4±0.1	0.14±0.04	0.013	-	-	-	-
Compex III / Citrate Synthase	0.82±0.	1.7±0.5	0.45±0.04	1.0±0.4	1.2±0.3	2.3±0.9	-	-	-	0.009	-
Complex IV / Citrate Synthase	0.08±0.03	1.1±0.2	0.11±0.04	0.8±0.2	0.063±0.04	1.4±0.2	<0.001	0.009	0.009	-	-
Number of animals/group	12	12	6	6	6	6					
ATP (nmol/mg)	3±2	0.70±0.05	5±4	0.76±0.08	0.82±0.08	0.63±0.05	0.028	-	-	-	-
ADP (nmol/mg)	11±2	7.9±0.7	14±5	8.7±0.8	8.0±1	7±1	-	-	-	-	-
AMP (nmol/mg)	75±8	77±7	70±13	84±8	81±8	69±11	-	-	-	-	-
TAN (nmol/mg)	89±8	86±7	89±14	94±7	90±8	77±12	-	-	-	-	-
AEC	0.09±0.03	0.06±0.006	0.13±0.06	0.05±0.01	0.05±0.005	0.06±0.002	-	0.05	-	0.033	-

Abbreviations: ATP-adenosine triphosphate; ADP-adenosine diphosphate; AMP-adenosine diphosphate; TAN-total adenine nucleotide pool; AEC-adenylate energy charge.

Data are means±SEM; n=5 or 6 (when separated by sex) or =10 or 12 (sexes combined) animals/group. Comparison between groups was performed using a non-parametric Mann-Whitney test. P-value<0.05 was considered significant and presented.

Table 2. Effects of maternal diet on indicators of antioxidant capacity and oxidative stress in fetal cardiac left ventricle from control *ad libitum*-fed pregnancies and in the presence of maternal nutrient reduction (MNR), based on a 70% reduction of the food eaten by the control mothers on a weight-adjusted basis at 0.9 gestation.

	Sexes combined		Male		Female		P-value				
	Control	MNR	Control	MNR	Control	MNR	C vs MNR	Male C vs MNR	Female C vs MNR	Control M vs F	MNR M vs F
Number of animals/group	10	10	5	5	5	5					
GSH (mM)	12±2	14±3	10±2	8±2	14±5	19±5	-	-	-	-	0.047
GSSG (mM)	4±2	3.1±0.9	3±1	1.6±0.5	5±3	5±2	-	-	-	-	-
GSH/GSSG	2.9±0.6	7±2	3.4±0.8	6±1	2.4±0.7	8±3	0.021				
Gl-Px (U/l)	28.5±2.5	23±2	27±3	23±2	30±4	23±3	-	-	-	-	-
Gl-Red (U/l)	79±7	83±5	79±6	87±6	78±14	80 ±9	-	-	-	-	-
Vit E (mM)	80±12	50±3	110±16	55±1	51±2	45±4	-	-	-	-	-
MDA (mM)	1.1±0.1	1.5±0.2	0.9±0.1	1.4±0.1	1.2±0.2	1.6±0.4	0.041	0.028	-	-	-

Data are means ± SEM; n=5 (when separated by sex) or =10 (sexes combined) animals/group. Comparison between groups was performed using a non-parametric Mann-Whitney test. P-value less than 0.05 was considered significant and presented.

12 Figures

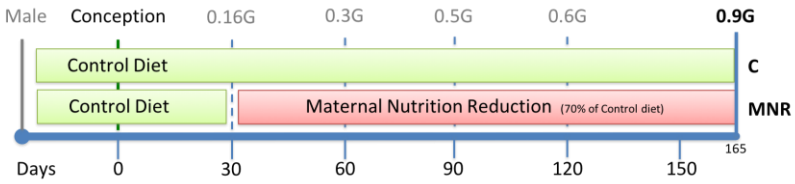

Fig. 1

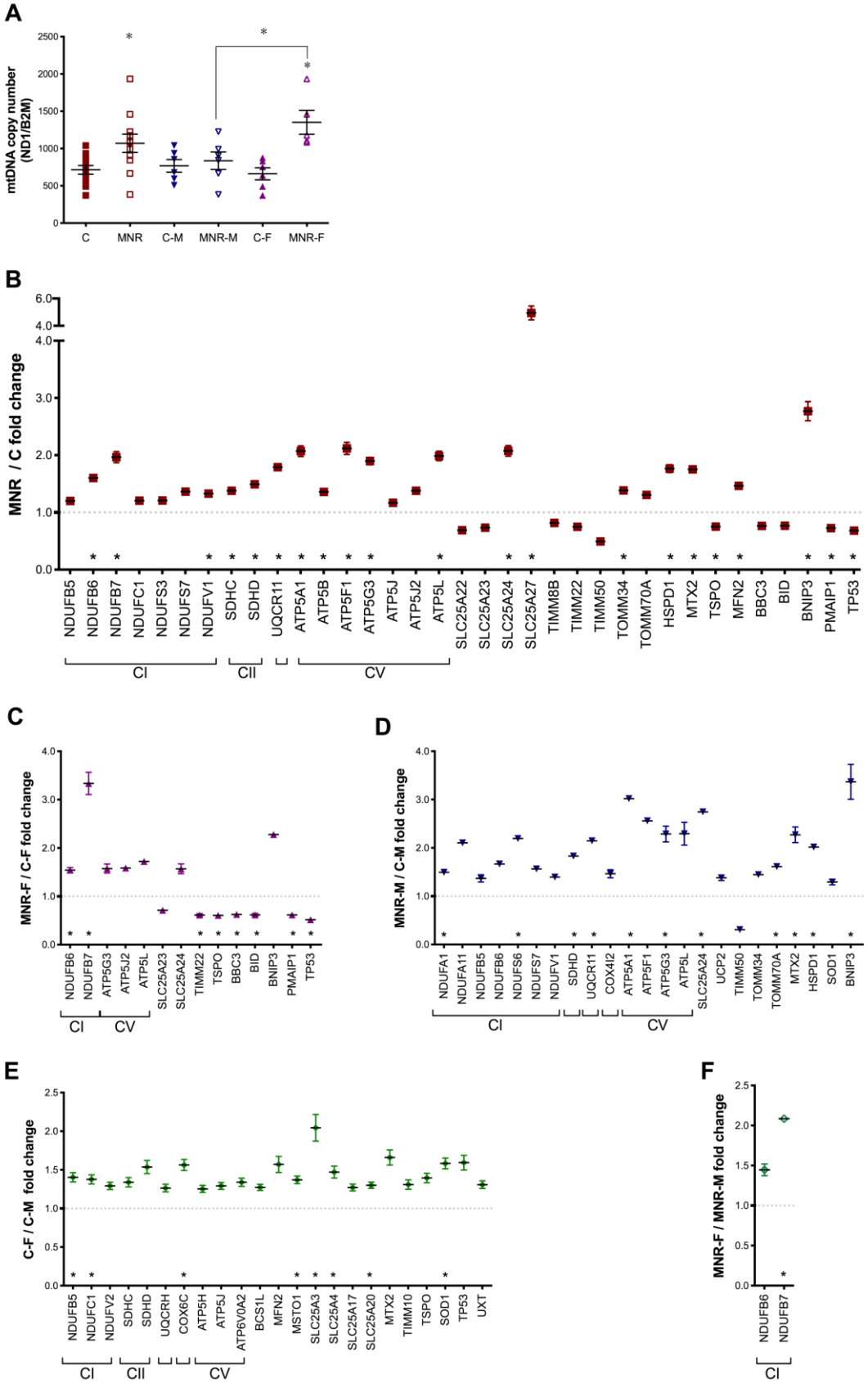
A
mtDNA copy number (ND1/B2M)
C
MNR
C-M
MNR-M
C-F
MNR-F
B
MNR / C fold change
NDUFB5
NDUFB6
NDUFB7
NDUFC1
NDUFS3
NDUFS7
NDUFV1
SDHC
SDHD
UQCR11
ATP5A1
ATP5B
ATP5F1
ATP5G3
ATP5J
ATP5J2
ATP5L
SLC25A22
SLC25A23
SLC25A24
SLC25A27
TIMM8B
TIMM22
TIMM50
TOMM34
TOMM70A
HSPD1
MTX2
TSPO
MFN2
BBC3
BID
BNIP3
PMAIP1
TP53
CI
CII
CV
C
MNR-F / C-F fold change
NDUFB6
NDUFB7
ATP5G3
ATP5J2
ATP5L
SLC25A23
SLC25A24
TIMM22
TSPO
BBC3
BID
BNIP3
PMAIP1
TP53
CI
CV
D
MNR-M / C-M fold change
NDUFA1
NDUFA11
NDUFB5
NDUFB6
NDUFS6
NDUFS7
NDUFV1
SDHD
UQCR11
COX4I2
ATP5A1
ATP5F1
ATP5G3
ATP5L
SLC25A24
UCP2
TIMM50
TOMM34
TOMM70A
MTX2
HSPD1
SOD1
BNIP3
CI
CV
E
C-F / C-M fold change
NDUFB5
NDUFC1
NDUFV2
SDHC
SDHD
UQCRH
COX6C
ATP5H
ATP5J
ATP6V0A2
BCS1L
MFN2
MSTO1
SLC25A3
SLC25A4
SLC25A17
SLC25A20
MTX2
TIMM10
TSPO
SOD1
TP53
UXT
CI
CII
CV
F
MNR-F / MNR-M fold change
NDUFB6
NDUFB7
CI

Fig. 2

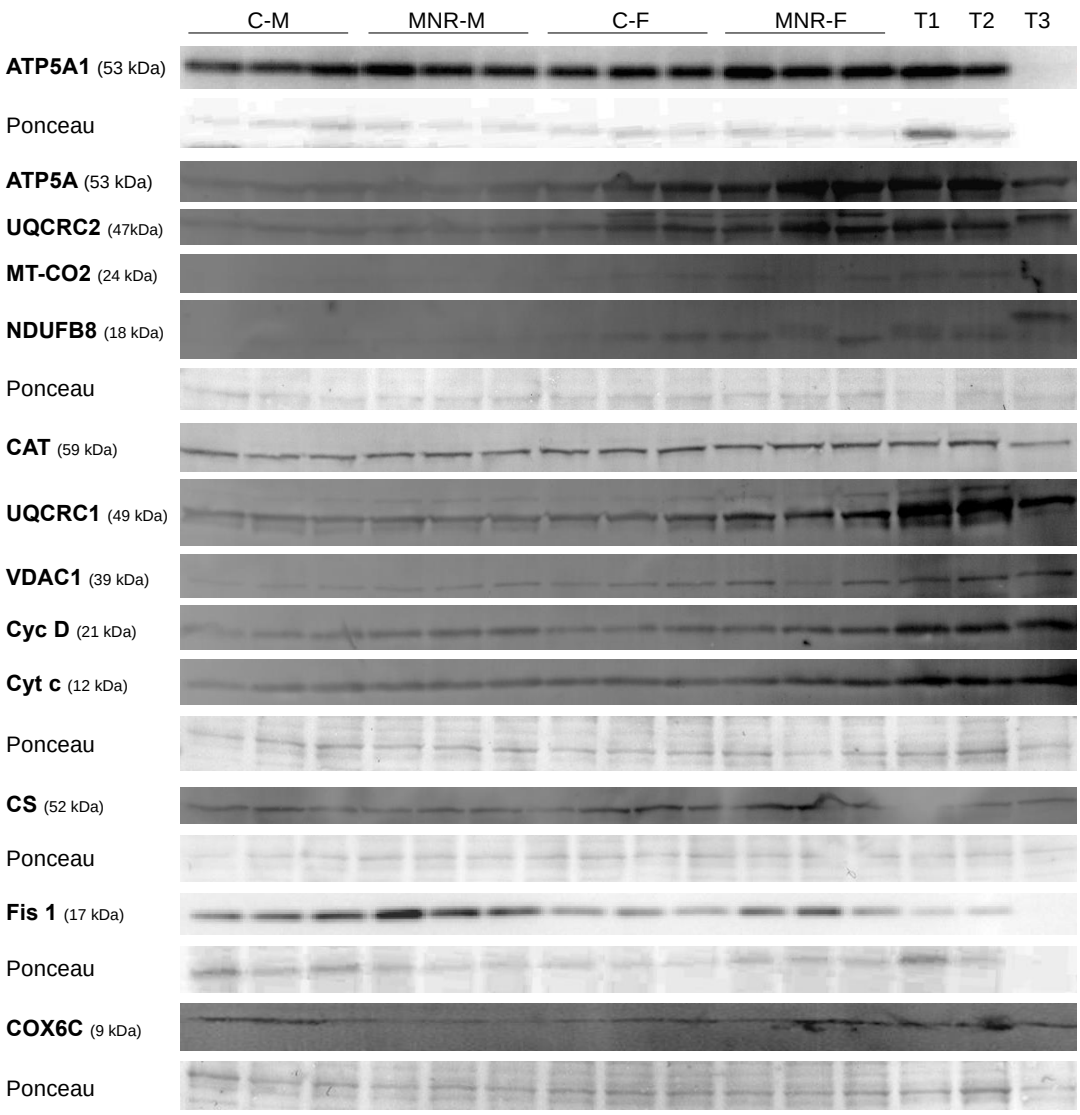

	Sexes combined		Male		Female		P-value by Mann-Whitney test				
	Control	MNR	Control	MNR	Control	MNR	C vs MNR	Male C vs MNR	Female C vs MNR	Control M vs F	MNR M vs F
Number of animals/group	12	12	6	6	6	6					
NDUFB8	1.11 ± 0.05	1.20 ± 0.05	1.00 ± 0.03	1.12 ± 0.01	1.21 ± 0.08	1.28 ± 0.10	0.033	0.010	-	-	0.037
UQCRC1	1.06 ± 0.03	1.17 ± 0.04	1.00 ± 0.02	1.09 ± 0.02	1.12 ± 0.03	1.24 ± 0.08	0.038	0.010	-	0.016	-
UQCRC2	1.12 ± 0.05	1.22 ± 0.05	1.00 ± 0.03	1.14 ± 0.01	1.24 ± 0.07	1.30 ± 0.09	-	0.016	-	0.016	-
MT-CO2	1.11 ± 0.05	1.20 ± 0.06	1.00 ± 0.03	1.11 ± 0.02	1.21 ± 0.08	1.29 ± 0.11	-	0.010	-	0.037	-
COX6C [a]	0.99 ± 0.01	1.01 ± 0.01	1.00 ± 0.01	0.99 ± 0.01	0.98 ± 0.01	1.03 ± 0.01	-	-	0.050	-	0.050
ATP5A1	1.07 ± 0.03	1.17 ± 0.05	1.00 ± 0.02	1.10 ± 0.02	1.14 ± 0.04	1.24 ± 0.09	-	0.025	-	0.006	-
ATP5A	1.11 ± 0.05	1.21 ± 0.05	1.00 ± 0.03	1.13 ± 0.02	1.22 ± 0.06	1.30 ± 0.09	-	0.016	-	0.010	-
CYT C	1.08 ± 0.04	1.20 ± 0.04	1.00 ± 0.02	1.13 ± 0.02	1.16 ± 0.04	1.27 ± 0.08	0.018	0.004	-	0.004	-
VDAC	1.08 ± 0.03	1.19 ± 0.05	1.00 ± 0.02	1.10 ± 0.02	1.16 ± 0.04	1.28 ± 0.09	0.043	0.006	-	0.004	-
CYC D	1.07 ± 0.03	1.17 ± 0.04	1.00 ± 0.02	1.11 ± 0.02	1.13 ± 0.03	1.23 ± 0.07	0.050	0.010	-	0.010	-
CS [b]	0.90 ± 0.04	0.79 ± 0.04	1.00 ± 0.07	0.85 ± 0.03	0.83 ± 0.04	0.73 ± 0.06	-	-	-	-	-
CAT [a]	1.02 ± 0.01	1.05 ± 0.01	1.00 ± 0.01	1.07 ± 0.01	1.04 ± 0.05	1.03 ± 0.06	-	0.050	-	0.050	0.050
FIS1 [a]	0.89 ± 0.08	1.33 ± 0.16	1.00 ± 0.11	1.61 ± 0.15	0.78 ± 0.11	1.05 ± 0.19	0.019	0.037	0.050	-	0.050

Fig. 3

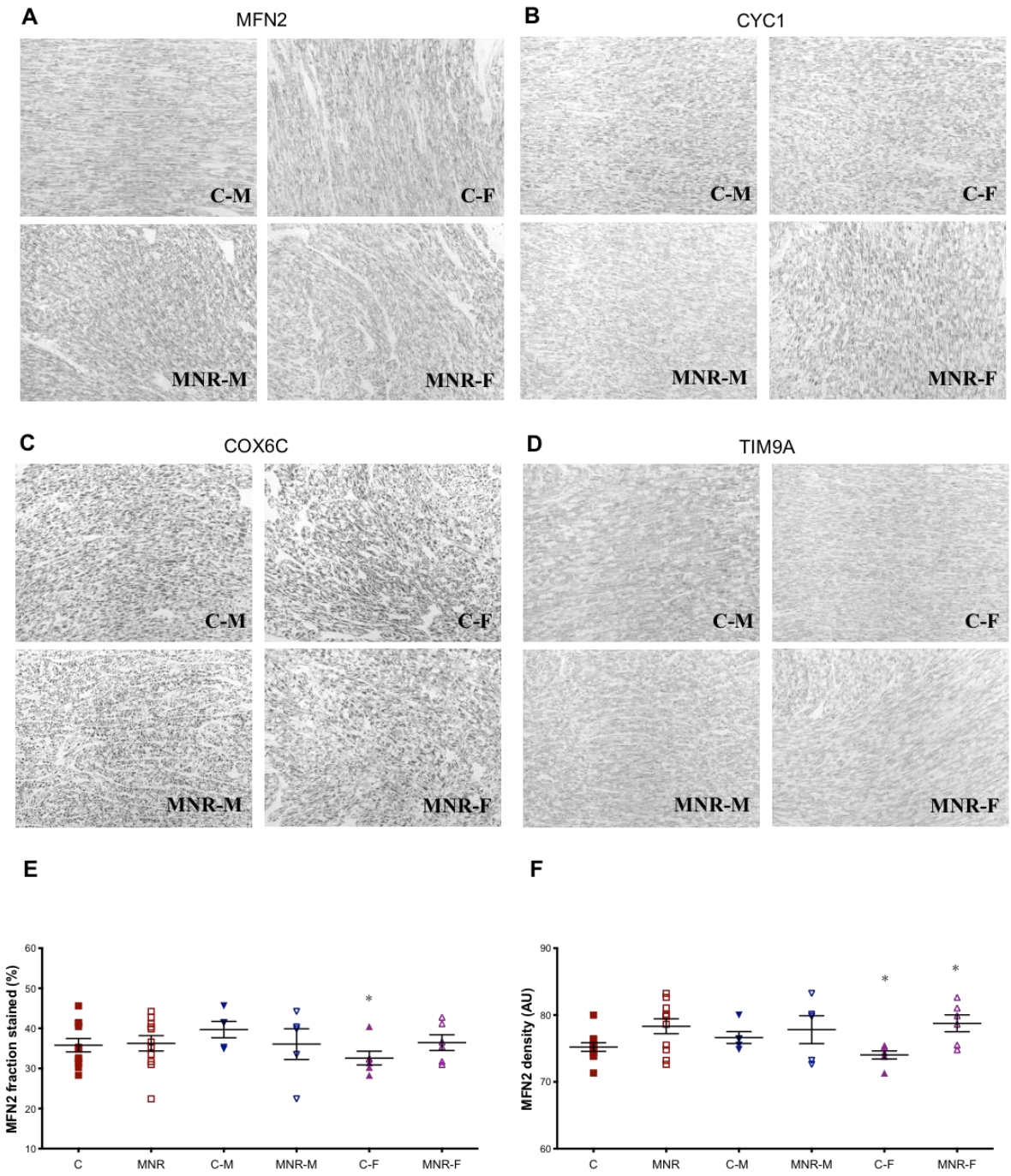
A
MFN2
C-M
C-F
MNR-M
MNR-F
B
CYC1
C-M
C-F
MNR-M
MNR-F
C
COX6C
C-M
C-F
MNR-M
MNR-F
D
TIM9A
C-M
C-F
MNR-M
MNR-F
E
MFN2 fraction stained (%)
60
50
40
30
20
10
C
MNR
C-M
MNR-M
C-F
MNR-F
*
F
MFN2 density (AU)
90
80
70
60
C
MNR
C-M
MNR-M
C-F
MNR-F
*
*

Fig. 4

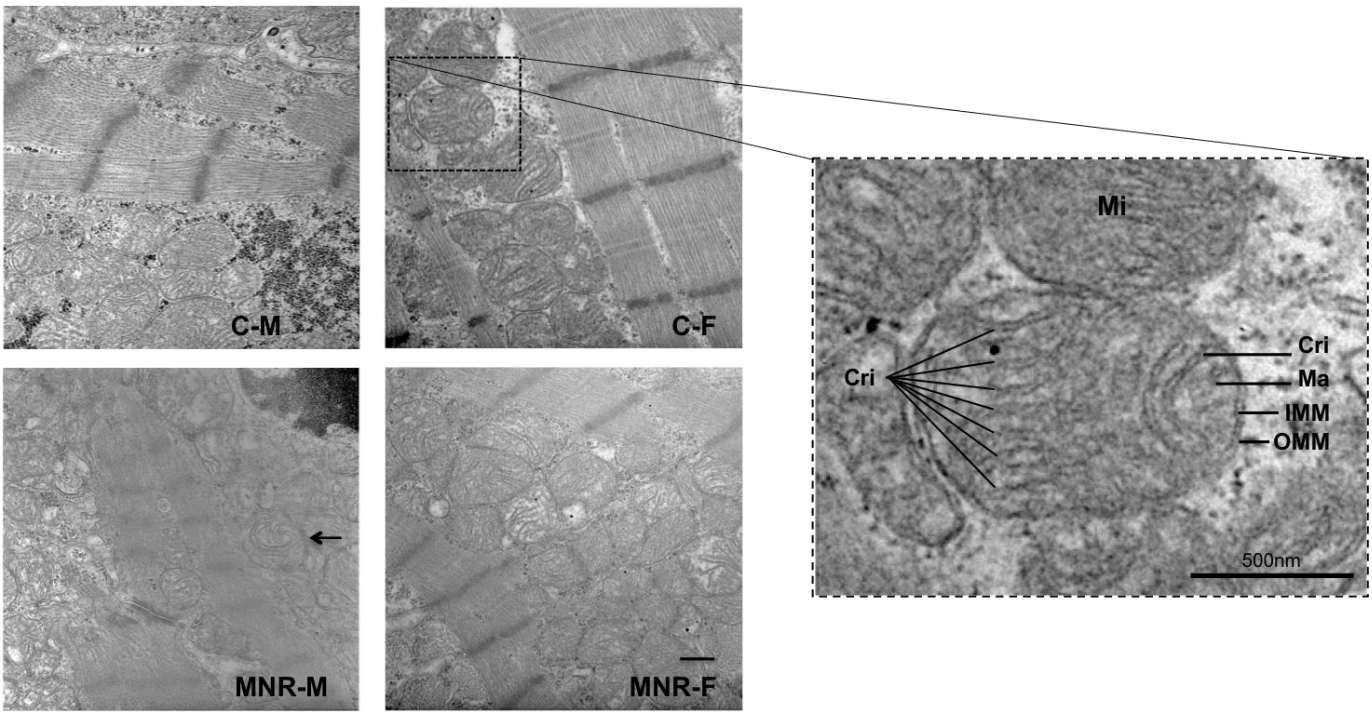

Fig. 5

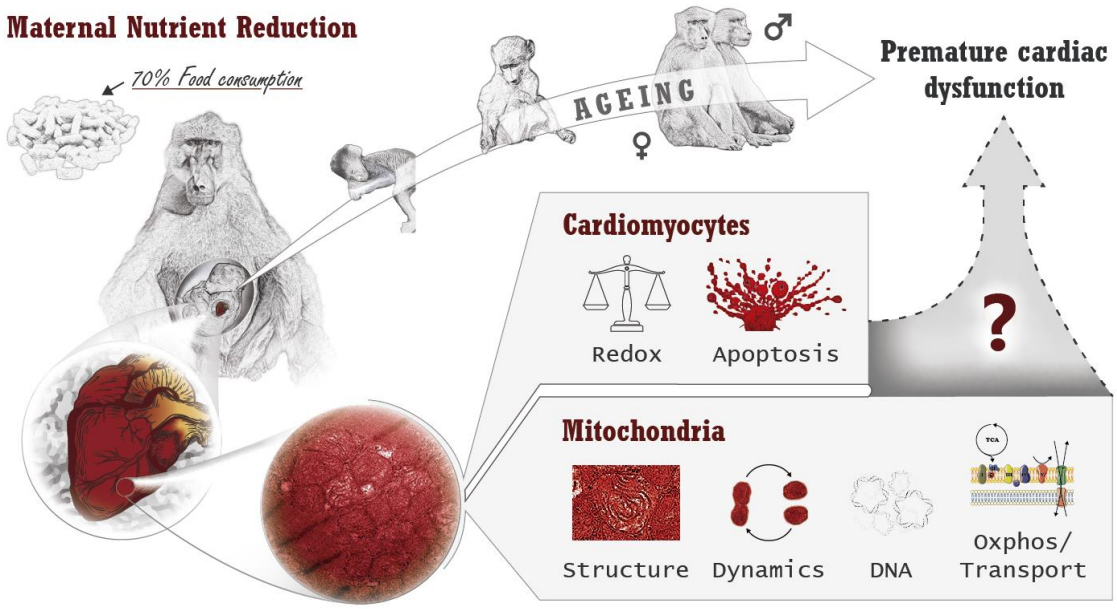
Maternal Nutrient Reduction
70% Food consumption
AGEING
Premature cardiac dysfunction
Cardiomyocytes
Redox
Apoptosis
?
Mitochondria
Structure
Dynamics
DNA
Oxphos/ Transport

Fig. 6

Supplemental material

Sex Dependent Vulnerability of Fetal Nonhuman Primate Cardiac Mitochondria to Moderate Maternal Nutrient Reduction

Susana P. Pereira PhD [a,b,c,*], Ludgero C. Tavares PhD [a,b], Ana I. Duarte PhD [a], Inês Baldeiras PhD [a,d], Teresa Cunha-Oliveira PhD [a], João D. Martins MSc [a], Maria S. Santos PhD [a,b], Alina Maloyan PhD [c,#], António J. Moreno PhD [b], Laura A. Cox PhD [e], Cun Li MD [f], Peter W. Nathanielsz MD [f], Mark J. Nijland PhD [c], and Paulo J. Oliveira PhD [a]

[a] CNC-Center for Neuroscience and Cell Biology, University of Coimbra, 3004-517 Coimbra, Portugal.
[b] Department of Life Sciences, University of Coimbra, 3004-517 Coimbra, Portugal.
[c] Center for Pregnancy and Newborn Research, University of Texas Health Science Center at San Antonio, 78229-3900 San Antonio, Texas, United States
[d] Neurological Clinic, Faculty of Medicine, University of Coimbra, 3004-517 Coimbra, Portugal.
[e] Department of Genetics, Texas Biomedical Research Institute, 78245-0549 San Antonio, Texas, United States.
[f] Wyoming Pregnancy and Life Course Health Center, University of Wyoming, Laramie, Wyoming, 82071-3684
[*] New address: Research Centre in Physical Activity Health and Leisure (CIAFEL), Faculty of Sports, University of Porto, 4200-450 Porto, Portugal.
[#] New address: Knight Cardiovascular Institute, Oregon Health and Science University, Portland, Oregon, USA, 97239

Address for correspondence

Paulo J. Oliveira, PhD,
CNC-Center for Neuroscience and Cell Biology, UC Biotech, Biocant Park, University of Coimbra, 3060-197 Cantanhede, PORTUGAL
phone: +351-231-249-235
fax: +351-239-853409
email: pauloliv@cnc.uc.pt
ORCID: 0000-0002-5201-9948

Susana P. Pereira, PhD,
CNC-Center for Neuroscience and Cell Biology, UC Biotech, Biocant Park, University of Coimbra, 3060-197 Cantanhede, PORTUGAL
phone: +351-231-249-170
fax: +351-239-853409
email: pereirasusan@gmail.com
ORCID: 0000-0002-1168-2444

Table S1. Panel of antibodies used in immunodetection.
Symbol denotes the protein identification, Description gives a summary information about the protein identification and/or function, Acession number denotes the reference from The Universal Protein Resource (UniProt) and Dilution represent the incubation conditions for the respective primary antibody.

Symbol	Description	Acession number[a]	Manufecturer code		Host Species	MW (KDa)	Dilution
NDUFB8	NADH dehydrogenase 1 beta subcomplex subunit 8	O95169	abcam	ab110242	Mouse	20	1:500
SDHB	Succinate dehydrogenase complex subunit B	P21912	abcam	ab14714	Mouse	29	1:500
SDHC	Succinate dehydrogenase complex subunit C	Q99643	Santa Cruz	sc-49491	Goat	12	1:100
UQCRC1	Ubiquinol-cytochrome c reductase core protein II	P31930	abcam	ab110252	Mouse	49	1:500
UQCRC2	Ubiquinol-cytochrome c reductase core protein II	P22695	abcam	ab14745	Mouse	47	1:500
MT-CO2	Cytochrome c oxidase subunit 2	P00403	abcam	ab110258	Mouse	24	1:500
COX6C	Cytochrome c oxidase subunit Vic	P09669	abcam	ab150422	Rabbit	9	1:1000
ATP5A1	ATP synthase subunit alpha, mitochondrial	P25705	abcam	ab14748	Mouse	53	1:500
ATP5A	ATP synthase subunit alpha	P25705	abcam	ab110273	Mouse	55	1:500
CYT C	Cytochrome c	P99999	abcam	ab110325	Mouse	12	1:500
VDAC1	Voltage-dependent anion-selective channel protein 1	P21796	abcam	ab14734	Mouse	39	1:500
CYC D	Cyclophilin D	P30405	abcam	ab110324	Mouse	21	1:500
CS	Citrate synthase	O75390	abcam	ab129088	Rabbit	52	1:1000
CAT	Catalase	P04040	abcam	ab1877	Rabbit	59	1:1000
SOD1	Superoxide dismutase 1	P00441	Santa Cruz	sc-11407	Rabbit	23	1:100
FIS1	Mitochondrial fission 1 protein	Q9Y3D6	Santa Cruz	sc48865	Goat	17	1:500

[a] as provided by the manufacturer and available on http://www.uniprot.org
Antibodies were diluted in 1% non-fat milk in PBS supplemented with 0.02% sodium azide, as a preservative, to a final volume of 5 ml and stored at 4ºC for no longer than 3 months or use to a maximum, of 5 times.

Table S2. List of secondary antibodies used in immunodetection.

Symbol	Description	Manufacturer code		Host Species	Dilution
G@R	goat anti-rabbit IgG-AP	Santa Cruz	sc-2007	Goat	1:5000
G@M	goat anti-mouse IgG-AP	Santa Cruz	sc-2008	Goat	1:5000
R@G	rabbit anti-goat IgG-AP	Santa Cruz	sc-2771	Rabbit	1:5000

Table S3. Panel of antibodies used in immunohistochemistry.
Symbol denotes the protein identification, Description gives a summary information about the protein identification and/or function, Acession number denotes the reference from The Universal Protein Resource (UniProt) and Dilution represent the incubation conditions for the respective primary antibody.

Symbol	Description	Accession number [a]	Manufacturer code		Host Species
CYC1	Cytochrome c-1, UQCR4	P08574	Sigma-Aldrich	HPA001247	Rabbit
COX6C	Cytochrome c oxidase subunit VIc	P09669	Santa Cruz	sc65240	Mouse
MFN2	Mitofusin 2	P25705	Santa Cruz	sc100560	Mouse
SIRT3	Sirtuin 3	Q9NTG7	Cell signaling	2627	Rabbit
SIRT3	Sirtuin 3	Q9NTG7	Cell signaling	5490	Rabbit
TIM9A	Translocase of inner mitochondrial membrane 9A	P25705	Santa Cruz	sc101285	Mouse

[a] as provided by the manufacturer and available on http://www.uniprot.org

Supplemental Figures and Legends

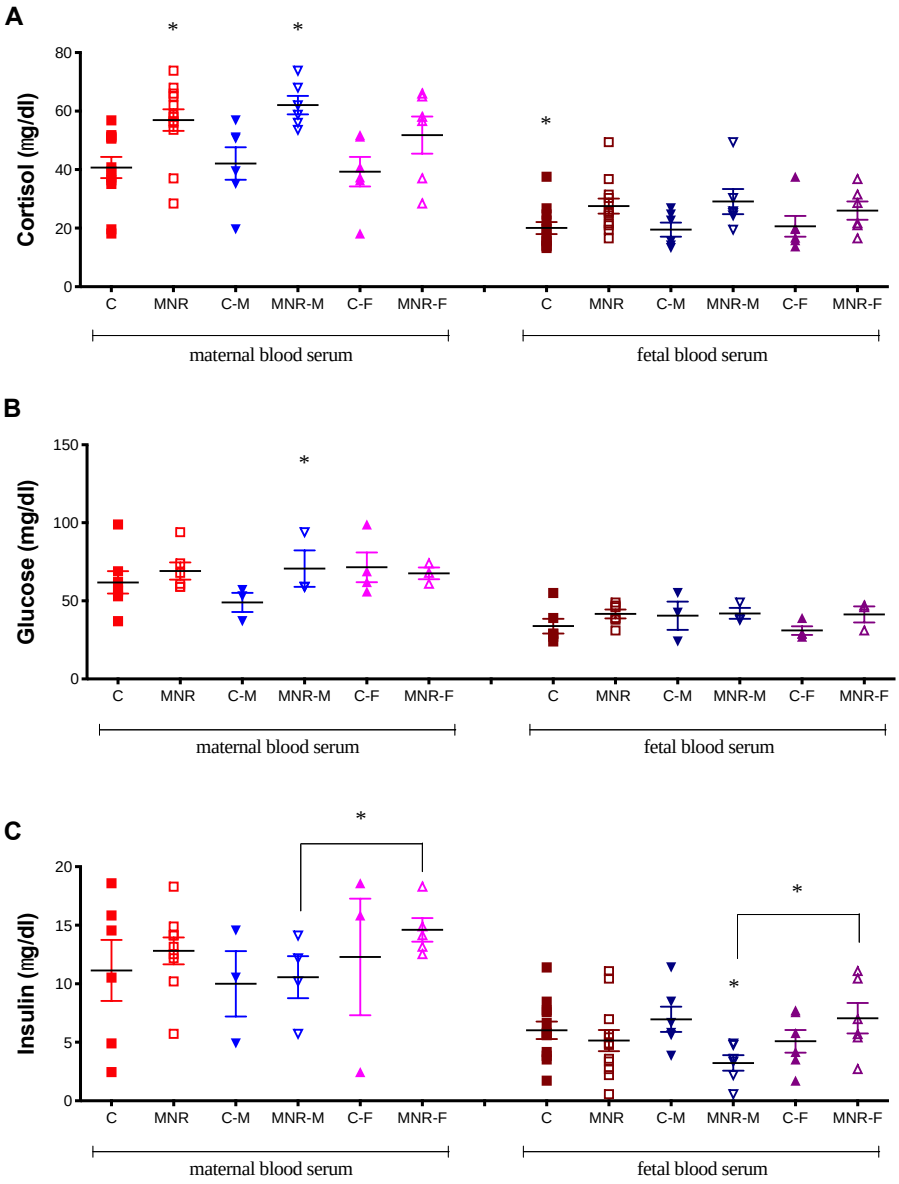

Fig. S1 Related to Table S4 and Table S5; Cortisol, glucose, and insulin levels in maternal and fetal plasma of control (C) and maternal nutrient reduction (MNR) groups. Metabolic parameters in maternal and fetal plasma of control ad libitum-fed pregnancies and in the presence of MNR, characterized as 70% of the food consumed by control mothers on a weight-adjusted basis of baboons at 0.9 gestation. A: cortisol concentrations. in maternal and fetal plasma of control and MNR baboons (male fetuses n=12; female fetuses n=12). C-M, male fetuses of control mothers (n=6); C-F, female fetuses of control mothers (n=6); MNR-M, male fetuses of MNR mothers (n=6); MNR-F, female fetuses of MNR mothers (n=6). B: glucose levels in maternal and fetal plasma of control and MNR baboons (C n=7; MNR n=6; C-M n=3; C-F n=4; MNR-M n=3; MNR-F n=3). C: insulin levels in maternal and fetal plasma of control and MNR baboons (C n=12; MNR n=12; C-M n=6; C-F n=6; MNR-M n=6; MNR-F n=6). Means ± SEM; Comparison between groups was performed using a non-parametric Mann-Whitney test. P-value less than 0.05 was considered significant. *P<0.05 vs. respective controls or as indicated.

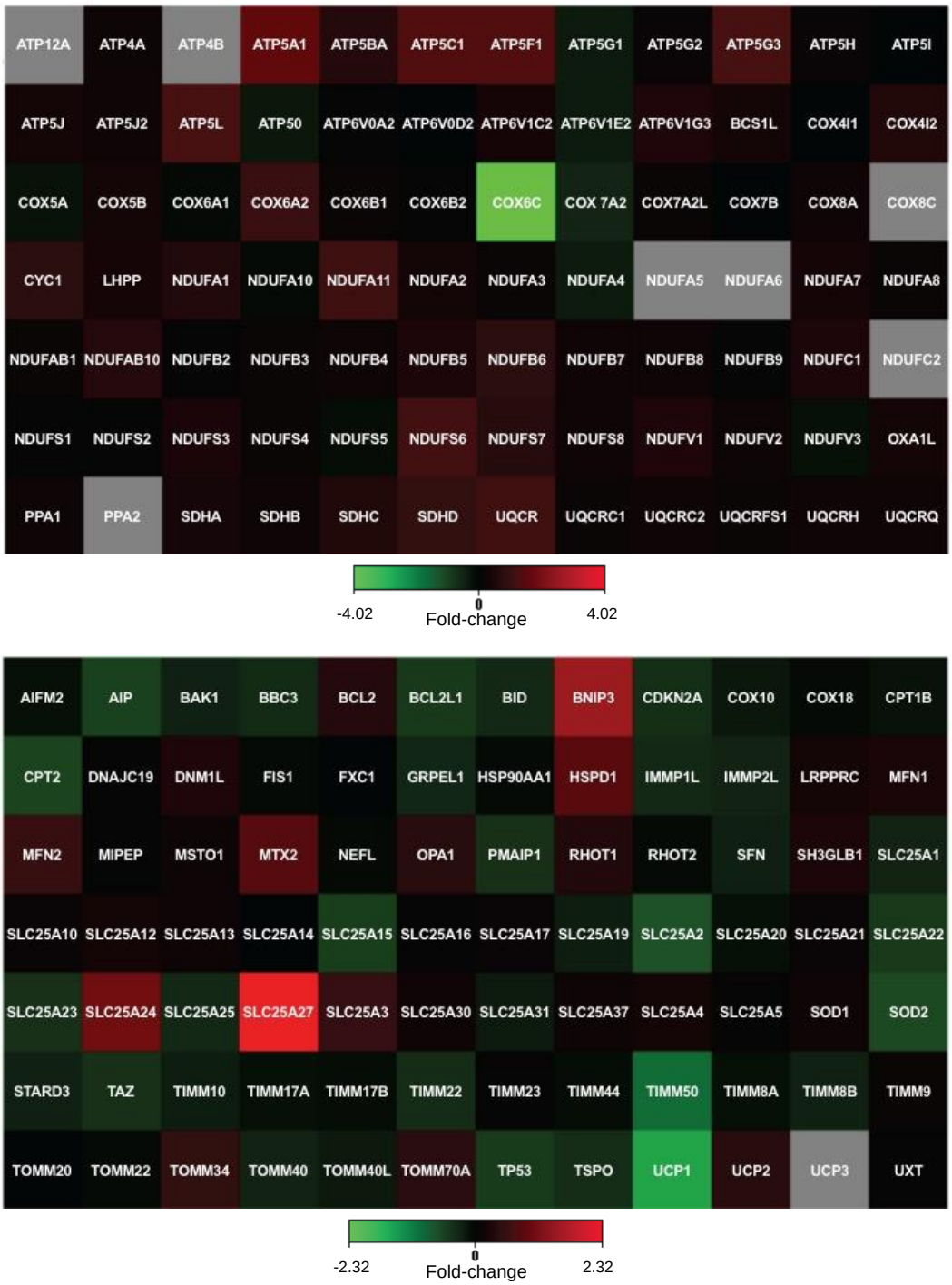

Fig. S2 Related to Fig. 2; Assessing the diet effects on gene expression profile by comparing control (C) and maternal nutrient reduction (MNR) groups.

Maternal nutrient reduction to 70% of the food eaten by the control mothers on a weight-adjusted basis leads to changes in gene expression profile in fetal cardiac left ventricle tissue. The heat map represents the transcriptome profile assessed in The Human Mitochondrial Energy Metabolism (top) and in the Human Mitochondria (bottom) pathway arrays in response to MNR when both sexes were combined. Red and green indicate increased and decreased expression, respectively, relative to the control group. Values were normalized to endogenous controls [hypoxanthine phosphoribosyltransferase 1 (*HPRT1*), ribosomal protein L13a (*RPL13A*), and Beta-actin (*ACTB*)] and expressed relative to their normalized values. n=12 animals/group (sexes combined). Cells in the heat map which are colored gray correspond to genes with erroneous fold changes, that is, this transcript average threshold cycle is either not determined or greater than the defined cut-off value (Ct = 35), in at least one of the groups, meaning that the fold-change must be considered erroneous and

uninterpretable.

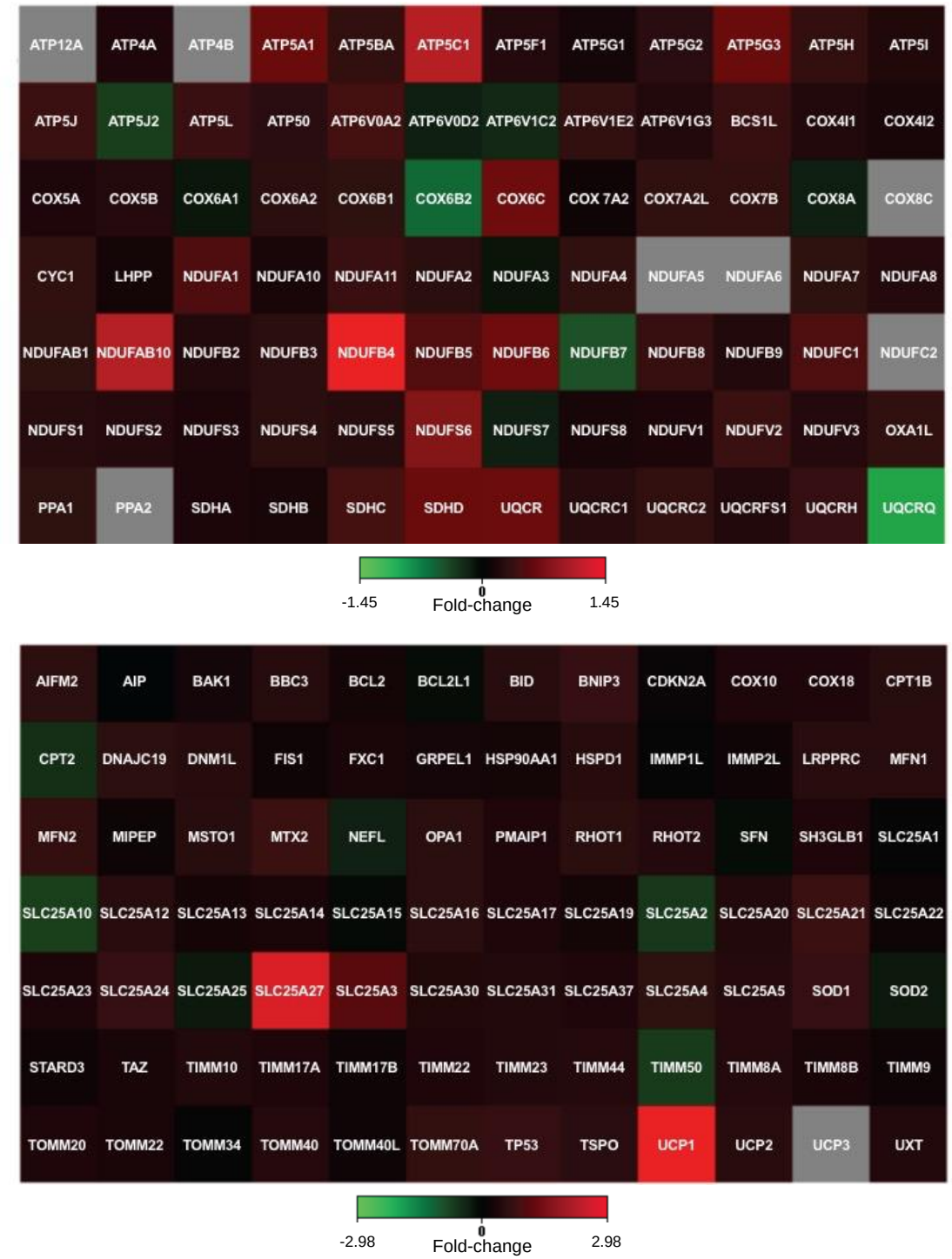

Fig. S3 Related to Fig. 2; Sex of fetus effects in the gene expression profile. Expression profile comparison for control fetal cardiac left ventricular tissue. The heat map represents the transcriptome profile assessed in The Human Mitochondrial Energy Metabolism (top) and in the Human Mitochondria (bottom) pathway arrays analyzed by fetal sex only for the control group. Red and green indicate increased and decreased expression, respectively, relative to control male fetuses. Values were normalized to endogenous controls [hypoxanthine phosphoribosyltransferase 1 (*HPRT1*), ribosomal protein L13a (*RPL13A*), and Beta-actin (*ACTB*)] and expressed relative to their normalized values. n=6 animals/group. Cells in the heat map which are colored gray correspond to genes with erroneous fold changes, that is, this transcript average threshold cycle was either not determined or greater than the defined cut-off value (Ct = 35), in at least one of the groups, meaning that its expression was undetected, making this fold-change result erroneous and uninterpretable.

Supplemental Tables

Table S4. Maternal and fetal morphometrics at 0.9 gestation in fetuses of control *ad libitum*-fed mothers and fetuses of mothers experiencing maternal nutrient reduction (MNR) to 70% of the food eaten by the control mothers on a weight-adjusted basis. See also Fig. S2 and Table S5.

	Sexes combined		Male		Female		P-value				
	Control	MNR	Control	MNR	Control	MNR	Diet	Male C vs MNR	Female C vs MNR	Control M vs F	MNR M vs F
Number of animals/group	12	12	6	6	6	6					
Maternal											
Weight preconception (Kg)	16.3±0.7	16.6±1.2	16.0±1.2	16.8±1.7	16.6±1.0	16.4±1.7	-	-	-	-	-
Weight at cesarean section (Kg)	18.3±0.7	16.4±1.1	18.5±1.2	15.9±1.7	18.12±0.9	17.0±1.5	-	-	-	-	-
Weight gain (%)	**12.8±2.1**	**-3.1±3.0**	**16.2±3.2**	**-7.1±3.7**	**9.5±2.3**	**1.8±4.2**	**0.001**	**0.006**	-	-	-
Placental weight (g)	**213.3±14.3**	**164.1±11.2**	**223.1±21.2**	**164.7±13.3**	**203.5±20.4**	**163.2±21.3**	**0.019**	**0.045**	-	-	-
Fetal											
Weight (g)	**816.93 ± 33.93**	**716.7±24.1**	**866.7±47.6**	**726.9±26.9**	**767.2±42.5**	**706.4±42.3**	**0.050**	**0.037**	-	-	-
Body length (cm)	37.54 ± 0.84	38.1±1.5	38.8±1.3	36.8±1.0	36.3±0.9	39.3±2.9	-	-	-	-	-
Femur length (cm)	**7.44 ± 0.18**	**6.9±0.2**	**7.3±0.2**	**7.0±0.3**	**7.5±0.3**	**6.8±0.1**	**0.032**	-	-	-	-
Chest circumference (cm)	**17.6±0.3**	**16.8±0.3**	**17.6±0.4**	**16.6±0.4**	**17.7±0.4**	**16.9±0.4**	**0.040**				
Body mass index (Kg/m^2)	5.8±0.2	5.1±0.3	5.8±0.3	5.4±0.3	5.8±0.2	4.8±0.6	-	-	-	-	-
Heart weight (g)	4.9±0.3	4.2±0.2	5.0±0.3	4.1±0.3	4.8±0.5	4.3±0.4	-	-	-	-	-
Heart weight/body weight (x1000)	6.0±0.2	5.4±0.5	5.8 ±0.2	4.7±1.0	6.2±0.4	6.0±0.2	-	-	-	-	-
Brain weight (g)	78.9±2.2	78.4±1.5	82.2±2.6	78.9±2.5	76.1±3.2	77.9±2.0	-	-	-	-	-
Brain weight/body weight (x1000)	**99.5±3.8**	**110.4±3.4**	**99.0±7.8**	**108.7±2.2**	**99.8±3.4**	**112.1±6.7**	**0.019**	-	-	-	-

Data are expressed as mean ± SEM. Comparison between groups was performed using a non-parametric Mann-Whitney test. P-value less than 0.05 was considered significant and presented.

Table S5. Maternal blood serum biochemical parameters at 0.9 gestation in fetuses of control *ad libitum*-fed mothers pregnancies and fetuses of mothers experiencing maternal nutrient reduction (MNR) to 70% of the food eaten by the control mothers on a weight-adjusted basis. Data are expressed as mean ± SE. Comparison between groups was performed using a non-parametric Mann-Whitney test. P-value less than 0.05 was considered significant and presented.

	Sexes combined		Male		Female		P-value				
	Control	MNR	Control	MNR	Control	MNR	Diet	Male C vs MNR	Female C vs MNR	Control M vs F	MNR M vs F
Number of animals/group	7	6	3	3	4	3					
Blood serum at cesarean section							-	-	-	-	-
Blood urea nitrogen (mg/dl)	8.9±0.5	9.3±1.0	8.0±0.6	7.7±0.3	9.5±0.7	11.0±1.5	-	-	-	-	-
Creatinine (mg/dl)	0.9±0.1	1.0±0.1	0.8±0.1	0.9±0.1	0.9±0.1	1.10±0.2	-	-	-	-	-
Blood urea nitrogen/Creatinine	10.1±0.7	9.6±1.4	9.7±0.8	8.3±0.9	10.4±1.1	10.8±2.8	-	-	-	-	-
Sodium (mEq/l)	140.9±0.8	140.5±1.1	140.3±1.7	142.0±1.2	141.3±0.8	139.0±1.5	-	-	-	-	-
Potassium (mEq/l)	3.56±0.1	3.7±0.2	3.8±0.2	3.7±0.1	3.4±0.1	3.6±0.3	-	-	-	-	-
Chloride (mEq/l)	**111.9±0.7**	**109.5±1.4**	**112.3±1.7**	**111.0±2.5**	**111.5±0.3**	**108.0±1.2**	**-**	**-**	**0.031**	**-**	**-**
Carbon dioxide (mEq/l)	22.1±0.7	21.2±1.1	23.0±0.6	22.3±0.7	21.5±1.2	20.0±2.0	-	-	-	-	-
Anion Gap (mEq/l)	10.4±1.1	13.5±1.5	8.8±0.4	12.4±2.2	11.7±1.7	14.6±2.2	-	-	-	-	-
Calcium (mg/dl)	8.5±0.1	8.4±0.1	8.4±0.2	8.2±0.0	8.5±0.1	8.7± 0.3	-	-	-	-	-
Phosphorus (mg/dl)	3.2±0.2	3.2±0.1	3.3±0.1	3.3±0.2	3.0±0.4	3.1±0.2	-	-	-	-	-
Albumin (g/dl)	2.9±0.2	2.7±0.1	2.9±0.0	2.7±0.1	2.8±0.3	2.7±0.1	-	-	-	-	-
Total protein (g/dl)	6.4±0.2	6.3±0.2	6.4±0.1	6.0±0.3	6.3±0.4	6.6 ±0.2	-	-	-	-	-
Total bilirubin (mg/dl)	0.3±0.1	0.3±0.1	0.3±0.1	0.3 ±0.1	0.2±0.0	0.4±0.2	-	-	-	-	-
Alkaline phosphatase (U/l)	130.1±25.3	178.7±43.5	171.3±53.4	163.3±13.9	99.3±8.5	194.0±95.0	-	-	-	-	-
Alanine aminotransferase (U/l)	45.1±9.1	58.5±12.5	36.0±10.0	53.3±14.0	52.0±14.3	63.7±23.7	-	-	-	-	-
Aspartate aminotransferase (U/l)	**21.7±2.3**	**37.3±7.0**	**22.0±2.7**	**38.7±11.8**	**21.5±3.8**	**36.0±10.2**	**0.038**	**-**	**-**	**-**	**-**
Gamma-glutamyl transferase (U/l)	31.5±1.4	32.4 ±1.0	31.0±2.7	32.7±1.8	32.0±1.5	32.0±1.0	-	-	-	-	-
Cholesterol (mg/dl)	60.6±6.0	64.2±7.5	62.3±14.3	57.3±8.2	59.3±4.5	71.0±13.0	-	-	-	-	-
Triglycerides (mg/dl)	32.0±4.1	51.8±7.0	29.3±5.7	52.7±8.4	34.7±6.7	50.5±16.5	-	-	-	-	-
Lactate dehydrogenase (U/l)	184.0±15.7	191.0±15.9	167.3±15.5	197.3±28.1	200.7±26.7	181.5±2.5	-	-	-	-	-
Creatine phosphokinase (U/l)	**281.0±52.2**	**357.4±128.2**	**376.7±61.0**	**390.7±230.4**	**185.3±27.5**	**307.5±33.5**	**-**	**-**	**-**	**0.050**	**-**

Table S6. Related to Fig. 2; mRNA abundance of mitochondrial proteins assessed by PCR. mRNA levels in cardiac left ventricle samples at 0.9 gestation from baboon fetuses of mothers fed *ad libitum* (controls, C) or 70% of the control diet (maternal nutrient reduction, MNR). Symbol denotes the gene identification, RefSeq denotes the Reference Sequence from the National Center for Biotechnology Information collection, Description gives summary information about the gene identification and/or function, Fold difference was calculated between the groups reported, positive values for up-regulation and negative values for a down-regulation. Fold differences relevant to the mitochondrial profile of the fetuses of control mothers (control female, C-F vs. control male, C-M) were presented in the C-F vs. C-M section, as well the comparison of transcripts expression based on maternal diet for the same sex (in the MNR-M vs. C-M and MNR-F vs. C-F sections), the sex dimorphism in the mitochondrial profile of the MNR fetus (in the MNR-F vs. MNR-M section) and global maternal diet-dependent effects in the mitochondrial expression profile (MNR vs. C section). The transcripts presented in bold have either a significance of $0.05<P<0.1$ or $P<0.05$.

Symbol	Refseq	Description	Fold difference	P-value
		C-F vs. C-M		
ATP6V0A2	NM_012463	ATPase, H+ transporting, lysosomal V0 subunit a2	1.339	0.070
BCS1L	NM_004328	BCS1-like (S. cerevisiae)	1.272	0.053
COX6C	NM_004374	Cytochrome c oxidase subunit VIc	**1.563**	**0.010**
NDUFB5	NM_002492	NADH dehydrogenase (ubiquinone) 1 beta subcomplex, 5	**1.404**	**0.034**
NDUFC1	NM_002494	NADH dehydrogenase (ubiquinone) 1, subcomplex unknown, 1	**1.376**	**0.042**
SDHC	NM_003001	Succinate dehydrogenase complex, subunit C, integral membrane protein	1.339	0.089
SDHD	NM_003002	Succinate dehydrogenase complex, subunit D, integral membrane protein	1.537	0.066
UQCRH	NM_006004	Ubiquinol-cytochrome c reductase hinge protein	1.264	0.086
MFN2	NM_014874	Mitofusin 2, mediator of mitochondrial fusion	1.570	0.092
MSTO1	NM_018116	Misato homolog 1, mitochondrial distribution and morphology regulator	**1.370**	**0.034**
MTX2	NM_006554	Metaxin 2, mitochondrial outer membrane import complex protein 2	1.661	0.068
SLC25A17	NM_006358	Solute carrier family 25 (mitochondrial carrier; peroxisomal membrane protein), member 17	1.271	0.073
SLC25A20	NM_000387	Solute carrier family 25 (carnitine/acylcarnitine translocase), member 20	**1.300**	**0.045**
SLC25A3	NM_002635	Solute carrier family 25 (mitochondrial carrier; phosphate carrier), member 3	**2.044**	**0.016**
SLC25A4	NM_001151	Solute carrier family 25 (mitochondrial carrier; adenine nucleotide translocator), member 4, ANT1	**1.471**	**0.049**
SOD1	NM_000454	Superoxide dismutase 1, soluble, Cu/Zn superoxide dismutase	**1.583**	**0.015**
TIMM10	NM_012456	Translocase of inner mitochondrial membrane 10 homolog (yeast)	1.309	0.099
TP53	NM_000546	Tumor protein p53, P53 tumor suppressor	1.593	0.070
TSPO	NM_000714	Translocator protein (18kDa), transport of cholesterol	1.395	0.083

UXT	NM_004182	Ubiquitously-expressed transcript	1.308	0.060
		MNR-M vs. C-M		
ATP5A1	NM_004046	ATP synthase, H+ transporting, mitochondrial F1 complex, alpha subunit 1	**3.019**	**0.012**
ATP5G3	NM_001689	ATP synthase, H+ transporting, mitochondrial Fo complex, subunit C3	**2.287**	**0.010**
ATP5L	NM_006476	ATP synthase, H+ transporting, mitochondrial Fo complex, subunit G	2.294	0.058
COX4I2	NM_032609	Cytochrome c oxidase subunit IV isoform 2	1.464	0.071
NDUFA1	NM_004541	NADH dehydrogenase (ubiquinone) 1 alpha subcomplex, 1	**1.495**	**0.041**
NDUFA11	NM_175614	NADH dehydrogenase (ubiquinone) 1 alpha subcomplex, 11	2.103	0.070
NDUFB5	NM_002492	NADH dehydrogenase (ubiquinone) 1 beta subcomplex, 5	1.368	0.079
NDUFB6	NM_182739	NADH dehydrogenase (ubiquinone) 1 beta subcomplex, 6	1.666	0.084
NDUFS6	NM_004553	NADH dehydrogenase (ubiquinone) Fe-S protein 6	**2.194**	**0.027**
NDUFS7	NM_024407	NADH dehydrogenase (ubiquinone) Fe-S protein 7	1.563	0.094
NDUFV1	NM_007103	NADH dehydrogenase (ubiquinone) flavoprotein 1	1.396	0.081
SDHD	NM_003002	Succinate dehydrogenase complex, subunit D, integral membrane protein	**1.830**	**0.047**
UQCR11	NM_006830	Ubiquinol-cytochrome c reductase, complex III subunit XI	**2.145**	**0.026**
BNIP3	NM_004052	BCL2/adenovirus E1B 19kDa interacting protein 3, pro-apoptotic factor	**3.367**	**0.023**
HSPD1	NM_002156	Heat shock 60kDa protein 1, chaperonin family, folding and assembly of proteins	**2.018**	**0.018**
MTX2	NM_006554	Metaxin 2, mitochondrial outer membrane import complex protein 2	**2.271**	**0.019**
SLC25A24	NM_013386	Solute carrier family 25 (mitochondrial carrier; phosphate carrier), member 24	**2.745**	**0.019**
SOD1	NM_000454	Superoxide dismutase 1, soluble, Cu/Zn superoxide dismutase	1.293	0.098
TIMM50	NM_001001563	Translocase of inner mitochondrial membrane 50 homolog (S. cerevisiae)	-3.232	0.053
TOMM34	NM_006809	Translocase of outer mitochondrial membrane 34	1.446	0.099
TOMM70A	NM_014820	Translocase of outer mitochondrial membrane 70 homolog A (S. cerevisiae)	**1.612**	**0.048**
UCP2	NM_003355	Uncoupling protein 2 (mitochondrial, proton carrier), SLC25A8, proton leak	1.380	0.073
		MNR-F vs. C-F		
ATP5G3	NM_001689	ATP synthase, H+ transporting, mitochondrial Fo complex, subunit C3	1.575	0.093
ATP5J2	NM_004889	ATP synthase, H+ transporting, mitochondrial Fo complex, subunit F2	1.586	0.082
ATP5L	NM_006476	ATP synthase, H+ transporting, mitochondrial Fo complex, subunit G	**1.721**	**0.037**

NDUFB6	NM_182739	NADH dehydrogenase (ubiquinone) 1 beta subcomplex, 6	**1.542**	**0.008**
NDUFB7	NM_004146	NADH dehydrogenase (ubiquinone) 1 beta subcomplex, 7	**3.336**	**0.001**
BBC3	NM_014417	BCL2 binding component 3	**-1.596**	**0.032**
BID	NM_001196	BH3 interacting domain death agonist	**-1.622**	**0.028**
BNIP3	NM_004052	BCL2/adenovirus E1B 19kDa interacting protein 3, pro-apoptotic factor	2.278	0.098
PMAIP1	NM_021127	Phorbol-12-myristate-13-acetate-induced protein 1, related to activation of caspases and apoptosis	**-1.624**	**0.025**
SLC25A23	NM_024103	Solute carrier family 25 (mitochondrial carrier; phosphate carrier), member 23	-1.405	0.080
SLC25A24	NM_013386	Solute carrier family 25 (mitochondrial carrier; phosphate carrier), member 24	1.570	0.052
TIMM22	NM_013337	Translocase of inner mitochondrial membrane 22 homolog (yeast)	**-1.631**	**0.024**
TP53	NM_000546	Tumor protein p53, P53 tumor suppressor	**-1.933**	**0.021**
TSPO	NM_000714	Translocator protein (18kDa), transport of cholesterol	**-1.651**	**0.020**
		MNR-F vs. MNR-M		
NDUFB6	NM_182739	NADH dehydrogenase (ubiquinone) 1 beta subcomplex, 6	1.447	0.057
NDUFB7	NM_004146	NADH dehydrogenase (ubiquinone) 1 beta subcomplex, 7	**2.084**	**0.014**
		MNR vs. C		
ATP5A1	NM_004046	ATP synthase, H+ transporting, mitochondrial F1 complex, alpha subunit 1	**2.071**	**0.004**
ATP5B	NM_001686	ATP synthase, H+ transporting, mitochondrial F1 complex, beta polypeptide	**1.360**	**0.048**
ATP5F1	NM_001688	ATP synthase, H+ transporting, mitochondrial Fo complex, subunit B1	**2.120**	**0.024**
ATP5G3	NM_001689	ATP synthase, H+ transporting, mitochondrial Fo complex, subunit C3	**1.898**	**0.002**
ATP5J	NM_001685	ATP synthase, H+ transporting, mitochondrial Fo complex, subunit F6	1.168	0.094
ATP5J2	NM_004889	ATP synthase, H+ transporting, mitochondrial Fo complex, subunit F2	1.380	0.069
ATP5L	NM_006476	ATP synthase, H+ transporting, mitochondrial Fo complex, subunit G	**1.987**	**0.003**
NDUFB5	NM_002492	NADH dehydrogenase (ubiquinone) 1 beta subcomplex, 5	1.202	0.088
NDUFB6	NM_182739	NADH dehydrogenase (ubiquinone) 1 beta subcomplex, 6	**1.603**	**0.004**
NDUFB7	NM_004146	NADH dehydrogenase (ubiquinone) 1 beta subcomplex, 7	**1.966**	**0.013**
NDUFC1	NM_002494	NADH dehydrogenase (ubiquinone) 1, subcomplex unknown, 1	1.207	0.090
NDUFS3	NM_004551	NADH dehydrogenase (ubiquinone) Fe-S protein 3	1.209	0.066
NDUFS7	NM_024407	NADH dehydrogenase (ubiquinone) Fe-S protein 7	1.363	0.051
NDUFV1	NM_007103	NADH dehydrogenase (ubiquinone) flavoprotein 1	**1.328**	**0.012**

SDHC	NM_003001	Succinate dehydrogenase complex, subunit C, integral membrane protein	**1.379**	**0.040**
SDHD	NM_003002	Succinate dehydrogenase complex, subunit D, integral membrane protein	**1.491**	**0.027**
UQCR11	NM_006830	Ubiquinol-cytochrome c reductase, complex III subunit XI	**1.790**	**0.023**
BBC3	NM_014417	BCL2 binding component 3	-1.309	0.054
BID	NM_001196	BH3 interacting domain death agonist	-1.304	0.066
BNIP3	NM_004052	BCL2/adenovirus E1B 19kDa interacting protein 3, pro-apoptotic factor	**2.770**	**0.003**
HSPD1	NM_002156	Heat shock 60kDa protein 1, chaperonin family, folding and assembly of proteins	**1.766**	**0.009**
MFN2	NM_014874	Mitofusin 2, mediator of mitochondrial fusion	**1.465**	**0.041**
MTX2	NM_006554	Metaxin 2, mitochondrial outer membrane import complex protein 2	**1.754**	**0.004**
PMAIP1	NM_021127	Phorbol-12-myristate-13-acetate-induced protein 1, related to activation of caspases and apoptosis	**-1.375**	**0.023**
SLC25A22	NM_024698	Solute carrier family 25 (mitochondrial carrier: glutamate), member 22	**-1.449**	**0.045**
SLC25A23	NM_024103	Solute carrier family 25 (mitochondrial carrier; phosphate carrier), member 23	-1.363	0.061
SLC25A24	NM_013386	Solute carrier family 25 (mitochondrial carrier; phosphate carrier), member 24	**2.076**	**0.001**
SLC25A27	NM_004277	Solute carrier family 25, member 27, UCP4	**4.942**	**0.044**
TIMM22	NM_013337	Translocase of inner mitochondrial membrane 22 homolog (yeast)	-1.336	0.051
TIMM50	NM_001001563	Translocase of inner mitochondrial membrane 50 homolog (S. cerevisiae)	-2.031	0.062
TIMM8B	NM_012459	Translocase of inner mitochondrial membrane 8 homolog B (yeast)	-1.223	0.052
TOMM34	NM_006809	Translocase of outer mitochondrial membrane 34	**1.383**	**0.026**
TOMM70A	NM_014820	Translocase of outer mitochondrial membrane 70 homolog A (S. cerevisiae)	1.305	0.100
TP53	NM_000546	Tumor protein p53, P53 tumor suppressor	**-1.468**	**0.027**
TSPO	NM_000714	Translocator protein (18kDa), transport of cholesterol	**-1.332**	**0.041**

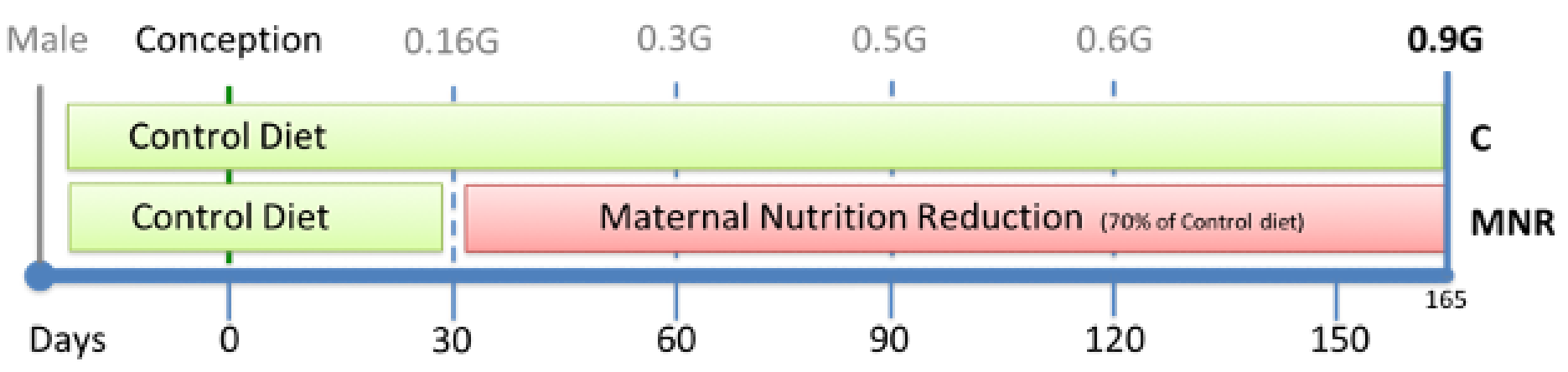
Male
Conception
0.16G
0.3G
0.5G
0.6G
0.9G
Control Diet
C
Control Diet
Maternal Nutrition Reduction (70% of Control diet)
MNR
165
Days
0
30
60
90
120
150

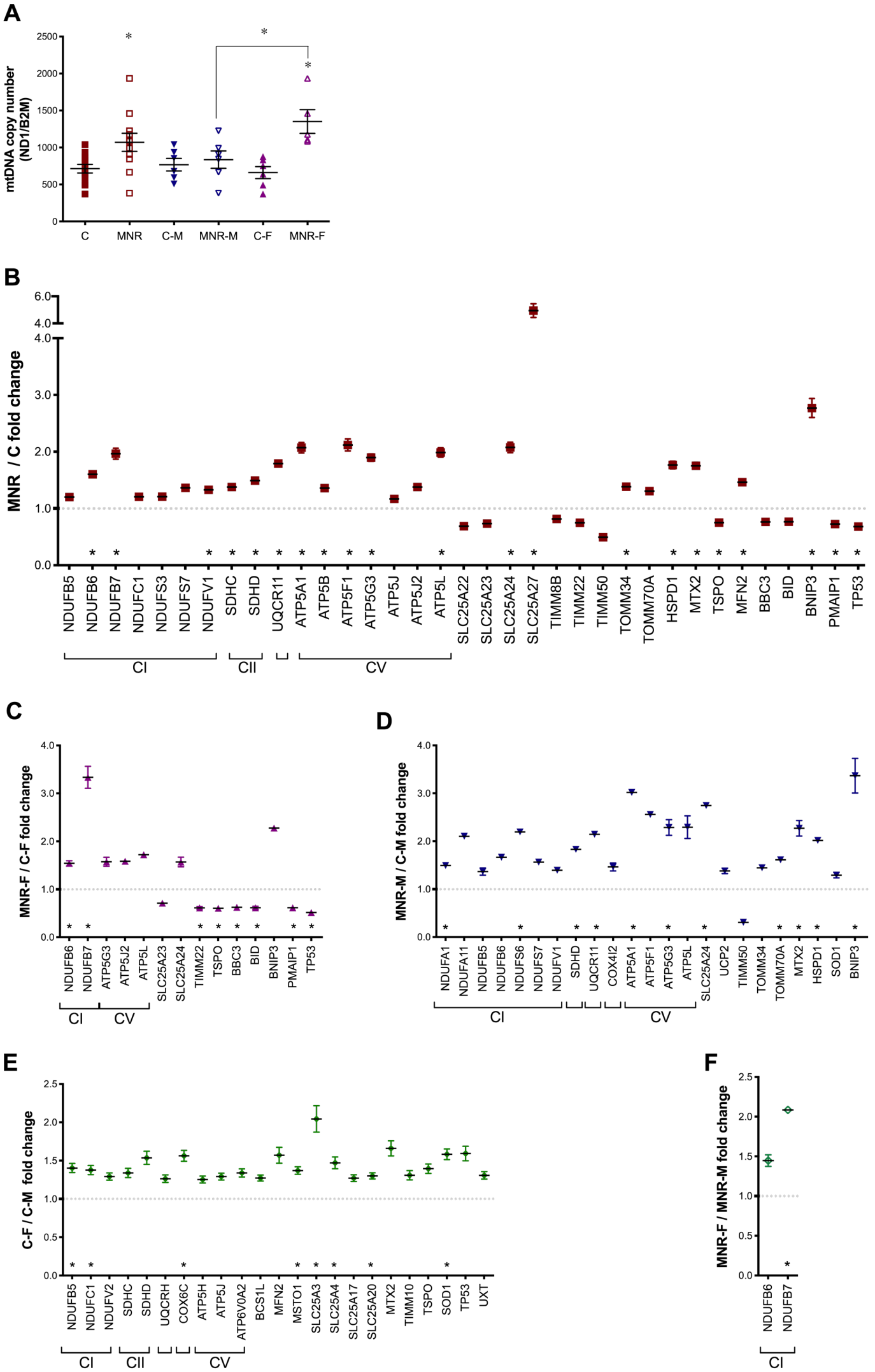
A
mtDNA copy number (ND1/B2M)
2500
2000
1500
1000
500
0
C
MNR
C-M
MNR-M
C-F
MNR-F
B
MNR / C fold change
6.0
4.0
4.0
3.0
2.0
1.0
0.0
NDUFB5
NDUFB6
NDUFB7
NDUFC1
NDUFS3
NDUFS7
NDUFV1
SDHC
SDHD
UQCR11
ATP5A1
ATP5B
ATP5F1
ATP5G3
ATP5J
ATP5J2
ATP5L
SLC25A22
SLC25A23
SLC25A24
SLC25A27
TIMM8B
TIMM22
TIMM50
TOMM34
TOMM70A
HSPD1
MTX2
TSPO
MFN2
BBC3
BID
BNIP3
PMAIP1
TP53
CI
CII
CV
C
MNR-F / C-F fold change
4.0
3.0
2.0
1.0
0.0
NDUFB6
NDUFB7
ATP5G3
ATP5J2
ATP5L
SLC25A23
SLC25A24
TIMM22
TSPO
BBC3
BID
BNIP3
PMAIP1
TP53
CI
CV
D
MNR-M / C-M fold change
4.0
3.0
2.0
1.0
0.0
NDUFA1
NDUFA11
NDUFB5
NDUFB6
NDUFS6
NDUFS7
NDUFV1
SDHD
UQCR11
COX4I2
ATP5A1
ATP5F1
ATP5G3
ATP5L
SLC25A24
UCP2
TIMM50
TOMM34
TOMM70A
MTX2
HSPD1
SOD1
BNIP3
CI
CV
E
C-F / C-M fold change
2.5
2.0
1.5
1.0
0.5
0.0
NDUFB5
NDUFC1
NDUFV2
SDHC
SDHD
UQCRH
COX6C
ATP5H
ATP5J
ATP6V0A2
BCS1L
MFN2
MSTO1
SLC25A3
SLC25A4
SLC25A17
SLC25A20
MTX2
TIMM10
TSPO
SOD1
TP53
UXT
CI
CII
CV
F
MNR-F / MNR-M fold change
2.5
2.0
1.5
1.0
0.5
0.0
NDUFB6
NDUFB7
CI

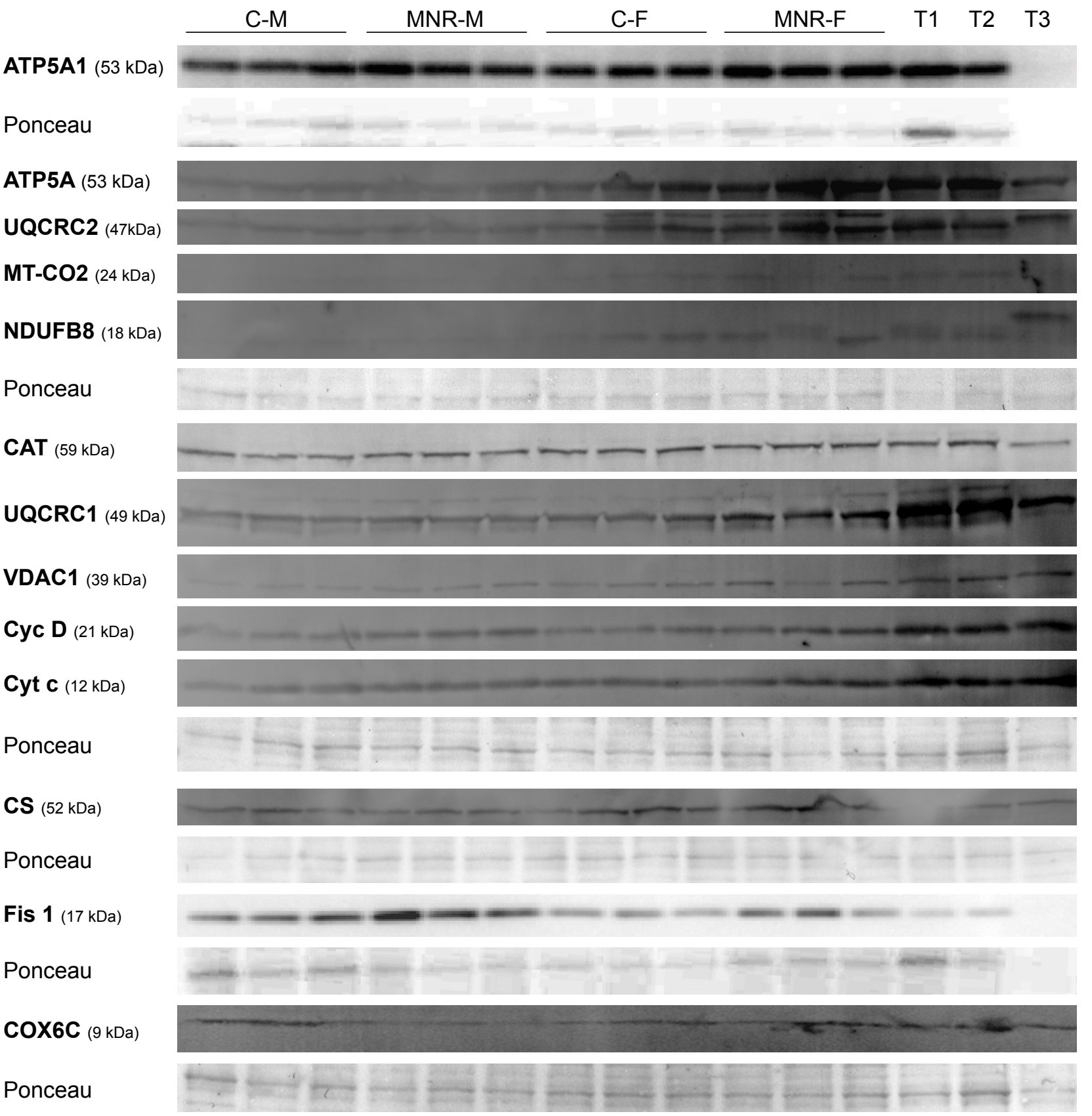

	Sexes combined		Male		Female		P-value by Mann-Whitney test				
	Control	MNR	Control	MNR	Control	MNR	C vs MNR	Male C vs MNR	Female C vs MNR	Control M vs F	MNR M vs F
Number of animals/group	12	12	6	6	6	6					
NDUFB8	1.11 ± 0.05	1.20 ± 0.05	1.00 ± 0.03	1.12 ± 0.01	1.21 ± 0.08	1.28 ± 0.10	0.033	0.010	-	-	0.037
UQCRC1	1.06 ± 0.03	1.17 ± 0.04	1.00 ± 0.02	1.09 ± 0.02	1.12 ± 0.03	1.24 ± 0.08	0.038	0.010	-	0.016	-
UQCRC2	1.12 ± 0.05	1.22 ± 0.05	1.00 ± 0.03	1.14 ± 0.01	1.24 ± 0.07	1.30 ± 0.09	-	0.016	-	0.016	-
MT-CO2	1.11 ± 0.05	1.20 ± 0.06	1.00 ± 0.03	1.11 ± 0.02	1.21 ± 0.08	1.29 ± 0.11	-	0.010	-	0.037	-
COX6C [a]	0.99 ± 0.01	1.01 ± 0.01	1.00 ± 0.01	0.99 ± 0.01	0.98 ± 0.01	1.03 ± 0.01	-	-	0.050	-	0.050
ATP5A1	1.07 ± 0.03	1.17 ± 0.05	1.00 ± 0.02	1.10 ± 0.02	1.14 ± 0.04	1.24 ± 0.09	-	0.025	-	0.006	-
ATP5A	1.11 ± 0.05	1.21 ± 0.05	1.00 ± 0.03	1.13 ± 0.02	1.22 ± 0.06	1.30 ± 0.09	-	0.016	-	0.010	-
CYT C	1.08 ± 0.04	1.20 ± 0.04	1.00 ± 0.02	1.13 ± 0.02	1.16 ± 0.04	1.27 ± 0.08	0.018	0.004	-	0.004	-
VDAC	1.08 ± 0.03	1.19 ± 0.05	1.00 ± 0.02	1.10 ± 0.02	1.16 ± 0.04	1.28 ± 0.09	0.043	0.006	-	0.004	-
CYC D	1.07 ± 0.03	1.17 ± 0.04	1.00 ± 0.02	1.11 ± 0.02	1.13 ± 0.03	1.23 ± 0.07	0.050	0.010	-	0.010	-
CS [b]	0.90 ± 0.04	0.79 ± 0.04	1.00 ± 0.07	0.85 ± 0.03	0.83 ± 0.04	0.73 ± 0.06	-	-	-	-	-
CAT [a]	1.02 ± 0.01	1.05 ± 0.01	1.00 ± 0.01	1.07 ± 0.01	1.04 ± 0.05	1.03 ± 0.06	-	0.050	-	0.050	0.050
FIS1 [a]	0.89 ± 0.08	1.33 ± 0.16	1.00 ± 0.11	1.61 ± 0.15	0.78 ± 0.11	1.05 ± 0.19	0.019	0.037	0.050	-	0.050

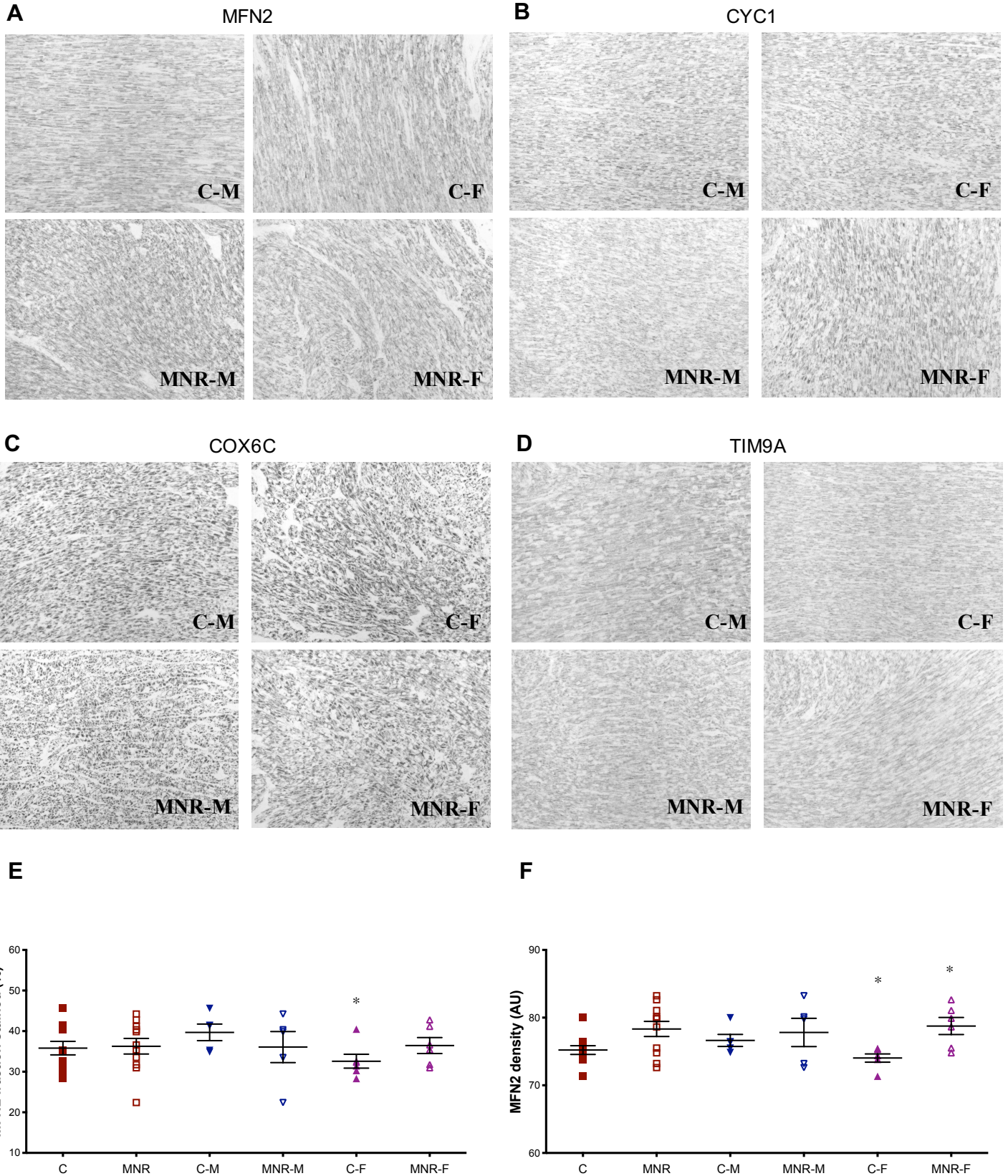
A
MFN2
C-M
C-F
MNR-M
MNR-F
B
CYC1
C-M
C-F
MNR-M
MNR-F
C
COX6C
C-M
C-F
MNR-M
MNR-F
D
TIM9A
C-M
C-F
MNR-M
MNR-F
E
MFN2 fraction stained (%)
60
50
40
30
20
10
C
MNR
C-M
MNR-M
C-F
MNR-F
*
F
MFN2 density (AU)
90
80
70
60
C
MNR
C-M
MNR-M
C-F
MNR-F
*
*

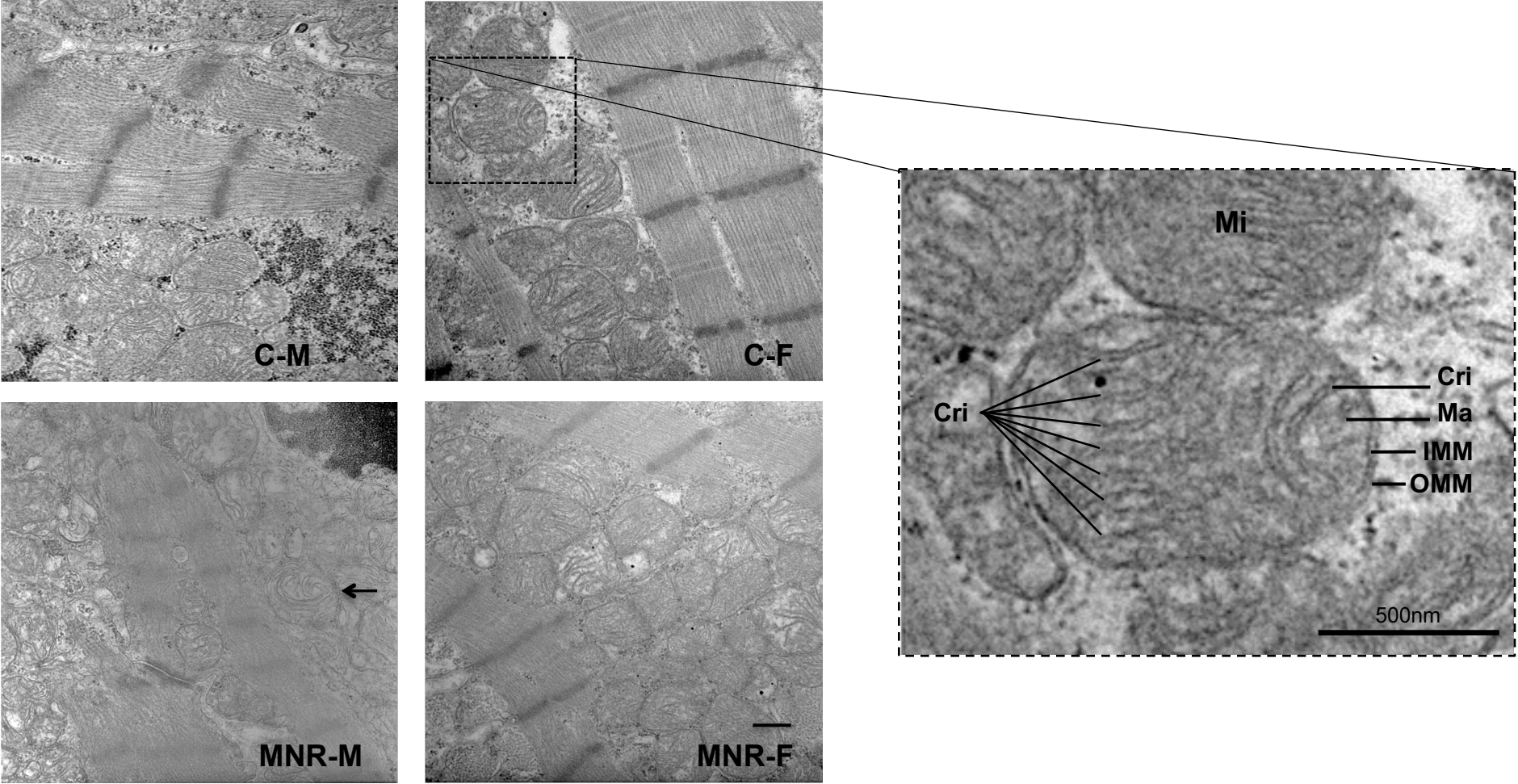
C-M
C-F
Mi
Cri
Cri
Ma
IMM
OMM
500nm
MNR-M
MNR-F

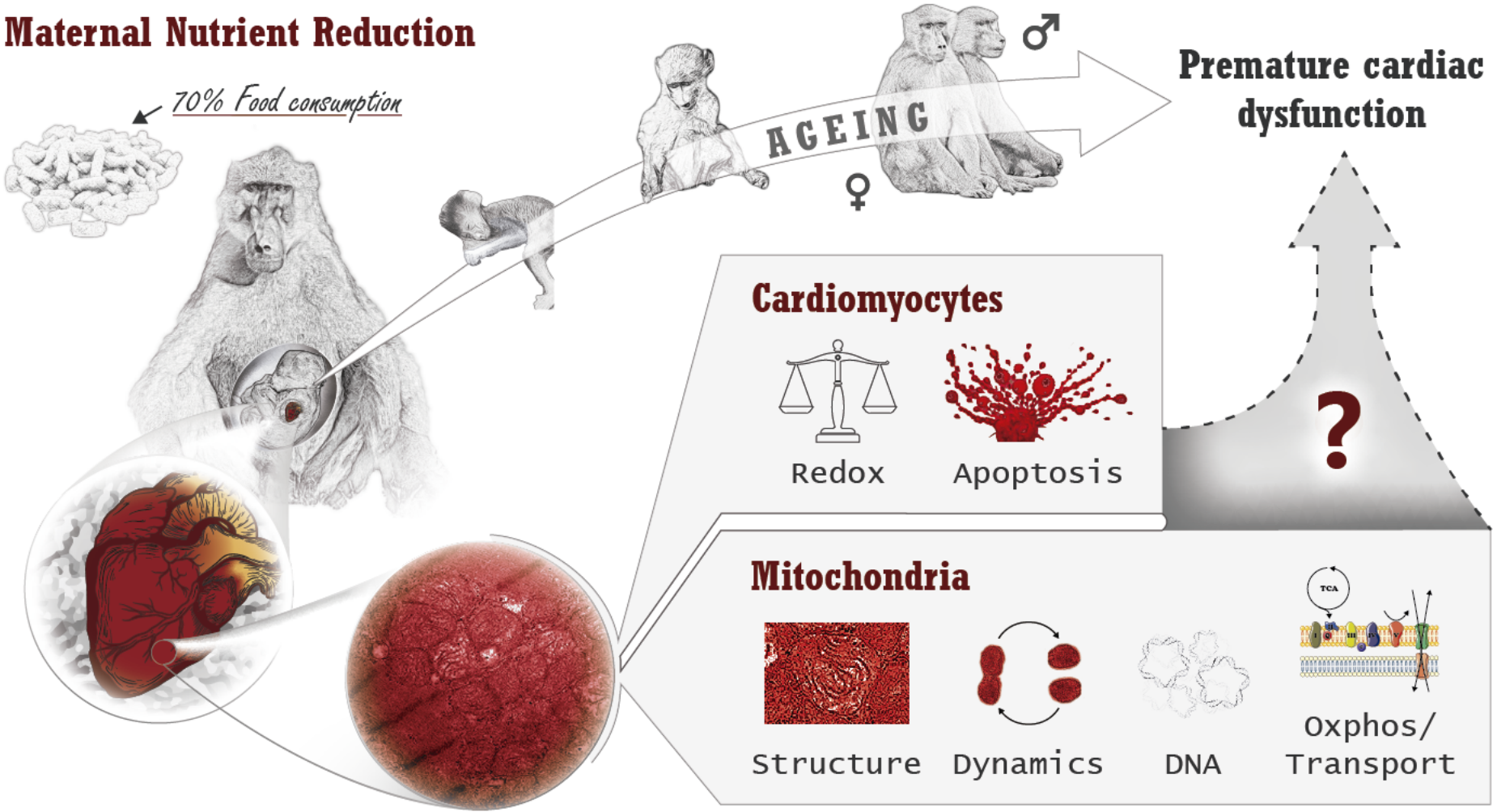
Maternal Nutrient Reduction
70% Food consumption
AGEING
♂
♀
Premature cardiac dysfunction
Cardiomyocytes
Redox
Apoptosis
?
Mitochondria
Structure
Dynamics
DNA
TCA
Oxphos/
Transport

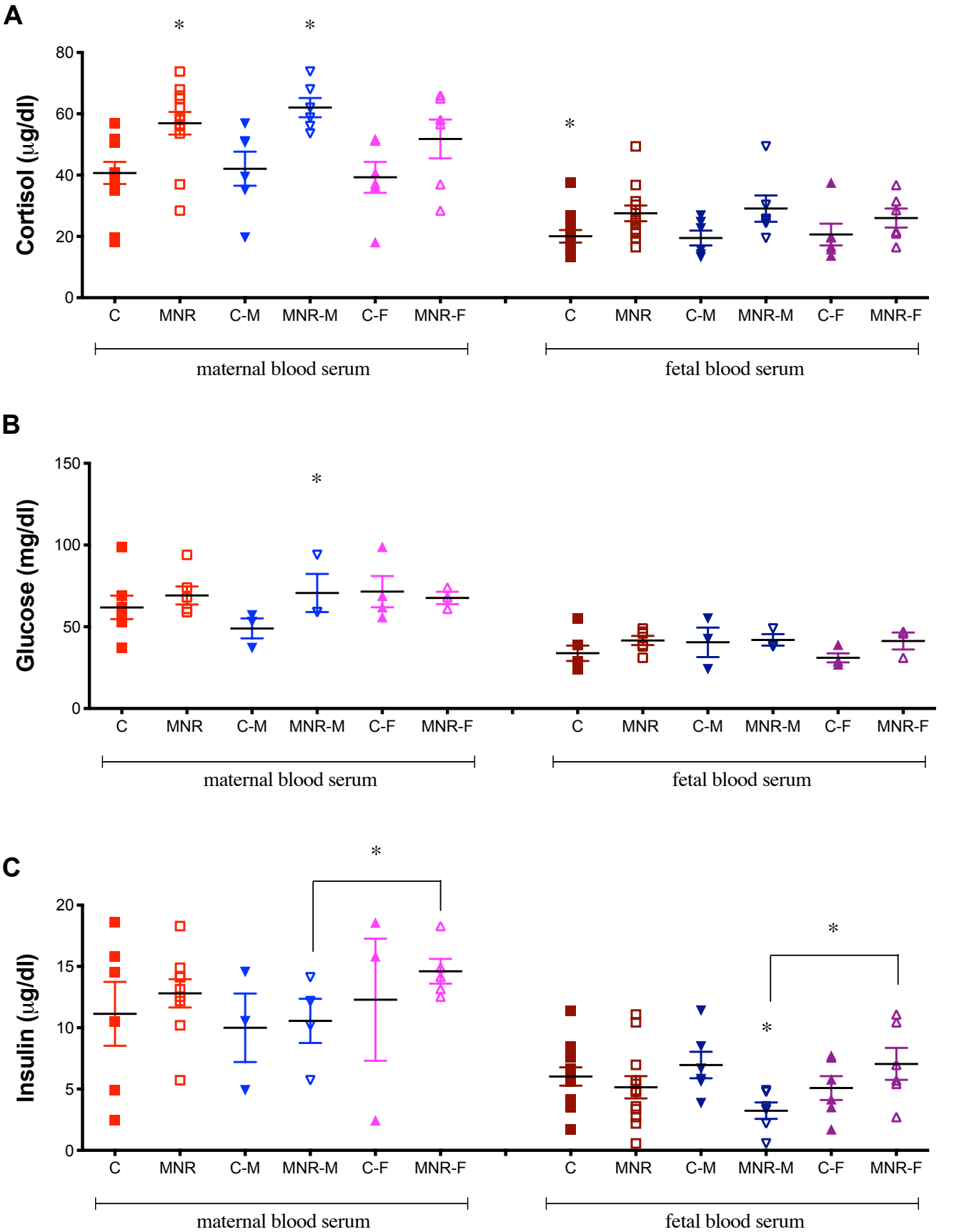
A
Cortisol (μg/dl)
80
60
40
20
0
*
*
*
C
MNR
C-M
MNR-M
C-F
MNR-F
maternal blood serum
fetal blood serum
B
Glucose (mg/dl)
150
100
50
0
*
C
MNR
C-M
MNR-M
C-F
MNR-F
maternal blood serum
fetal blood serum
C
Insulin (μg/dl)
20
15
10
5
0
*
*
*
C
MNR
C-M
MNR-M
C-F
MNR-F
maternal blood serum
fetal blood serum

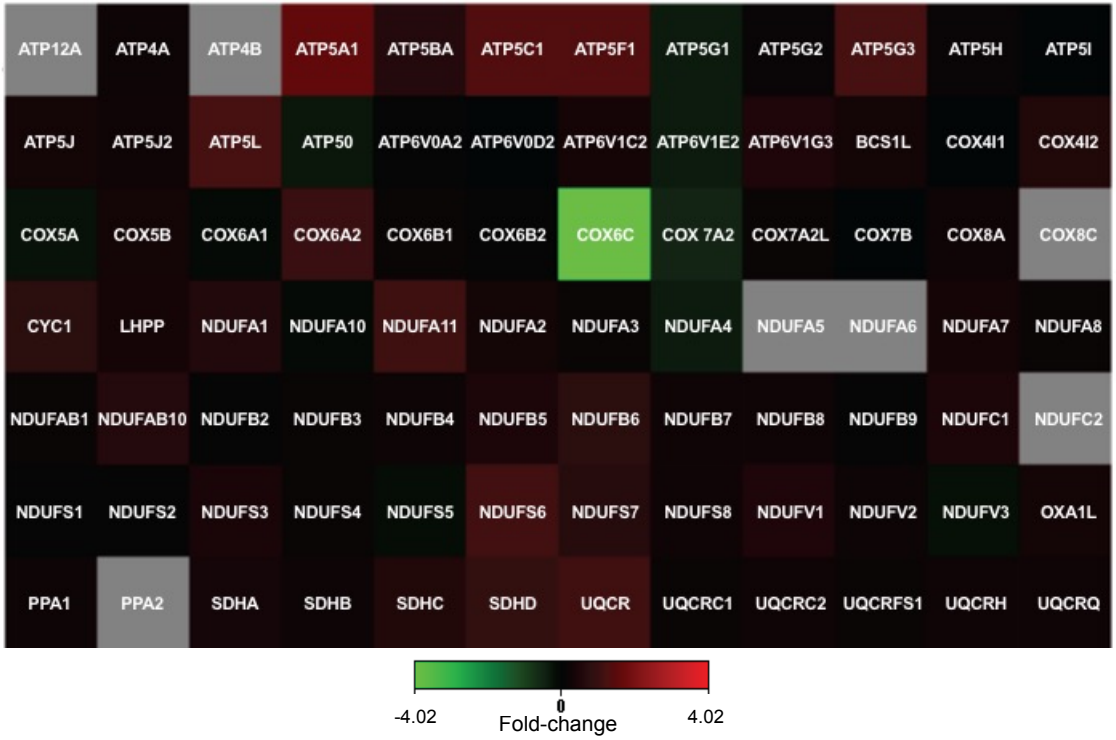
ATP12A ATP4A ATP4B ATP5A1 ATP5BA ATP5C1 ATP5F1 ATP5G1 ATP5G2 ATP5G3 ATP5H ATP5I
ATP5J ATP5J2 ATP5L ATP50 ATP6V0A2 ATP6V0D2 ATP6V1C2 ATP6V1E2 ATP6V1G3 BCS1L COX4I1 COX4I2
COX5A COX5B COX6A1 COX6A2 COX6B1 COX6B2 COX6C COX 7A2 COX7A2L COX7B COX8A COX8C
CYC1 LHPP NDUFA1 NDUFA10 NDUFA11 NDUFA2 NDUFA3 NDUFA4 NDUFA5 NDUFA6 NDUFA7 NDUFA8
NDUFAB1 NDUFAB10 NDUFB2 NDUFB3 NDUFB4 NDUFB5 NDUFB6 NDUFB7 NDUFB8 NDUFB9 NDUFC1 NDUFC2
NDUFS1 NDUFS2 NDUFS3 NDUFS4 NDUFS5 NDUFS6 NDUFS7 NDUFS8 NDUFV1 NDUFV2 NDUFV3 OXA1L
PPA1 PPA2 SDHA SDHB SDHC SDHD UQCR UQCRC1 UQCRC2 UQCRFS1 UQCRH UQCRQ
-4.02
0
Fold-change
4.02

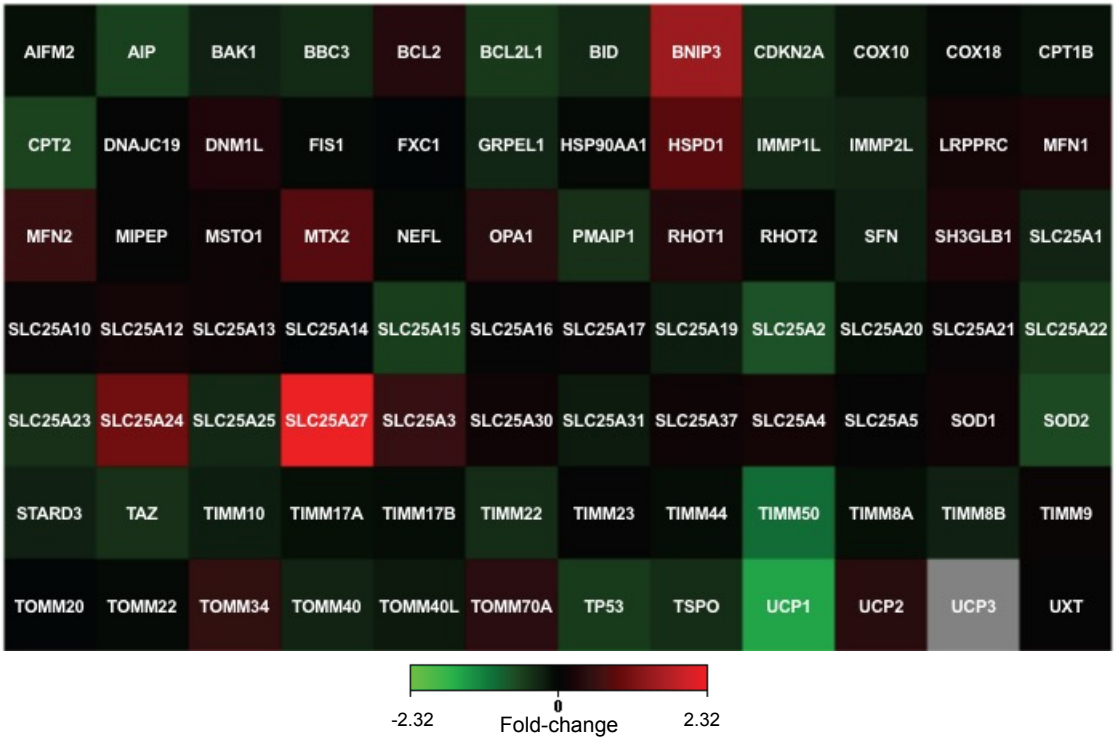
AIFM2 AIP BAK1 BBC3 BCL2 BCL2L1 BID BNIP3 CDKN2A COX10 COX18 CPT1B
CPT2 DNAJC19 DNM1L FIS1 FXC1 GRPEL1 HSP90AA1 HSPD1 IMMP1L IMMP2L LRPPRC MFN1
MFN2 MIPEP MSTO1 MTX2 NEFL OPA1 PMAIP1 RHOT1 RHOT2 SFN SH3GLB1 SLC25A1
SLC25A10 SLC25A12 SLC25A13 SLC25A14 SLC25A15 SLC25A16 SLC25A17 SLC25A19 SLC25A2 SLC25A20 SLC25A21 SLC25A22
SLC25A23 SLC25A24 SLC25A25 SLC25A27 SLC25A3 SLC25A30 SLC25A31 SLC25A37 SLC25A4 SLC25A5 SOD1 SOD2
STARD3 TAZ TIMM10 TIMM17A TIMM17B TIMM22 TIMM23 TIMM44 TIMM50 TIMM8A TIMM8B TIMM9
TOMM20 TOMM22 TOMM34 TOMM40 TOMM40L TOMM70A TP53 TSPO UCP1 UCP2 UCP3 UXT
-2.32
0
Fold-change
2.32

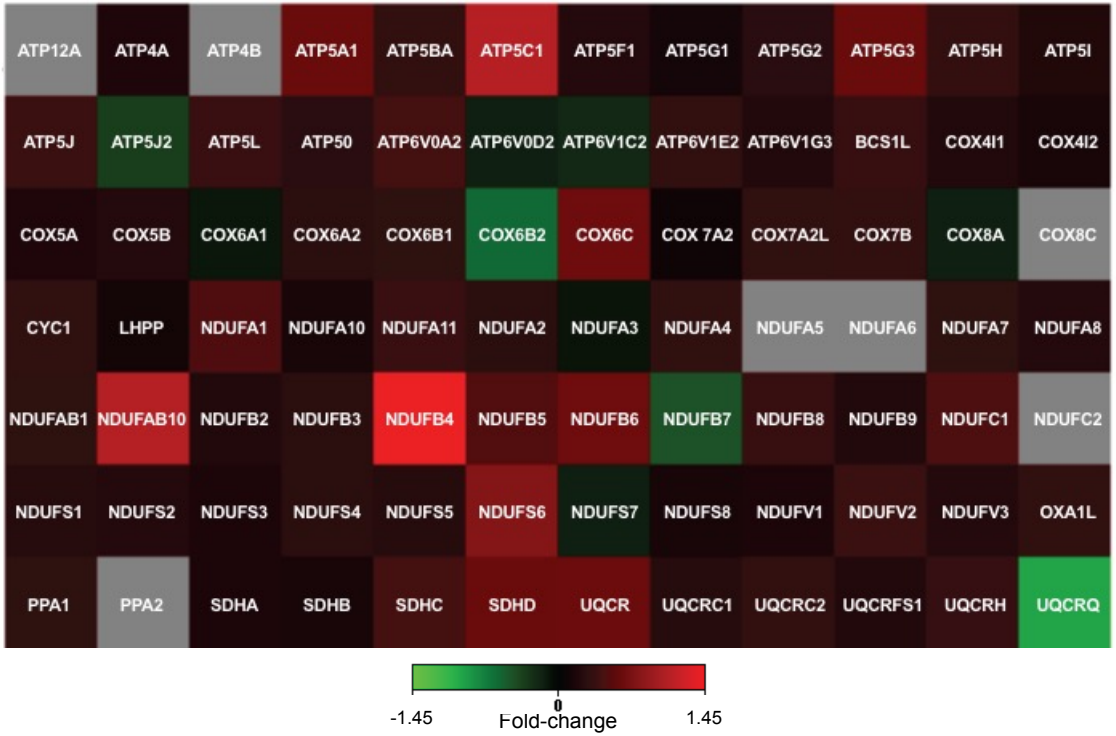
ATP12A ATP4A ATP4B ATP5A1 ATP5BA ATP5C1 ATP5F1 ATP5G1 ATP5G2 ATP5G3 ATP5H ATP5I
ATP5J ATP5J2 ATP5L ATP50 ATP6V0A2 ATP6V0D2 ATP6V1C2 ATP6V1E2 ATP6V1G3 BCS1L COX4I1 COX4I2
COX5A COX5B COX6A1 COX6A2 COX6B1 COX6B2 COX6C COX 7A2 COX7A2L COX7B COX8A COX8C
CYC1 LHPP NDUFA1 NDUFA10 NDUFA11 NDUFA2 NDUFA3 NDUFA4 NDUFA5 NDUFA6 NDUFA7 NDUFA8
NDUFAB1 NDUFAB10 NDUFB2 NDUFB3 NDUFB4 NDUFB5 NDUFB6 NDUFB7 NDUFB8 NDUFB9 NDUFC1 NDUFC2
NDUFS1 NDUFS2 NDUFS3 NDUFS4 NDUFS5 NDUFS6 NDUFS7 NDUFS8 NDUFV1 NDUFV2 NDUFV3 OXA1L
PPA1 PPA2 SDHA SDHB SDHC SDHD UQCR UQCRC1 UQCRC2 UQCRFS1 UQCRH UQCRQ
-1.45
0
Fold-change
1.45

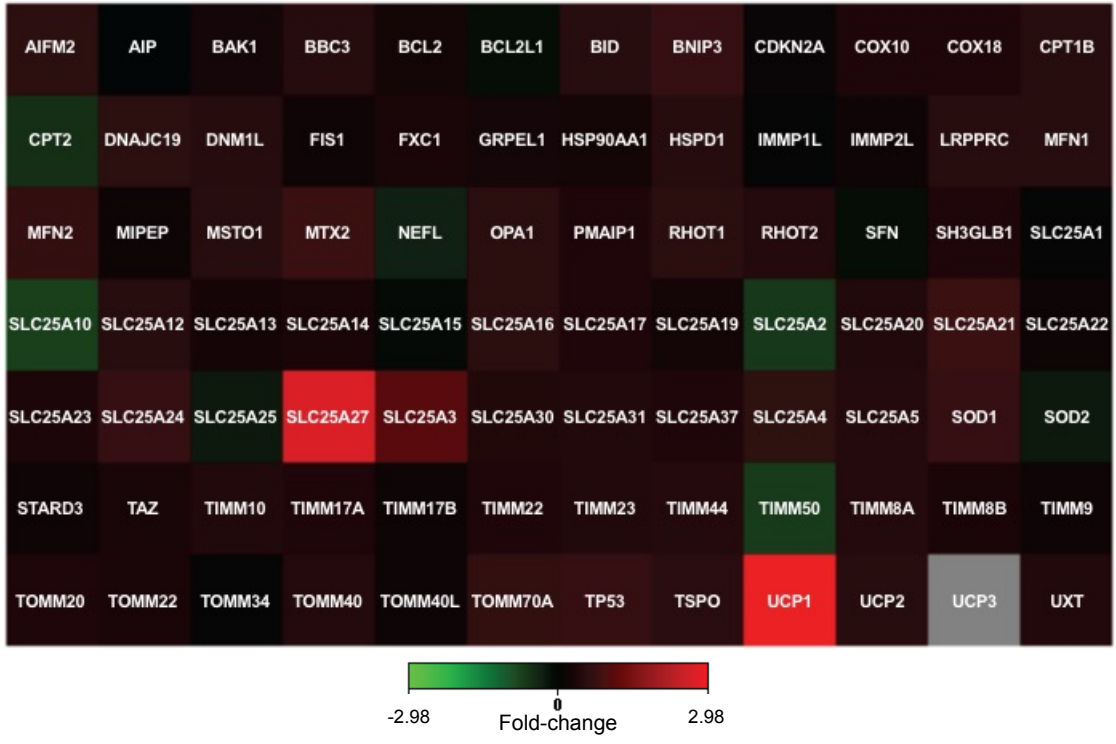
AIFM2 AIP BAK1 BBC3 BCL2 BCL2L1 BID BNIP3 CDKN2A COX10 COX18 CPT1B
CPT2 DNAJC19 DNM1L FIS1 FXC1 GRPEL1 HSP90AA1 HSPD1 IMMP1L IMMP2L LRPPRC MFN1
MFN2 MIPEP MSTO1 MTX2 NEFL OPA1 PMAIP1 RHOT1 RHOT2 SFN SH3GLB1 SLC25A1
SLC25A10 SLC25A12 SLC25A13 SLC25A14 SLC25A15 SLC25A16 SLC25A17 SLC25A19 SLC25A2 SLC25A20 SLC25A21 SLC25A22
SLC25A23 SLC25A24 SLC25A25 SLC25A27 SLC25A3 SLC25A30 SLC25A31 SLC25A37 SLC25A4 SLC25A5 SOD1 SOD2
STARD3 TAZ TIMM10 TIMM17A TIMM17B TIMM22 TIMM23 TIMM44 TIMM50 TIMM8A TIMM8B TIMM9
TOMM20 TOMM22 TOMM34 TOMM40 TOMM40L TOMM70A TP53 TSPO UCP1 UCP2 UCP3 UXT
-2.98
0
Fold-change
2.98